ADDIS ABABA UNIVERSITY

ETHIOPIAN INSTITUTE OF WATER RESOURCES

Hydrological and Hydrogeological Characterizations and Classifications Using Remote Sensing Datasets and Models

BY

GUTA WAKBULCHO ABESHU

June, 2013

Addis Ababa

Ethiopia

Hydrogeological and Hydrological Characterizations and Classification Using Remote Sensing Datasets and Models

By

Guta Wakbulcho Abeshu

The thesis is submitted to Ethiopian Institute of Water Resources, Addis Ababa University in partial fulfillment of the requirements for the degree of Scientific Masters degree in Water Resources Engineering and Management (Surface Water Hydrology).

Assessment Board

Ms. Adanech Yared	Chair Person
Dr. Solomon Gebreyohanis	External Examiner
Dr. Ing. Dereje Hailu	Internal Examiner
Prof. Dr. Ing. Joseph L. Awange	Primary Supervisor
Dr. Mekonnen Gebremichael	Second Supervisor

Ethiopian Institute of Water Resources

Addis Ababa University

Addis Ababa, Ethiopia

STATEMENT OF THE AUTHOR

I, **Guta Wakbulcho Abeshu**, declare that this thesis is my original work and that all sources of materials used for this thesis have been duly acknowledged. Also, the work presented here has not been submitted for any academic degree award at any University. Further I declare that when research paper is published from the thesis following sentence will appear at the bottom of the first page of the article or at the end of the article. © 2013 Guta Wakbulcho Abeshu

Guta Wakbulcho Abeshu

Signature:.....

Date:.....

Addis Ababa, Ethiopia

Disclaimer

This document describes work undertaken as part of program of study at Ethiopian Institute of Water Resources, Addis Ababa University. All views and opinions expressed therein remains the sole responsibility of the author, and do not necessarily represent those of the institute.

Dedicated To

My parents, Mr. Wakbulcho Abeshu and Mrs. Tejitu Jirata,

who thought me the art of fortitude and survival.

and

My brothers and sisters,

with whom I wish I could live under same roof forever

Biographical Sketch

Mr. Guta Wakbulcho was born on 27th of June 1987 at the foot of Mount Walal in West Wollega region of Oromia, Ethiopia. He was raised in a houseful of brothers and sisters who kept him enthusiastic regardless of a situation, they thought him how to read and write before he even became a first grader. Moving with his family from place to place, Mr. Guta took his elementary and middle school classes in different village towns of West Wollega region. He attended his high school education at Guliso High School and preparatory school at Ghimbi Comprehensive High School. In 2005 Mr. Guta joined Arba Minch University (AMU), Water Technology Institute where he graduated with a BSc. in Hydraulic and Water Resources Engineering with distinction in 2009. Following his graduation Mr. Guta joined the hydraulic and water resources engineering department faculty at AMU. After teaching undergraduate courses for about one and half years, in May, 2011 he joined Ethiopian Institute of Water Resources to study his MSc. in Water Resources Engineering and Management. His major research interest includes hydrologic remote sensing, hydrologic modeling, stochastic hydrology, catchment hydrology and water resources system.

Acknowledgement

Foremost, I would like to address my paramount gratitude to my supervisors, Prof. Dr. Ing. Joseph L. Awange and Dr. Mekonnen Gebremichael for all their help and support without which the completion of the thesis might not been possible. Deep gratitude goes to Mr. Ehsan Forootan and Mr. Taye Alemayehu who has helped me thoughtfully throughout the work carried out in the thesis, despite the distance and their busy schedules. I would like to extend my deepest appreciation to Dr. Phlip Omondi for reviewing the whole thesis. I owe my deepest gratitude to those, in one way or another, contributed their valuable assistances in the preparation and completion of this study. Also, I would like to extend my deepest appreciation to the USAID and Arba Minch University for their financial support throughout my stay at EIWR.

ABSTRACT

Ethiopian water resource is facing a range of challenges in water management caused by several natural and man-made impacts, namely over exploitation, deforestation, land degradation and climate variability. Understanding the spatio-temporal characteristics of water storages is therefore crucial for the country, since the welfare of the society depends on the availability of water. The prime objective of this study is to apply remotely sensed and model data to Ethiopia in order to i) analyze the inter-annual, intra-annual and seasonal variabilities of Total Water Storage (TWS), ii) understand the relationship between TWS variations, rainfall and soil moisture anomaly, and iii) study the relationship between the characteristics of aquifers' and TWS anomalies. The data used in this study includes; monthly gravity field data from the Gravity Recovery And Climate Experiment (GRACE) mission to assess the variation in TWS; monthly rainfall data from the Tropical Rainfall Measuring Mission (TRMM) to assess the response of water storages to the incoming water mass and the effect of rainfall on TWS, and the hydrological model data of Global Land Data Assimilation System (GLDAS) to obtain soil moisture. Our investigation covers a period of 8 years from 2003 to 2011. The results of the study shows that the western part and the north-eastern lowland of the country lost water at a rate of not less than 0.108 cm/year, whereas all the other regions gained water mass at a rate of more than 0.60 cm/year. The impact of rainfall seasonality was also seen on TWS changes, with losing seasons being summer and autumn, and gaining seasons being spring and winter for majority of the regions. From the TWS duration curve (TDC), the percentage time of water mass loss in all regions is also observed as 55% of the study period. Applying the statistical method of Principle Component Analysis (PCA) on TWS, soil moisture, and rainfall variations shows the dominant annual water variability in the western, north-western, northern and central regions, and the dominant seasonal variability in the western, north western and the eastern regions. A correlation

analysis between TWS and rainfall indicate a minimum time lag of zero and maximum of six months, whereas no lag has been seen between soil moisture anomaly and TWS. A significant increase in TWS deficit has also been seen in the central highlands of the country over the period of three years (2003 to 2006) with Total Storage Deficit Index (TSDI) ranging from nearly zero in 2003 to -500 % in western region and -800 % in the central and northern regions of the country in 2006. A classification of the country based on TWS Duration Curve shows that TWS variation is high in the western and low in the north eastern parts. The delay response and correlation coefficient between rainfall and TWS is also related to recharge mechanism and revealed that most regions of the country receive indirect recharge. The hydrological characterizations and classification has been carried out as Part-II, separately from the hydrogeologic characterization section only for watersheds in one selected basin which is located in region 2.

The Part-II finding shows the possibility of characterizing and classifying watersheds in a data limited regions through the help of remote sensing instruments and models. Here, the characterization and classification has been made using the catchment climate, catchment function and catchment structure descriptors. The detailed findings of this section have been described in a separate "Abstract" provided at the beginning of Part-II.

Keywords: Ethiopia, GRACE-TWS, TRMM, Duration Curve, Hydrogeological Characterization

TABLE OF CONTENTS

List of Figures

List of Tables

Abbreviations

AET	Actual Evapotranispiration
AMSR-E	Advanced Microwave Scanning Radiometer for the Earth Observing
AMSU	Advanced Microwave Scanning Unit
ASTER	Advanced Spaceborn Thermal Emission and Reflection
CSR	Center for Space Research
CLM	Community Land Modelling
DMSP	Defense Metrological Satellite Program
DKUR	Density Kurtosis
DSK	Density Skewness
DDK	Different Degree Kusche Filtering
DEM	Digital Elevation Model
DEWA	Division Early Warning and Assessment
DI	Dryness Index
ENSO	El Nino Southern Oscillation
MetOp	European Operational Metrological Satellite
EI	Evaporative Index
EOF	Empirical Orthogonal Function
GFZ	German Research Center for Geosciences
GDEM	Global DEM
GLDAS	Global Land Data Assimilation System
GES DISC	Goddard Earth Science Data and Information Services Center
GSFC	Goddard Space Flight Center
GRACE	Gravity Recovery ad Climate Experiment
HC	Hypsometric Curve
ICGEM	International Center for Global Earth Modeling
KBRR	K-Band Range Rate
KU	Kurtosis
LIS	Land Information System
LE	Latent Heat flux
LEO	Low Earth Orbiting
MHS	Microwave Humidity Sounder
MoWR	Ministry of Water Resources
MODIS	MODerate Resolution Imaging Spectroradiometer
NASA	National Aeronautics and Space Administration
NCEP	National Center for Environmental Prediction
NOAA	National Oceanic and Atmospheric Administration
PET	Potential Evapotranispiration
PLE	Potential Latent Heat flux
PCA	Principal Component Analysis

RC	Runoff Coefficient
SWIR	Shortwave Infrared
SK	Skewness
SSM/I	Special Sensor Microwave/Imager
SE	Stream flow Elasticity
TIR	Thermal Infrared
TWI	Topographic Wetness Index
TSD	Total Storage Deficit
TWS	Total Water Storage
TMI	TRMM Microwave Imager
TMPA	TRMM Multi satellite Precipitation Analysis
TRMM	Tropical Rainfall Measuring Mission
TDC	TWS Duration Curve
UNEP	United Nation Environmental Program
VIC	Variable Infiltration Capacity

PART – I

Characterization of Ethiopia's Mega Hydrogeological Regimes using Remote Sensing Datasets and Models

CHAPTER ONE

INTRODUCTION

1.1. General Background

Large portion of major freshwater basins in the world fall within the jurisdiction of more than one nation, and nearly half of the planet's land areas are covered by transboundary river basins (Uitto and Duda, 2002). While more than 86% of the country's lands are drained by international basins, water resources of Ethiopia overreach other countries in the Eastern and North-Eastern Africa (e.g., Sudan, Kenya, Somalia and Egypt) in intense ways. Extreme hydrological variability and seasonality in addition to the international nature of its most significant surface water resources are the primary challenges of water resources management in the country (World Bank, 2006). For instance, being the headwater of the Nile basin, Ethiopia contributes ~86 % of the total annual flow of Nile (Gebeto, 2010; Melesse, 2011; Sutcliffe and Parks, 1999), and also approximately 90 % of Lake Turkana inflow (Ferguson and Harbott, 1982). Any local or regional effect on the water resources of the country, therefore, influenced either by natural, anthropogenic or their inter-linked factor may have substantial consequences, not only on Ethiopia, but also on the downstream countries such as Egypt, Sudan and Kenya (Conway, 1996; Taye and Willems, 2012; UNEP/DEWA, 2012).

The basins within the country have experienced several inter-linked natural and anthropogenic calamities activated by several factors that have caused loss of lives, famines, diseases and damage to the economy for over a century. Among all, frequent droughts and floods in particular have the most severe impacts (World Bank, 2009). On the one hand, depletion in

water storage influenced by shortage of rainfall, over exploitation and mismanagement of the natural resources are causing water deficiency. This leads to an important negative shock that can destabilize livelihoods (Gray and Mueller, 2012), as it imposes frequent crop failures due to dry spells and droughts resulting in low agricultural production leading to famine that affects millions of rural poor farmers, pastoralists, domestic and wild animals (Awulachew et al., 2007). On the other hand, some studies in well instrumented small head water catchments in Ethiopian highlands reveal the effects of catchment management on the hydrological responses. For instance, Nyssen et al. (2010) described that in northern Ethiopia, catchment managements has resulted in higher infiltration rates and reduction in direct runoff volume, implying that it has had a positive influence on the catchment water balance. Another stud in the same region by Berhane et al. (2013) claims that human influence in the past, through construction of micro-dams has resulted in the return of old springs, emergence of new springs, wetlands and increase in stream discharges.

Hydrogeological investigations refer to the study of lithological, stratigraphical and structural aspects of a territory using basic geological methods leading to the understanding of the factors that regulate effective infiltration, groundwater reserve, the circulation and outflow of the groundwater. The prime aim is to provide the general information on the groundwater resource potential (Alemayehu, 2006). According to Chernet (1993), Ethiopia has diverse hydrogeological conditions which are highly controlled by its geologic, topographic and climatic conditions. MacDonald et al. (2001) noted that the groundwater availability in Ethiopia is controlled by two main factors; the geology and aquifer recharge. Characterizing hydrogeological regimes of the country through its geologic behaviors have been subject of numerous studies in the past few decades (Ayenew et al., 2008; Chernet, 1993; Damilie et al.,

2007, 2008; Furi et al., 2011, 2012; Kebede et al., 2005, 2008; Yitbarek et al., 2012). However, since such kind of study requires data collected at fine spatial and temporal domains, as a result, most of them are limited to small scales. For instance, Ayenew et al. (2008), Furi et al. (2012), Kebede et al. (2005, 2008), Yitbarek et al. (2012) carried out hydrogeological investigations over different segments of Ethiopia using environmental isotopes and hydrochemicals, and found that the approach to be the most effective tool for differentiating various forms of geochemical reaction and to infer environmental factors affecting groundwater quality and its flow in the region. But such type of studies are costly, requires skilled experts, and are often difficult to apply over large areas, which are not easy to venture, particularly in developing countries like Ethiopia.

Climatic characteristics have also been the theme of various studies over the past few decades. For instance, Conway et al. (2011), Degefu (1987), Gamachu (1977), Haile (1988), Seleshi and Camberlin (2006) and Seleshi and Zanke (2004) studied the spatio-temporal variability of climate over different segments of Ethiopia and reported that climate is one of the major driving forces of hydrological partitions in Ethiopia, while effects of topography are also noticeable. There are also several attempts to study the influence of warming of the Indian Ocean on the hydrological events in the region (Funk et al., 2011). Wolde-Georgis (1997) considered the relation between the El Niño Southern Oscillation (ENSO) phenomenon and drought in Ethiopia and suggested that it is important to consider ENSO for improving drought early warning by providing longer lead times to respond. According to Taye and Willems (2012), changes occurring on the Pacific Ocean are responsible for the decadal oscillations in climate and related high and low Abbay basin water availability for Ethiopia, Sudan, and Egypt. In this context, Shang et al. (2011) studied the trend of extreme precipitation in the north western

highlands of Ethiopia and found no increasing/decreasing trend in extreme precipitation in the region. Inferring the water availability in the region through climatic study might not be good enough while the roles of anthropogenic factors are also noteworthy. Consequently, more studies are needed to reinforce them. Therefore, studies on parameters which hold the chronicles of anthropogenic, climatic or their interlinked factors are of more importance.

Total Water Storage (TWS), which is defined as all forms of water stored above and underneath the surface, is a key component of the terrestrial and global hydrological cycles that exerts important control over water, energy and biogeochemical fluxes. Therefore, it plays a major role in the Earth's climate system (Rodell et al., 2004; Syed et al., 2008; Tapley et al., 2004). Characterizing water storages at all stages (surface, soil water and groundwater) and their responses to the incoming and outgoing water masses are of great importance in terms of understanding the magnitude of anthropogenic and natural disasters on the water resource systems. This is of interest especially in areas where seasonality of rainfall is strong and the welfare of the society relies on the availability of water. For characterization of water storage, soil moisture and groundwater have been documented to play a significant role, e.g., in Frappart et al. (2011), Rodell et al. (2007), Rodell and Famiglietti (2001) and Swenson et al. (2008). For developing countries like Ethiopia, in-situ data for soil moisture and groundwater levels are among the most difficult water budget parameters to obtain. This indicates an important role of remote sensing data along with modeling approaches to obtain such parameters.

1.2. Relevance of the Research

While most of the previous studies concentrated on the climatic characteristics (Degefu, 1987; Haile 1988) and the use of environmental isotopes and hydrochemicals to trace the water

availability in Ethiopia (Damilie et al., 2007, 2008; Kebede et al., 2005, 2008), this contribution focuses on the TWS variations in the region. In regions like Ethiopia, where the conventional in-situ data are sparse and not distributed uniformly, or not available in the areas where they are mostly needed, understanding of the surrounding environment and water storage characterizations are not easy. To overcome such difficulties, a top-down method provides a possible approach. For instance, rather than computing the TWS from groundwater, surface water storage anomaly, snow water equivalent and soil moisture, a reverse computation of the required parameters from TWS can be performed where these parameters are remotely sensed (Rodell et al., 2004). Gravity Recovery And Climate Earth Experiment (GRACE) satellites offers such possibility of remotely sensing groundwater depletion in data poor regions of the world (Rodell et al., 2007).

To date, however, except studies which have been done at continental or global scale (Ramillien et al., 2005; Reager and Famiglietti, 2009; Schmidt et al., 2008; Schmidt et al., 2006) and those in connection with the Nile basin (Bedada, 2007; Bonsor et al., 2010; Melesse et al., 2010), GRACE satellite product have not been applied to the Ethiopian basins at a local level. One of the major challenges in applying the GRACE satellite gravity potential product to estimate total water storage variations in Ethiopian basins is the fact that only two of the 12 basins (Abbay and Wabishebele) can barely fulfill the smallest required basin area (200,000km^2; Tapley et al., 2004) for GRACE satellite applications. To overcome this drawback, in the current study, Ethiopia is divided into ten regions of equal size of 4^0 x 4^0. For each region, the TWS are computed from GRACE data using approaches presented in Wahr et al. (1998). Rainfall and soil moisture data have been used from Tropical Rainfall Measuring Mission (TRMM) and the Global Land Data Assimilation System (GLDAS), respectively.

1.3. Research Objectives

General Objective

The general objective of this study is to characterize large scale hydrogeological regimes of Ethiopia through the use of remotely sensed data and models.

Specific Objectives

The major contributions of this study are:

- To understanding the responses of Ethiopian aquifers, through information obtained from the analysis of inter-annual (i.e., between years variability), intra-annual (i.e., processes that occur on a time scale of less than one year but more than one month), and their TWS duration curve (i.e., the frequency of occurrence).
- To depict the reaction of each region to the incoming water mass (rainfall) in order to obtain the lag time that helps in estimating the longest period over which the available stored groundwater can be exploited after rainy seasons without going beyond the mean TWS.
- To examine the TWS deficit obtained from GRACE with the dry spells, and
- To identifying the dominant variability pattern of GRACE TWS, soil moisture and rainfall over Ethiopia at intra-annual, annual and seasonal time scales.

1.4. Hypothesis

- The Inter-annual, Intra-annual and seasonal variability of total water storage is governed by rainfall seasonality in the region.
- Groundwater is the dominant controlling factor for total water storage variation.

- There will be a poor correlation between total water storage and rainfall over Ethiopia, as more than 75% of the countries aquifers get their recharge through indirect mechanism (Kebede, 2012).

1.5. Thesis Structure

The remainder of the study is organized as follows; in Chapter 2, the overall Theorical framework of the study are discussed. Chapter 3 presents the description of study area, data used and the analysis methods. The results and discussions of the study are presented in Chapter 4 and 5 respectively, while Chapter 6 summarizes the major findings of the study and recommendation provided.

CHAPTER TWO

THEORICAL FRAMEWORK

2.1.Time-Variable Gravity

The Earth's gravity field is a product of its mass distribution (mass, both deep within the Earth, and at and above its surface); this mass distribution is constantly changing. Tides in the ocean and solid Earth cause short time large mass variations (at 12-hour and 24-hour periods) (Wahr et al, 2007). Atmospheric disturbances associated with synoptic storms, seasonal climatic variations, etc., lead to variations in the distribution of mass in the atmosphere, the ocean, and the water stored on land (Wahr, et al 2007). Mantle convection causes mass variability throughout the mantle that has large amplitudes compared to those associated with climatic variability, but it generally occurs slowly relative to human timescales. Because of these and other processes, the Earth's gravity field varies with time.

One serious limitation when interpreting gravity observations is that the inversion of gravity for density is non-unique. There are always an infinite number of possible internal density distributions that can produce the same external gravity field. Even perfect knowledge of the external gravity field would not provide a unique density solution. Non-uniqueness is much less of an issue for short human timescale varying gravity. If the time-varying signals vary rapidly enough, it can usually be assumed to come from mass variability at the Earth's surface rather than from deep within the Earth. It is almost certain that this signal is coming from some combination of the atmosphere, the oceans, and the water/snow/ice stored on or just below the land surface. But also few solid Earth processes are likely to vary this rapidly, let alone to show an annual or monthly cycle. The only exceptions are the body tide, which can be modeled and

removed at a very good accuracy. Loading signal, which is typically only a few percent of the signal from the load itself, can be linearly related to the load signal through scale-dependent, well-modeled, proportionality factor called Load love numbers.

2.2.Changes in the Earth's Oblateness

The first satellite identification of a non-tidal time-varying signal was the recovery of a secular change in the Earth's oblateness. The oblateness is a global-scale component, and is the easiest laterally varying component to detect with a satellite. Let N (θ, φ) be the height of the geoid above the Earth's mean spherical surface at latitude θ and eastward longitude φ (Fig. 2).

$$N(\theta,\varphi) = a\sum_{l=2}^{\infty}\sum_{m=0}^{l}\widetilde{P}_{lm}(\cos\theta)(C_{lm}\cos(m\emptyset) + S_{lm}\sin(m\emptyset)) \quad 1$$

Where a, is the radius of the Earth, the P_{lm} are normalized associated Legendre functions, the C_{lm} and S_{lm} are dimensionless (Stokes) coefficients. Global gravity field solutions are typically provided in the form of a set of spherical harmonic coefficients also called Stokes coefficients. The indices l and m are the degree and order of the Legendre function respectively.

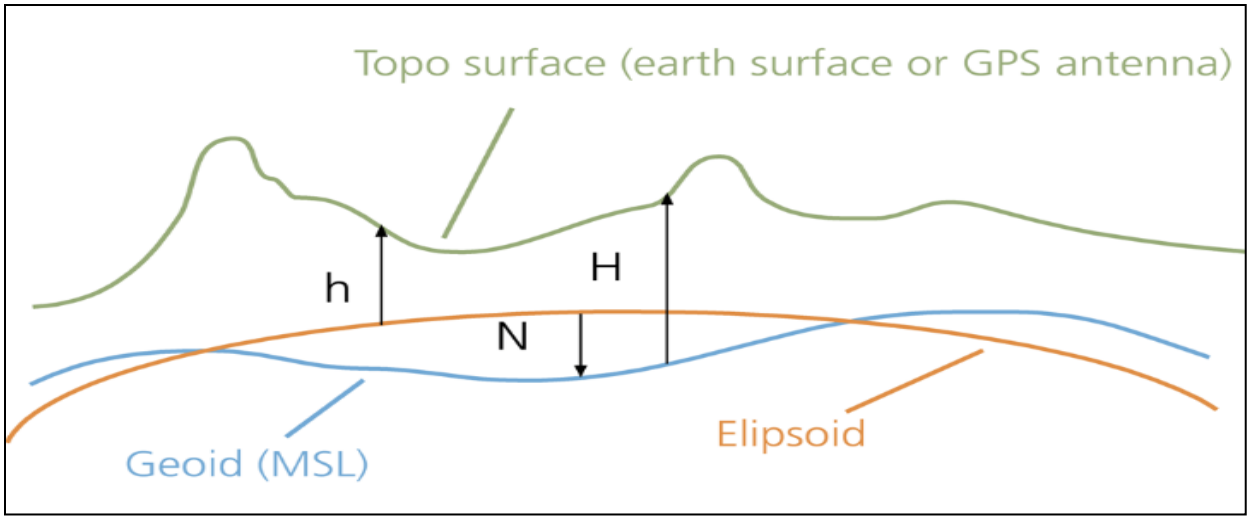

Figure 1: Geoid height (N), Orthometric height (H) and Ellipsoidal height (h)

2.3. Using the Spherical Harmonic Solutions to Solve for Mass

The time-variable component of the gravity field can be obtained by removing the long-term mean of the Stokes coefficients from each monthly value. The mean can be derived from one of the static fields available or more usefully, it can be estimated by simply constructing the average of all the monthly fields used in the analysis. The reason for removing the mean field is that it is dominated by the static density distribution inside the solid Earth. It thus has no bearing on attempts to learn about, the distribution of masses like water stored on land or in the ocean. Removing the static field, though, means that all contributions from the mean stored water are also removed. Thus, only the time-variable component of the water storage can be recovered. The time-variable gravity field is then used to solve for the time-variable mass field. This solution is non-unique. Let ΔClm and ΔSlm, be the time-variable components of the (l, m) Stokes coefficients for some month. Let $\Delta\rho$(r, θ, φ) be the density redistribution that causes this time-dependent change in gravity. Then the time-variable part of spherical harmonic coefficients can be expressed as:

$$\begin{pmatrix}\Delta C_{lm}\\ \Delta S_{lm}\end{pmatrix} = \frac{3}{4\pi a \rho_{ave}(2l+1)} \int \Delta\rho(r,\theta,\varphi) \left(\frac{r}{a}\right)^{l+2} \tilde{P}_{lm}(cos\ \theta) \begin{pmatrix}cos(m\varphi)\\ sin(m\varphi)\end{pmatrix} sin\,\theta\ d\theta d\varphi dr \qquad 2$$

Where ρ_{ave} is the average density of the Earth, which is 5517 kg/m^3.

If the density is expanded as a sum of Legendre functions we will get:

$$\Delta\rho(r,\theta,\varphi) = \sum_{l=0}^{\infty}\sum_{m=0}^{l} \tilde{P}_{lm}\,(cos\,\theta)(\Delta\rho_{lm}^{c}(r)\,cos(m\varphi) + \Delta\rho_{lm}^{s}(r)\,sin(m\varphi) \qquad 3$$

Using the above equations (2 and 3), and employing orthogonality relations for Legendre functions we obtain,

$$\begin{pmatrix}\Delta C_{lm}\\ \Delta S_{lm}\end{pmatrix} = \frac{3}{a\rho_{ave}(2l+1)}\int \begin{pmatrix}\Delta\rho^{c}_{lm}(r)\\ \Delta\rho^{s}_{lm}(r)\end{pmatrix}\left(\frac{r}{a}\right)^{l+2} dr \qquad 4$$

Suppose, we have reason to believe the observed ΔClm and ΔSlm are caused by mass variability concentrated within a thin layer of thickness H near the Earth's surface; a layer containing those regions of the atmosphere, oceans, ice sheets, and land water storage that are subject to significant mass fluctuations. H, in this case, would be mostly determined by the thickness of the atmosphere, and is of the order of 10 km. If H is thin compared to the horizontal resolution of the observations, then the amplitude of the density anomaly can be uniquely determined, as follows. Suppose the observed gravity field is accurate enough to resolve gravity anomalies down to scales of R km. That means the ΔClm and ΔSlm's contain useful information for values of l up to lmax = 20000/R. Suppose H is thin enough that:

$$\frac{(l_{max}+2)H}{a} \ll 1 \qquad 5$$

Then $\left(\frac{r}{a}\right)^{l+2} \approx 1\ for\ all\ usable\ values\ of\ l, and\ also\ (2)\ reduces\ to$

$$\begin{pmatrix}\Delta C^{surf\ mass}_{lm}\\ \Delta S^{surf\ mass}_{lm}\end{pmatrix} = \frac{3}{4\pi\rho_{ave}(2l+1)}\int \Delta\sigma(\theta,\varphi)\tilde{P}_{lm}(cos\theta)\begin{pmatrix}cos\,(m\varphi)\\ sin\,(m\varphi)\end{pmatrix} sin\theta d\theta d\varphi \qquad 6$$

where Δσ is the change in surface density (i.e. mass/area), defined as the radial integral of $\Delta\rho$ through surface layer

$$\Delta\sigma(\theta,\varphi) = \int_{thin\ layer}\Delta\rho(r,\theta,\varphi)dr \qquad 7$$

$$\begin{pmatrix}\Delta C^{solid\ Earth}_{lm}\\ \Delta S^{solid\ Earth}_{lm}\end{pmatrix} = k_l\begin{pmatrix}\Delta C^{surf\ mass}_{lm}\\ \Delta S^{surf\ mass}_{lm}\end{pmatrix} \qquad 8$$

Thus, the total dependence of stokes coefficients on the surface mass density is

$$\begin{pmatrix}\Delta C_{lm}\\ \Delta S_{lm}\end{pmatrix} = \frac{3}{4\pi a\rho_{ave}}\frac{1+k_l}{(2l+1)}\int \Delta\sigma(\theta,\varphi)\tilde{P}_{lm}(cos\theta)\begin{pmatrix}cos(m\varphi)\\ sin(m\varphi)\end{pmatrix} sin\theta d\theta d\varphi \quad 9$$

By expanding Δσ (θ, φ) as a sum of Legendre coefficients, similar to the expansion shown in (3) for Δρ, and using the orthogonality of the Legendre functions to obtain a result similar to (4), we find:

$$\Delta\sigma(\theta,\varphi) = \frac{a\rho_{ave}}{3}\sum_{l=0}^{\infty}\sum_{m=0}^{l}\frac{2l+1}{1+k_l}\tilde{P}_{lm}(cos\theta)(\Delta C_{lm}\, cos(m\varphi) + \Delta S_{lm}\, sin(m\varphi) \quad 10$$

The results above assume the surface layer is thin enough that (5) is valid. If we assume that lmax = 65, and that the layer includes the atmosphere so that H~10 km, then (5) is violated at about the 10% level. Equation (10) is the starting point for using GRACE estimates of ΔClm and ΔSlm to recover changes in surface mass density. The methods and procedural computations of love numbers and normalized associated Legendre polynomial in equation 10 are described below

2.4. Remote Sensing of Total Water Storage – GRACE

GRACE is a joint satellite gravimetry mission of the US National Aeronautics and Space Administration (NASA) and the German Space Agency (DLR). It was launched in March, 2002 with an assignment to track changes in the Earth's gravity field. GRACE consists of two satellites moving one after the other in near-circular orbit at an altitude of ~460 Km above the Earth with an inclination of 89.5 ^{0} and the distance between them being 220 Km. The microwave K-Band Range Rate system (KBRR) is used to continually monitor their separation distance to an accuracy of better than 1 μm (Tapley et al., 2004).

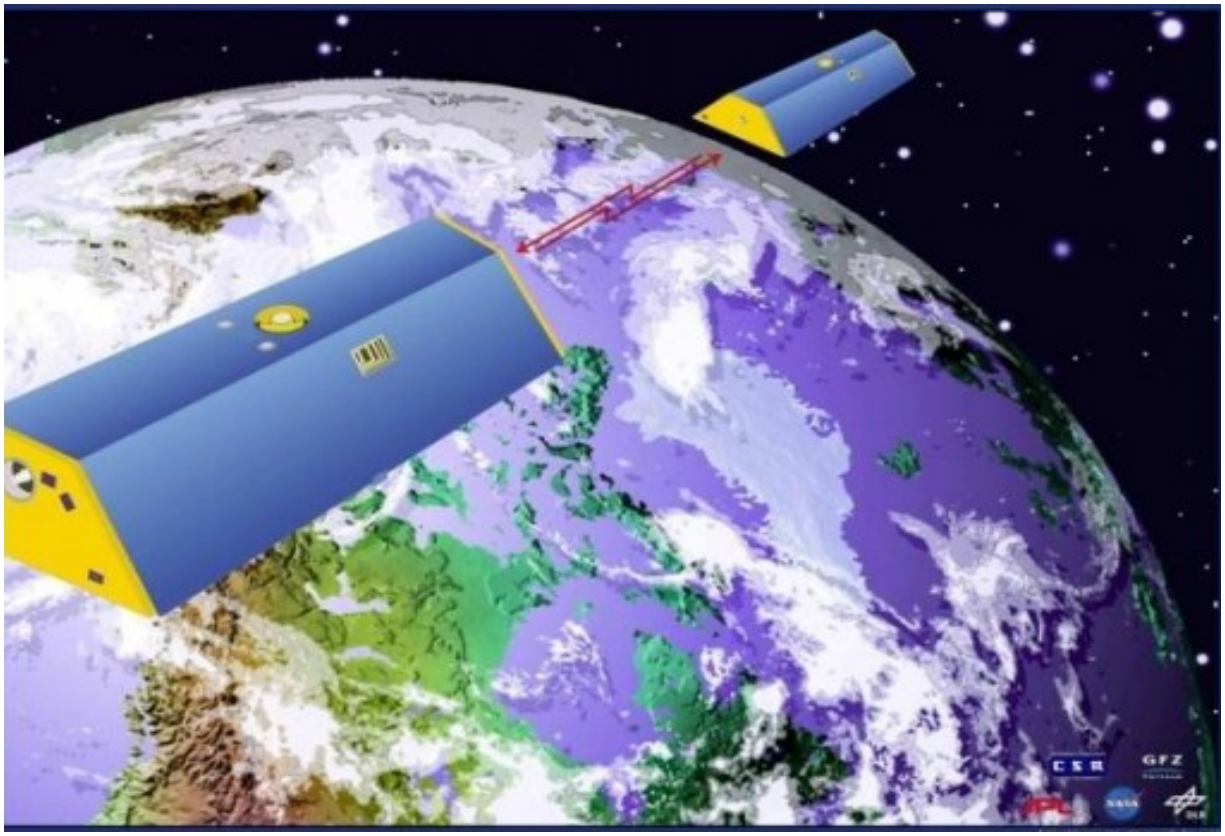

Figure 2: GRACE twin satellites (Source: GRACE web page)

2.4.1. Spherical Harmonic Coefficients

Spherical harmonics are the angular portion of a set of solutions to Laplace's equation represented in a system of spherical coordinates**.** Observations of mass variability using either satellites or ground-based instrumentation can be used to study a wide variety of geophysical processes that involve changes in mass (Dickey et al., 1997).

The GRACE satellite gravimetry mission has been one of the most commonly exploited satellite in the past decade for computing TWS and proved to have the capacity to remotely sense water storage changes at regional and global scale. For instance, changes in TWS and drought characterization have been reported, (see, e.g., Awange et al., 2011; Awange et al., 2007; Chen et al., 2010; Crowley et al., 2006; Crowley et al., 2008; Forootan et al., 2012; Rodell et al., 2007; Strassberg et al., 2009; Yirdaw et al., 2008). Yeh et al. (2006) studied groundwater storage

changes in Illinois using GRACE and reported that GRACE-based method of estimating monthly to seasonal groundwater storage changes performs reasonably well at a basin size of better than 200,000 km^2. The potential for using GRACE gravity measurements to monitor TWS over large semiarid regions subjected to intense irrigation is also shown e.g., see, Strassberg et al., (2009).

2.4.2. The Normalized Associated Legendre Polynomial

The concept of Legendre function is first introduced by French mathematician named Adrien-Marie Legendre. It is an important application of power series method of solution to the Legendre differential equation in which $\alpha \geq 0$ is a real parameter. The equation arises in a variety of applications, but mainly in connection with physical problems in which spherical symmetry is present. The equation finds its origin in the study of Laplace's equation when expressed in spherical coordinates.

$$(1 - x^2)y'' - 2xy' + \alpha(\alpha + 1)y = 0, \qquad 11$$

It is one of the functions considered as special functions so-called higher transcendental functions, as distinct from elementary functions such as sine, cosine, exponential, and logarithm. We first develop the series solutions for arbitrary $\alpha \geq 0$, and then consider the cases α = n = 0, 1,2,...,which lead to a special class of polynomial solutions $P_n(x)$ called Legendre polynomials in which n is the degree of the polynomial.

There are different ways computing the associated Legendre polynomial function values of a given degree and order. The method presented here is adopted from Bethencourt et al., (2005). The starting values for computing normalized Legendre polynomial function values of certain l-max and m-max are $\tilde{P}_{00}(t) = 1$ and $\tilde{P}_{11}(t) = \sqrt{3u}$, with u = $\sin\theta$. From them one can proceed through the diagonal terms (m = n) by means of equation 11.

$$\tilde{P}_{mm}(t) = u\sqrt{\frac{2m+1}{2m}}\tilde{P}_{m-1,m-1} \quad 12$$

The next terms, $\tilde{P}_{l+1,l}$ *or* $P_{m,m-1}$ necessary to initialize the previous recurrence relations can be obtained by the same relations (equation 12) and (13) taking into account the fact that the constants the associated Legendre function don't exist to m > l and $b_{l+1,l} = h_{m,m-1} = 0$ in these cases.

$$\tilde{P}_{lm}(t) = a_{lm}t\tilde{P}_{l-1,m}(t) - b_{lm}\tilde{P}_{l-2,m}(t) \quad 13$$

$$where \quad a_{lm} = \sqrt{\frac{(2l-1)(2l+1)}{(l-m)(l+m)}} \quad 14$$

$$b_{lm} = \sqrt{\frac{(2l+1)(l+m-1)(l-m-1)}{(l-m)(l+m)(2l-3)}} \quad 15$$

$$\tilde{P}_{lm}(t) = \frac{1}{\sqrt{j}}\left(g_{lm}\frac{t}{u}\tilde{P}_{l,m+1}(t) - h_{lm}\tilde{P}_{l,m+2}(t)\right) \quad 16$$

$$where \quad g_{lm} = \frac{2(m+1)}{\sqrt{(l-m)(l+m+1)}} \quad 17$$

$$h_{lm} = \sqrt{\frac{(l+m+2)(l-m-1)}{(l-m)(l+m+1))}} \quad 18$$

Then one can go 'Forward' increasing sequentially the degree n in (equation 12), or decreasing sequentially the order m in (equation 13), they are called as recursive relations 'Forward Column' (FC) and 'Forward Row' (FR) recursive methods respectively (Fig. 3)

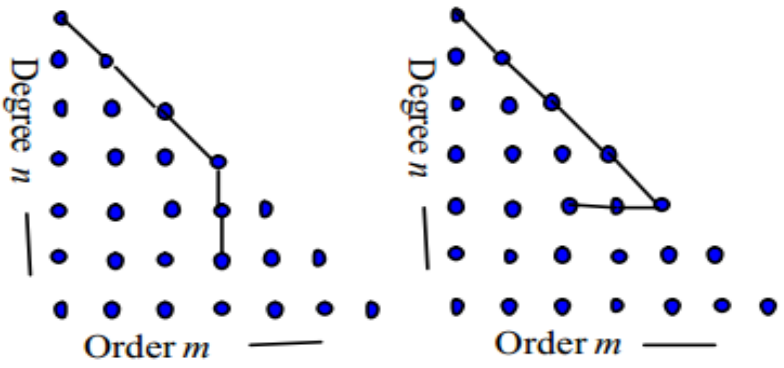

Figure 3: Row and Column Schematic Recursion of Associated Legendre Polynomial

2.4.3. Load Love Number, k_l

The use of equation 10 to recover surface mass requires knowledge of the load Love numbers, kl. The l = 0 term is proportional to the total mass of the Earth, where the Earth includes not only the solid Earth, but also its fluid envelope (the oceans, atmosphere, etc.). This total mass does not change with time, and so ΔC_{00} from GRACE can be assumed to vanish. The l = 1 terms are proportional to the position of the Earth's center of mass relative to the center of the coordinate system and so depend on how the coordinate system is chosen. One possibility is to choose a system where the origin always coincides with the Earth's instantaneous center of mass. In that case all l = 1 terms in the geoid are zero by definition, and so the GRACE results for ΔClm = ΔSlm = 0 for all l = 1. Another possibility is to define the coordinate system so that its origin coincides with the center of figure of the Earth's solid outer surface. That is the most sensible way of defining the origin when recovering the Earth's time-variable mass distribution, since hydrological, oceanographic, and atmospheric models are invariably constructed in a system fixed to the Earth's surface. In that case the l =1 GRACE results for ΔClm =ΔSlm need not vanish, and the Love number kl=1 is defined so that the l = 1 terms in (10) describe the offset between [the center of mass of the surface mass + deformed solid Earth] and [the center of figure

of the deformed solid Earth surface]. It is shown by Trupinet al. (1992; equation (10)) that for this coordinate system $k_{l=1}$=− (hl=1+2l=1)/3, where hl=1and l=1are the l = 1 displacement Love numbers when the origin is the center of mass of the deformed solid Earth. For this choice of origin, the numerical value of kl=1=− (hl=1+2`l=1)/3 is given in Table 1.

Table 1: Elastic Love Numbers, kl Computed by Dazhong Han as described by Han and Wahr (1995), for Earth Model PREM (Dziewonski and Anderson, 1981) (adopted from Wahr et al. 2007).

l	K_l
0	0.000
1	0.027
2	-0.303
3	-0.194
4	-0.132
5	-0.104
6	-0.089
7	-0.081
8	-0.076
9	-0.072
10	-0.069
12	-0.064
15	-0.058
20	-0.051
30	-0.040
40	-0.033
50	-0.027
70	-0.020
100	-0.014
150	-0.010
200	-0.007

2.4.4. Smoothing

The unphysical striping error pattern, seen in typical monthly solutions of the GRACE project when geoid or surface mass anomaly maps are constructed, can be understood as an

individual realization of a noise process with a spatially distinct correlation (Kusche et al., 2009). Errors in the GRACE derived spherical harmonic coefficients become large for large l (i.e. short scales), and because terms with large l values can make important contributions to the sum in (10) (note the 2l+1 factor in the numerator of (10)), the use of (10) as written can lead to highly inaccurate results (Wahr et al., 1998), see Figure 3. To obtain accurate results it is necessary to somehow reduce the large-l contributions to the sum (10). This involves the insertion of some additional multiplicative factor into (10) that is small for large values of l. Figure 3 shows the TWS derived from unsmoothed GRACE spherical harmonic coefficients.

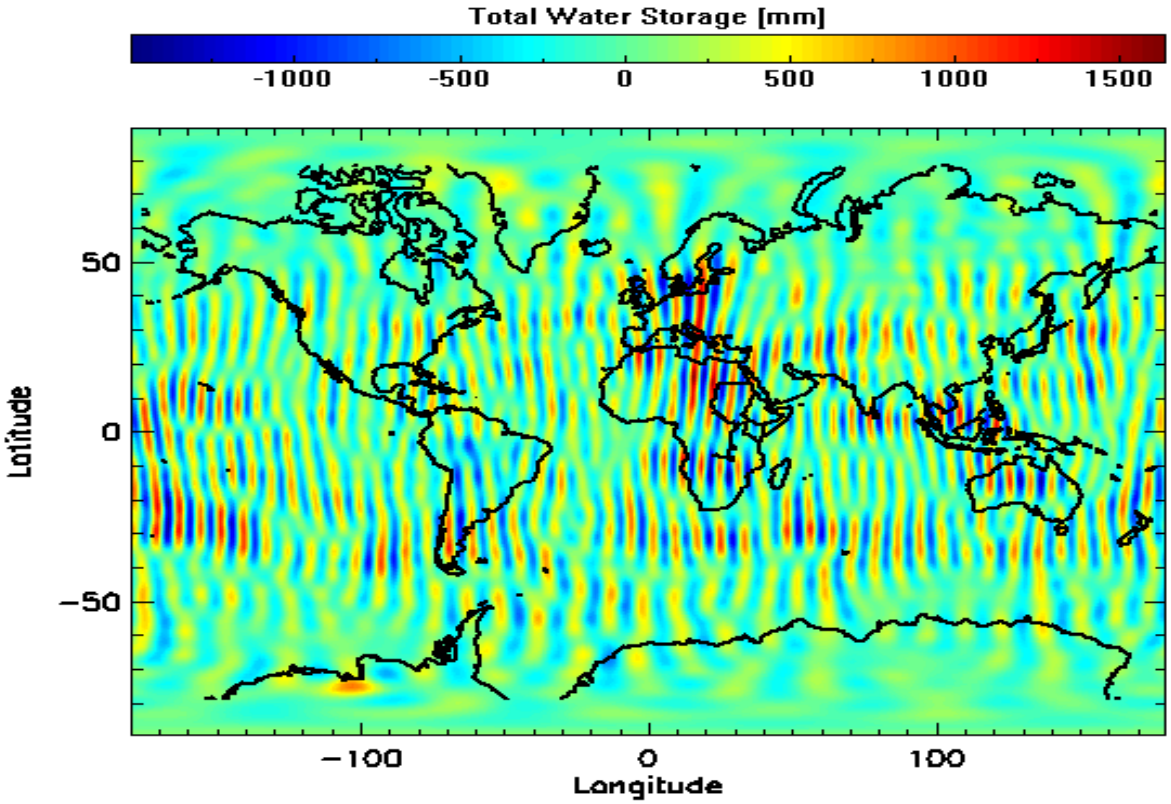

Figure 4: Unfiltered Global GRACE-TWS for December 2006 (computed by Equation 10)

A variety of methods have been devised and used for improving the GRACE mass estimates in this way, some among them are Wahr, et al., 1998; Swenson and Wahr, 2002; Swensonet al., 2003; Seo and Wilson, 2005; Chen et al., 2006; Han et al., 2005, Swenson and

Wahr, 2006, Kusche, 2009 and Zhang et al., 2009. These methods fall into one of two categories as most of them are similar to one another: smoothing the surface mass results or averaging over specific regions (Wahr et al., 2007). Here, we discuss about two methods from the first group, which are employed in this study of the first category only, Gaussian Smoothing and Different Degree Kusche (DDK) smoothing.

A) Gaussian Smoothing

Gaussian smoothing is the simplest way of modifying equation 10 to obtain accurate results, is to introduce degree-dependent weighting factors W_l into the sum, so that

$$\overline{\Delta\sigma}(\theta,\varphi) = \frac{a\rho_{ave}}{3}\sum_{l=0}^{\infty}\sum_{m=0}^{l}\frac{2l+1}{1+k_l}W_l\tilde{P}_{lm}(cos\theta)(\Delta C_{lm}\,cos(m\varphi) + \Delta S_{lm}\,sin(m\varphi)\,, \qquad 19$$

where $\overline{\Delta\sigma}$ is the smoothed version of surface mass anomaly.

A convenient choice of smoothing coefficients is the use of Gaussian values developed by Jekeli (1981) to improve estimates of the Earth's gravity field (Wahr et al., 1998). Those coefficients can be found using the recursion relations.

$$W_o = 1 \qquad 20$$

$$W_1 = \frac{1+e^{-2b}}{1-e^{-2b}} - \frac{1}{b} \qquad 21$$

These coefficients correspond to a smoothing function

$$W(\alpha) = \frac{bexp[-b(1-cos\,\alpha)]}{1-e^{-2b}} \qquad 23$$

$$b = \frac{ln\,(2)}{\left(1 - cos\,(\frac{r}{a})\right)} \qquad 24$$

and r is the distance on the Earth's surface at which W has decreased to 1/2 its value at α = 0 (the distance on the Earth's surface = aα). When data mapped shown in Fig.3 is smoothed with this method, the improvement looks like shown in Fig. 4.

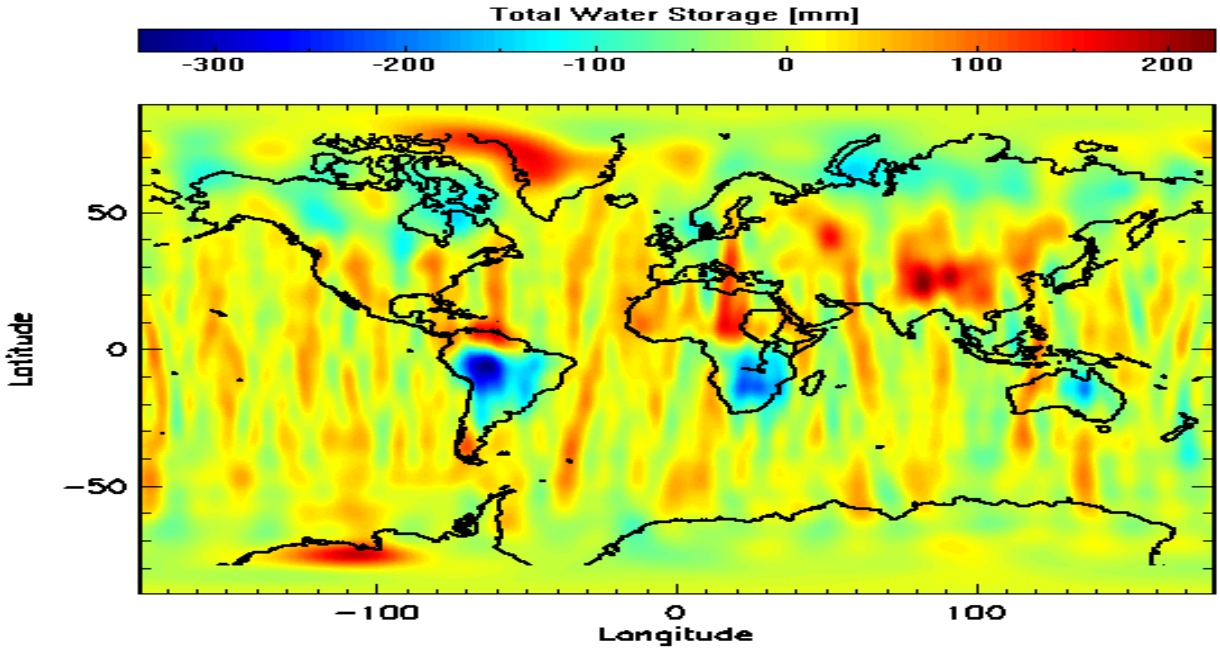

Figure 5: Global GRACE derived TWS Map after Gaussian Smoothing is applied (the smoothing radius is 450 Km).

B) DDK Smoothing

This method was devised by J. Kusche in 2007. The method was originally based on computing and applying a filter matrix with as many rows and columns as there are spherical harmonic coefficients (Kusche, 2007). In this method with smoothing parameter a, each spherical harmonic coefficient ($\sigma_{lmq} = c_{lm}^{\sigma} for\ q = 0\ and\ \sigma_{lmq} = s_{lm}^{\sigma}\ for\ q = 1$) of the surface

mass anomaly σ (λ, θ) (or any other functional of gravity change) is decorrelated and smoothed in the following way.

$$\sigma_{lmq}^{filt} = \sum_{l'=l_{min}}^{lmax} \sum_{m'=0}^{l'} \sum_{q'=0}^{1} w_{lmq}^{l'm'q'}(a)\sigma_{l'm'q'} \qquad 25$$

Kusche methods (DDK1, DDK2 and DDK3) filtered GRACE spherical harmonic coefficients data can be obtained from official distributors of the GRACE data.

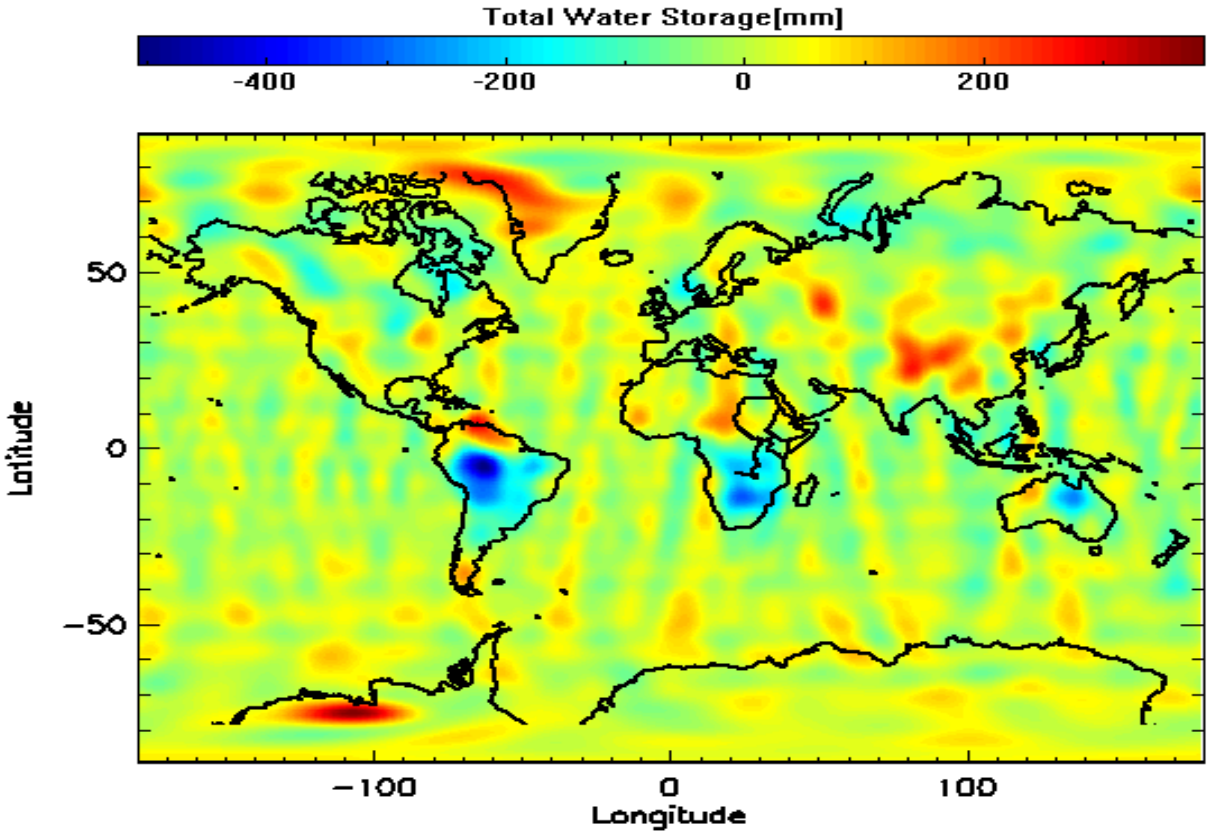

Figure 6: Global GRACE derived Total Water Storage Map of December 2006 after DDK3 Smoothing is applied

2.5. Remote Sensing of Rainfall-TRMM

TRMM, a joint USA/Japan satellite mission designed to survey the rain structure, rate and distribution in tropical and subtropical regions (latitude range ± 50°). It was launched in November, 1997 and has a circular orbit of altitude 400 km and inclination angle of 35˚ (Huffman and Bolvin, 2012; Huffman et al., 2007; Kummerow et al., 1998; Kummerow et al., 2000; Simpson et al., 1988). In its rainfall measuring package, TRMM has three instruments; Precipitation Radar (PR), Microwave Imager (MI), and Visible and Infrared Scanner (VlRS). The mission aims at monitoring tropical and sub-tropical amount of rainfall, rain profiles, and brightness temperature (Kummerow et al., 1998).

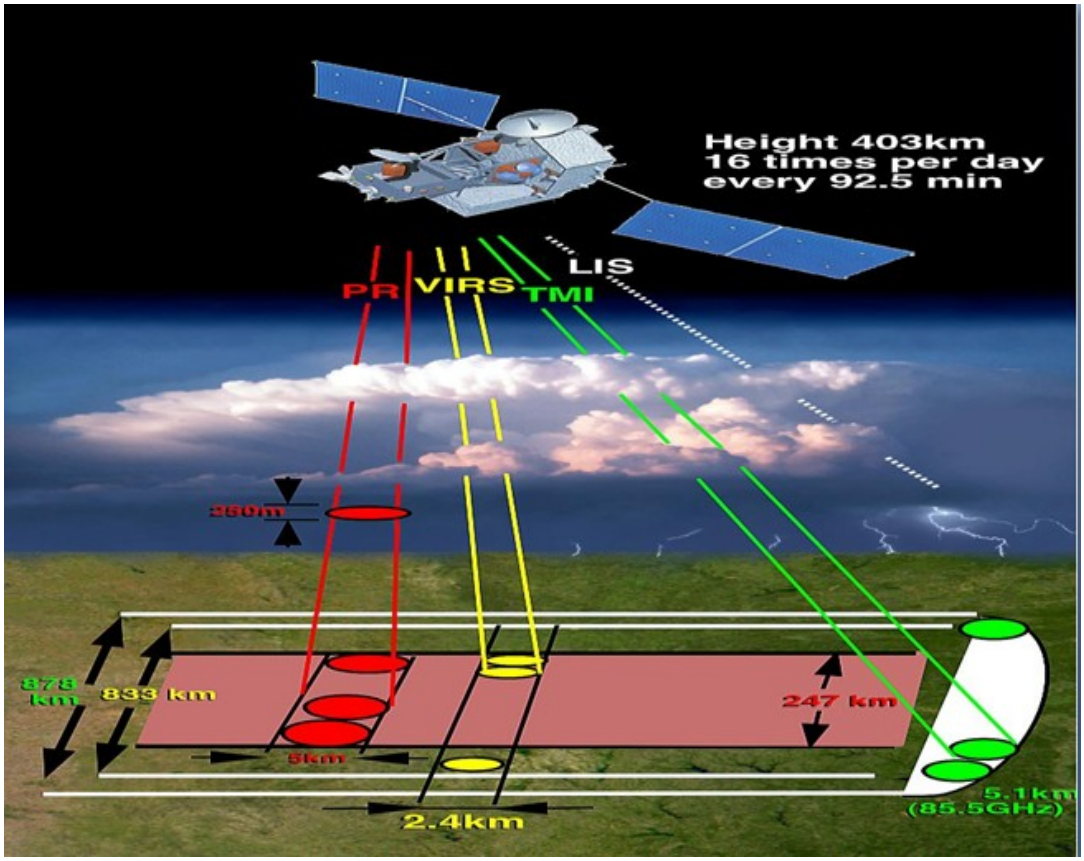

Figure 7: Tropical Rainfall Measuring Mission Satellite

2.5.1. TRMM Multi-Satellite Precipitation Analysis (TMPA)

The TMPA depends on input from two different types of satellite sensors, namely microwave and IR. First, precipitation-related microwave data are being collected by a variety of low earth orbiting (LEO) satellites, including the TRMM Microwave Imager (TMI) on TRMM, Special Sensor Microwave/Imager (SSM/I) and Special Sensor Microwave Imager/Sounder (SSMIS) on Defense Meteorological Satellite Program (DMSP) satellites, Advanced Microwave Scanning Radiometer for the Earth Observing System (AMSR-E) on Aqua, the Advanced Microwave Sounding Unit (AMSU) on the National Oceanic and Atmospheric Administration (NOAA) satellite series, and the Microwave Humidity Sounders (MHS) on later NOAA-series satellites and the European Operational Meteorological (MetOp) satellite (Huffman et al., 2009).

2.5.2. TRMM Precipitation Retrieval Algorithm

The TMPA product is computed in four stages; (1) the microwave precipitation estimates are inter-calibrated and combined, (2) IR precipitation estimates are created using the calibrated microwave precipitation, (3) the microwave and IR estimates are combined, and (4) rain gauge data are integrated. The real-time TMPA lacks the fourth step and has a few simplifications (Huffman et al., 2009). The TRMM-3B42 is one of the TMPA products developed with the aim to provide high quality satellite rainfall estimates. The data includes retrieval from six different sources: VIRS, TMI, PR and combination with other satellites (GPI, GPCP and SSMM).

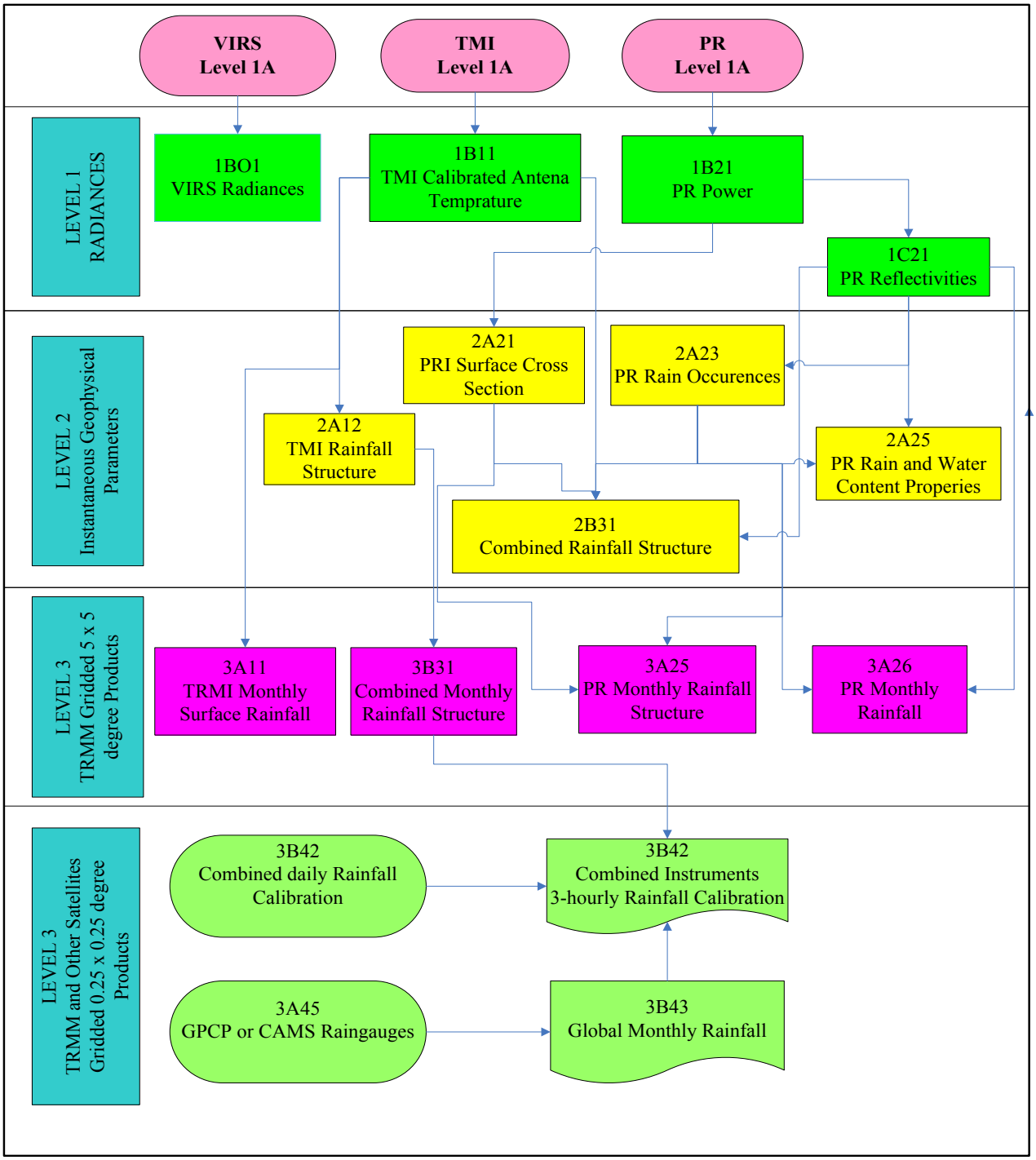

Figure 8: TRMM Rainfall Estimation Algorithm (Adopted from TRMM V6 Data Processing Overview Manual)

2.6. Global Land Surface Models

2.6.1. Development of Land Surface Model

Table 2: Land Surface Model development Chronology

Generation	Starting period	Description
Gen-0	Prior to 60s	Lack of land-surface processes (prescribed diurnal cycle of surface temperature)
Gen-1a	Mid 60s	Surface model with time fixed soil moisture
Gen-1b	Late 60s	Bucket Model (Manabe, 1969): time- and space-varying soil moisture
Gen-2	70s	Big-leaf model (Deardorff, 1978): explicit vegetation treatment, major milestone
Gen-3	Late 80s	Development of more sophisticated models including hydrological, biophysical, biochemical and ecological processes (e.g., BATS, SiB, NCARLSM, Century)
	Mid 90s	Implementation of advanced LSMs at major operational numerical weather prediction (NWP) centers.

2.6.2. Global Land Data Assimilation System (GLDAS)

GLDAS model is developed jointly by NASA Goddard Space Flight Center (GSFC), the National Oceanic and Atmospheric Administration (NOAA), and National Centers for Environmental Prediction (NCEP) (Rodell et al., 2004). It drives multiple offline (not coupled to the atmosphere) land surface models that integrate huge quantities of observation based data. GLDAS executes its outputs globally at relatively high spatial resolutions ranging from 2.5° to 0.01^0 with temporal resolution ranging from 3-hourly to monthly enabled by the Land Information System (LIS) (Fang et al., 2009). There are four different land surface models (LSM) in the system: MOSAIC model, National Centers for Environmental Prediction/Oregon State University/Air Force/Hydrologic Research Lab Model (NOAH) model, the Community Land Model (CLM), and the Variable Infiltration Capacity (VIC) (Rui, 2011). Here, we only discuss the

model we used in this study, NOAH model. A key input into the NOAH LSM includes land-use (vegetation) type, soil texture and slope, while other secondary parameters can be specified as function of the three primary parameters. The NOAH LSM structure is as shown in Fig 8.

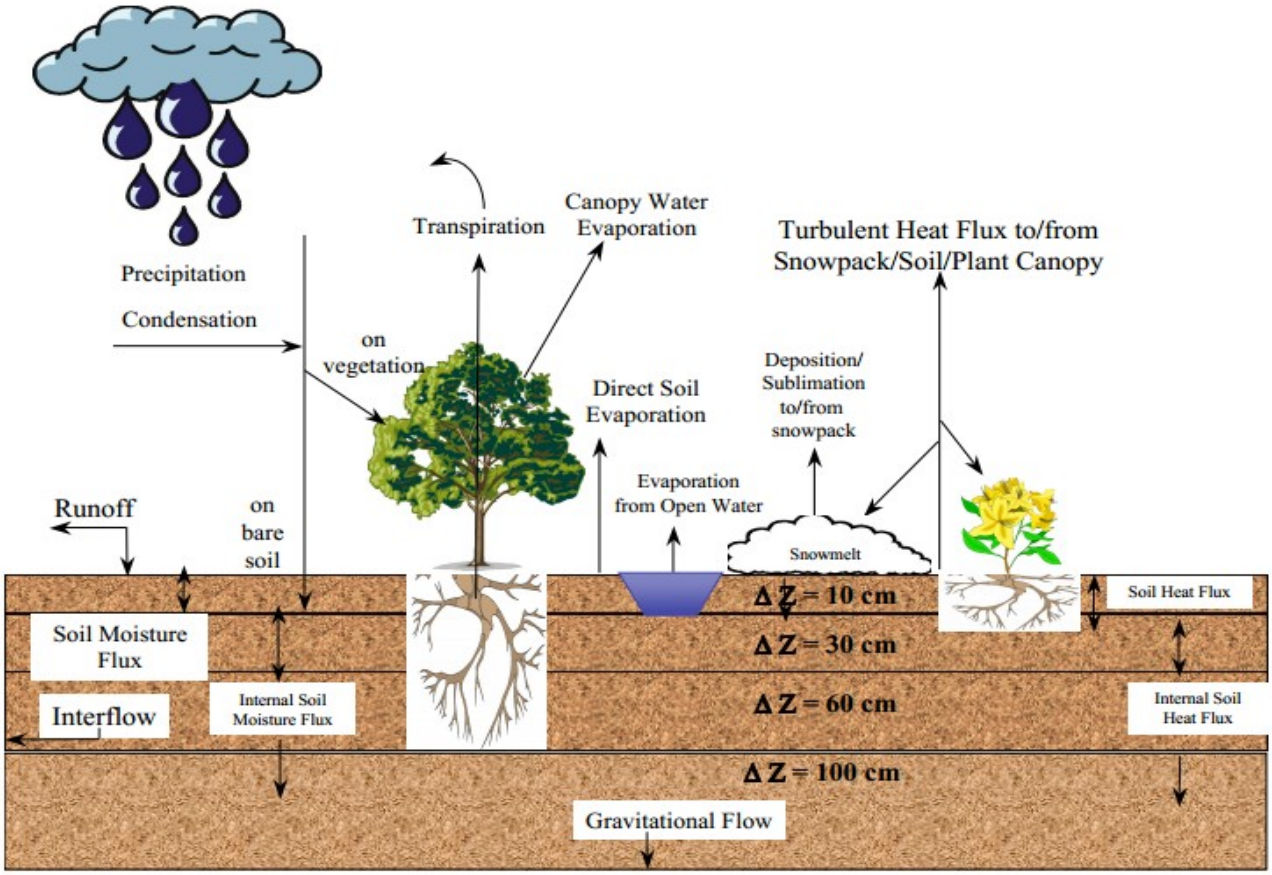

Figure 9: NOAH LSM model structure

2.6.3. GLDAS- Soil Moisture

The soil moisture data from GLDAS is available up to 2 m below the earth surface. On its computation they recommended that each succeeding soil layer downward should not exceed three times the thickness of soil layer above it. Based on this concept the NOAH LSM has four common layers configured as 0.1 m (Layer 1), 0.3 m (Layer 2), 0.6 m (Layer 3) and 1.0 m (Layer 4), see Fig. 8. The physical equation (Richards's equation for soil water movement (Equation FFF)) in LSM predicts the soil moisture at midpoint of each model soil layer.

$$\frac{\partial \theta}{\partial t} = \frac{\partial}{\partial z}\left(D\frac{\partial \theta}{\partial z}\right) + \frac{\partial K}{\partial z} + F_\theta \qquad 24$$

Where D, K functions (soil texture, soil moisture), F_Θ represents source (rainfall) and sinks (evaporation)

The results shown below are global maps of soil moisture derived by NOAH LSM in kg/m2 for each layers.

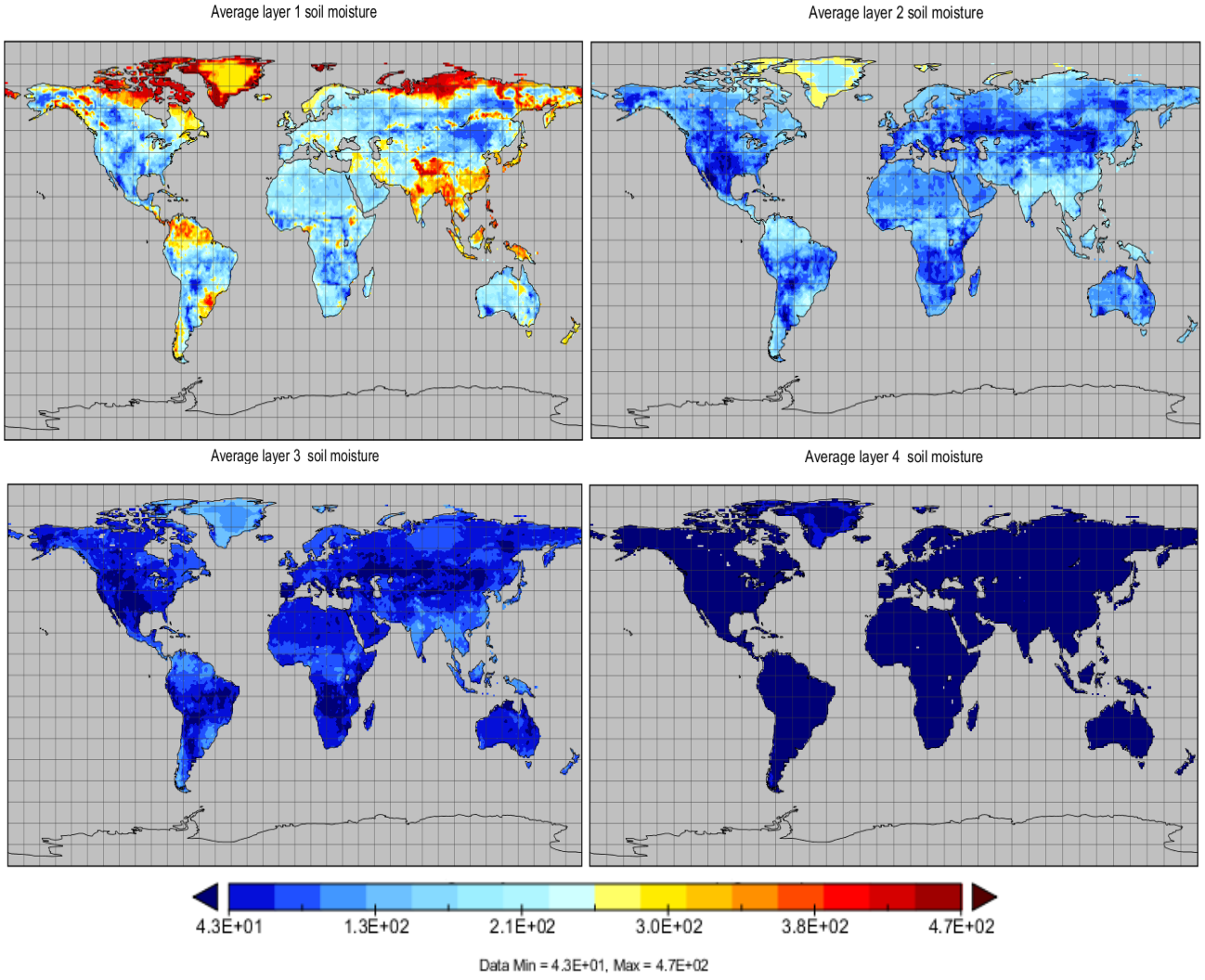

Figure 10: Four Layers of Soil Moisture for August 2011

2.7. Principal Component Analysis

2.7.1. Theory of PCA

Principal component analysis (PCA) is a multivariate technique that analyzes a data table in which observations are described by several inter-correlated quantitative dependent variables. It is one of a family of techniques for taking high-dimensional data, and using the dependencies between the variables to represent it in a more tractable, lower-dimensional form, without losing too much information. The goals of PCA are to (i) extract the most important information from the data table, (ii) compress the size of the data set by keeping only this important information, (iii) simplify the description of the data set, and (iv) analyze the structure of the observations and the variables. In order to achieve these goals, PCA computes new variables called principal components which are obtained as linear combinations of the original variables. To have the largest possible variance, i.e., inertia and therefore this component will 'explain' or 'extract' the largest part of the inertia of the data table. The second component is computed under the constraint of being orthogonal to the first component and to have the largest possible inertia.

2.7.2. Derivation of Principal Components

Suppose that x is a vector of p random variables, and that the variances of the p random variables and the structure of the covariances or correlations between the p variables are of interest. Unless p is small, or the structure is very simple, it will often not be very helpful to simply look at the p variances and all of the ½ p (p−1) correlations or covariances. An alternative approach is to look for a few (p) derived variables that pre-serve most of the information given by these variances and correlations or covariances. Although PCA does not ignore covariances and correlations, it concentrates on variances. The first step is to look for a linear function α1xof

the elements of x having maximum variance, whereα_1 is a vector of p constants α_{11}, α_{12},..., α_{1p},and denotes transpose, so that

$$\alpha_1' x = \alpha_{11}x_1 + \alpha_{12}x_2 + \cdots + \alpha_{1p}x_p = \sum_{j=1}^{p} \alpha_{1j}x_j \qquad 25$$

Next, look for a linear function α_2x, uncorrelated with α_1x having maximum variance, and so on, so that at the k^{th} stage a linear function α_kx is found that has maximum variance subject to being uncorrelated with α_1x, α_2x,...,α_{k-1}x.The k^{th} derived variable, α_kx is the k^{th} PC. Up to p PCs could be found, but it is hoped, in general, that most of the variation in x will be accounted for by m PCs, where $m \ll p$.

CHAPTER THREE

MATERIAL AND METHODS

3.1. Description of Study Area

Ethiopia is a landlocked country bounded by Eritrea (N), South Sudan (SW), Sudan (NW), Kenya (S), Somalia (E) and Djibouti (NE). Geographically it is located between latitudes $3^0$15' N to 15^0 N and longitudes 33^0 E to 48^0 E, with a surface area of 1,127,127 km^2. The altitude ranges from nearly 120 m below mean sea level in the Dallol depression to ~4620 m above mean sea level at mount Ras Dashen. The country has three major physiographic regions, including the western highlands and associated lowlands, the eastern highlands and associated lowlands, and the rift valley in between, running from north-east to south-west separating the eastern and western highlands (Fig.12). It is because of these physiographic influences on the drainage systems that Ethiopia is counted as the water tower of East Africa. The country has 12 major basins, eight of which are River basins, one is Lake basin and the remaining three are dry basins with no or insignificant out flow (FAO, 2005). All emanates in the central highlands except Aysha and Ogaden, which are totally located in the lowlands.

Ethiopia contributes to three major drainage systems, the Mediterranean Sea drainage system (Abbay, Baro-Akobo, Mereb and Tekeze), the Great East African Rift-valley drainage system (Omo-Ghibe, Awash, Rift-valley Lakes, Denakil and Aysha) and the Indian Ocean drainage system (Genale-Dawa, Wabishebelle and Ogaden) (Fig. 11). The total annual runoff of the country is estimated to be 122 BCM (MoW, 1999). Groundwater resources of Ethiopia and its distribution vary depending on the geologic, structural and climatic setups. With regard to the groundwater potential, there is no agreed figure yet, the values vary from 2.6 to hundreds of

BCM (Alemayehu, 2006; Kebede, 2012). The near surface geological pattern that mainly govern hydrogeological characteristics of the country constitutes oldest basement rocks (18%), paleozoic and mesozoic sedimentary rocks (25%), tertiary volcanic (40%), and quaternary sediments and volcanic (17%) (Alemayehu, 2006).

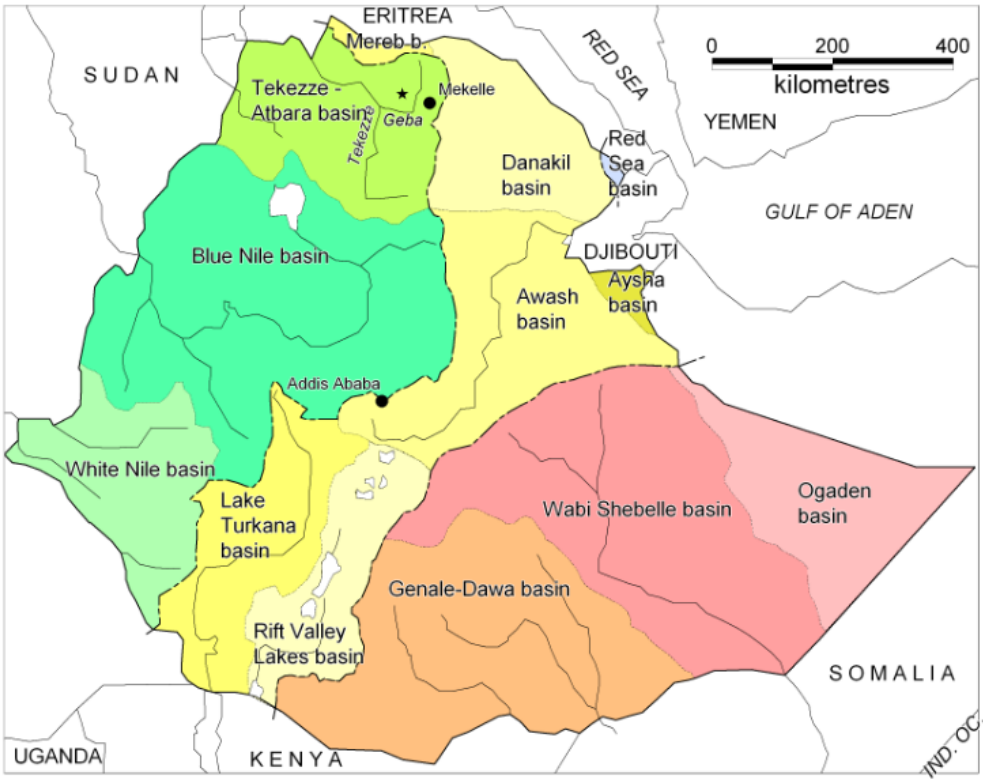

Figure 11: Major drainage basins in Ethiopia. The bold dashed line (— —) represents major water divides between the Mediterranean Sea basin (west), the Rift Valley endorheic basins (centre), and Indian Ocean basin (east), Figure adopted from Nyssen et al. (2010) with permission from the lead author.

In Ethiopia, there are tremendous diversities of climatic, biophysical and socio-economic settings (MoW, 2002). The climate ranges from equatorial rainforest in the south and southwest, which is characterized by high rainfall and humidity to afro-alpine on the summits of the Semien

(western highlands) and Bale (eastern highlands) mountains to desert like conditions of the Northeast, East and Southeast lowlands. The temperature ranges from ~60^0 C at Dallol depression to a freezing temperature in the mount Ras Dashen Plateau (MoW, 2012). The mean annual rainfall varies from ~3000 mm at Masha in the western highlands to barely 200 mm in the eastern lowlands (Engida and Esteves, 2011; Romilly and Gebremichael, 2011; Seleshi and Zanke, 2004). The mean annual evapotranspiration of the country ranges from 1300 mm to 1800 mm (MoW, 2012).

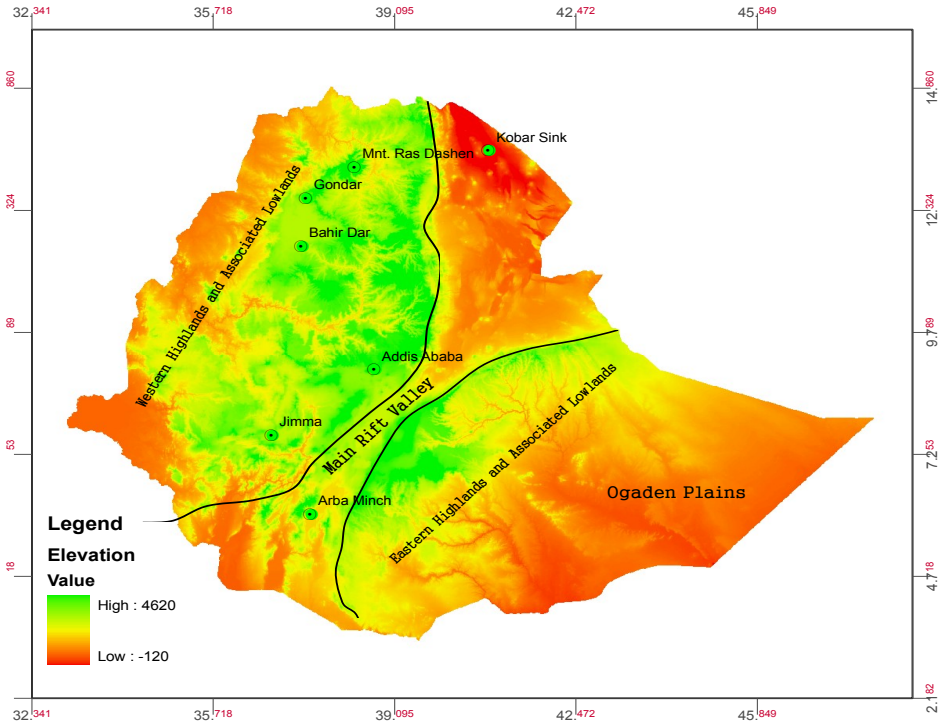

Figure 12: Physiographic regions of Ethiopia (Source: modified from Chernet, 1993)

3.2. Data

3.2.1. Gravity Recovery And Climate Experiment (GRACE)

The GRACE satellite gravimetry mission has been one of the most commonly exploited satellite in the past decade for computing TWS and proved to have the capacity to remotely sense

water storage changes at regional and global scale. For instance, changes in TWS and drought characterization have been reported, (see, e.g., Awange et al., 2011; Awange et al., 2007; Chen et al., 2010; Crowley et al., 2006; Crowley et al., 2008; Forootan et al., 2012; Rodell et al., 2007; Strassberg et al., 2009; Yirdaw et al., 2008). Yeh et al. (2006) studied groundwater storage changes in Illinois using GRACE and reported that GRACE-based method of estimating monthly to seasonal groundwater storage changes performs reasonably well at a basin size of better than 200,000 km^2. The potential for using GRACE gravity measurements to monitor TWS over large semiarid regions subjected to intense irrigation is also shown e.g., see, Strassberg et al., (2009).

This study used GRACE Level-2 data set, which consists of the processed time-variable gravity field products (Flechtner, 2007). The Level-2 products are provided as sets of spherical harmonics averaged on certain time periods (usually monthly). There are three official institutions responsible for providing the gravity field data, while each having their own modeling approaches and sometimes using different background models. The centers are University of Texas, Center for Space Research (CSR), University of California, Jet Propulsion Laboratory (JPL) and German Research Centre for Geosciences (GFZ). The Release 04 of gravity solution data from CSR which is reported as the most downloaded products was used in this study.

GRACE level-2 spherical harmonics at high degrees are affected by correlated noise (Kusche, 2007; Kusche et al., 2009). To reduce the errors present in short wave-length, known as striping pattern in spatial domain, they need to be smoothed before being used for hydrological analysis. Here, GRACE monthly solutions were smoothed using Kusche et al. (2009)'s DDK3 filter. The data are available from the official website of the International Centre for Global Earth

Models (ICGEM) [1] . The suitability of the DDK filter for hydrological studies is discussed in (e.g., Werth et al., 2009). Our investigations cover the period from January, 2003 to December, 2010 using 96 months of GRACE RL04 products.

3.2.2. Global Land Data Assimilation System (GLDAS)

GLDAS executes its outputs globally at relatively high spatial resolutions ranging from 2.5° to 0.01^0 with temporal resolution ranging from 3-hourly to monthly enabled by the Land Information System (LIS) (Fang et al., 2009). The parameters in GLDAS-monthly data falls into three main categories: water balance (WB), energy balance (EB), and forcing parameters. WB includes the important soil moisture parameter and other water related variables, such as rainfall rate and surface runoff. EB has surface temperature and heat fluxes. To investigate the spatial and temporal variation of soil moisture over Ethiopia, we used the WB monthly data generated by NOAA LSM at spatial resolution of 1^0 x 1^0. The data was obtained freely from NASA, Goddard Earth Science Data and Information Services Center (GES DISC)[2].

3.2.3. Tropical Rainfall Measuring Mission (TRMM) Satellite Rainfall

There are several versions of TRMM-3B42 products. The version used herein is version 7 data (Huffman and Bolvin, 2012), which was made available to the public on 22 May, 2012, following the end of the most recent versions (6 and 6a). The major difference between the previous versions and the one used in this study is that the later has additional gauge relative weighting in the processing of the products (Huffman and Bolvin, 2012). TRMM data used here has a fair spatial resolution of 0.25^0 x 0.25^0 and temporal resolution of 3-hour. The data was

1.http://icgem.gfz-potsdam.de/ICGEM/TimeSeries.html

2 .http://disc.sci.gsfc.nasa.gov/hydrology/data-holdings

obtained from NASA GES DISC[3]. In this study the 3-hourly rainfall rates have been converted to rainfall amount and aggregated to monthly basis.

Numerous satellite rainfall product validation studies have been carried out in different regions of Ethiopia over the past decade. For example, Dinku et al, (2007, 2008), reported validation 16 satellite products over complex terrain of Ethiopia. Hirpha et al, (2010) revealed that IR-based rainfall algorithms have major limitations in reproducing rainfall fields in mountainous regions of East Africa stating that, additional information, e.g., relative humidity and/or rain gauge data at different elevations may be needed to improve the accuracy of rainfall estimates from IR-based algorithms. Romilly and Gebremichael, (2011) also reported that in Ethiopia, the microwave-based products outperform the infrared-based product. Beyene et al. (2010) validated the NOAA rainfall product (RFE) against weather station data's all over Ethiopia and found that RFE can reasonably be used for Early warning systems. With their work on the validation of satellite product (RFE, TRMM-3B42, TRMM-3B42RT, CMORPH, GSMaP-MVK and GSMaP-MVK+) in desert locust recession region, a region which includes nearly half of Ethiopia, Dinku et al. (2010) reported that a comparison of the different products shows that no single product stands out as having the best or the worst overall performance. Based on these validations and recommendations, the present study uses only the TRMM rainfall product.

3.3. Methods

For an accuracy of a few millimeters in TWS derived from GRACE to be achieved, some studies urge that the basin sizes should be greater than 200,000 km^2(Rodell and Famiglietti, 2001; Tapley et al., 2004). On the one hand, only two of the Ethiopian basins (Abbay and

3 http://mirador.gsfc.nasa.gov/

Wabishebele) can barely fulfill this criterion. On the other hand, Ethiopian catchments exhibit very different characteristics as they are climatically and environmentally extremely heterogeneous (section 2). In this respect, computing the TWS over Ethiopia as a whole might lead to wrong conclusions, since basins averages will follow the variability of the region with dominant signal. To overcome this, Ethiopia is divided into 4^0 x 4^0 (approximately 440 km x 440 km) spatial resolution size. This enables (i) attaining the GRACE application requirements, and (ii) minimizing errors which might result from generalizing the country as a whole. This way, ten regions are obtained, whose minimum/maximum latitude and longitude, and designation to be used in this paper from now onwards are described in Table 1. The boundaries tend to fit to larger physiographic regions of Ethiopia to the extent that is possible.

Table 3: Locations and designation of the 10 (4^0 x 4^0) regions of Ethiopia.

Min Lat/Lon	**Max Lat/Lon**	**Designation**
$02^0/33^0$	$06^0/37^0$	Region 1
$06^0/33^0$	$10^0/37^0$	Region 2
$10^0/33^0$	$14^0/37^0$	Region 3
$10^0/37^0$	$14^0/41^0$	Region 4
$06^0/37^0$	$10^0/41^0$	Region 5
$02^0/37^0$	$06^0/41^0$	Region 6
$02^0/41^0$	$06^0/45^0$	Region 7
$06^0/41^0$	$10^0/45^0$	Region 8
$10^0/41^0$	$14^0/45^0$	Region 9
$05^0/45^0$	$09^0/49^0$	Region 10

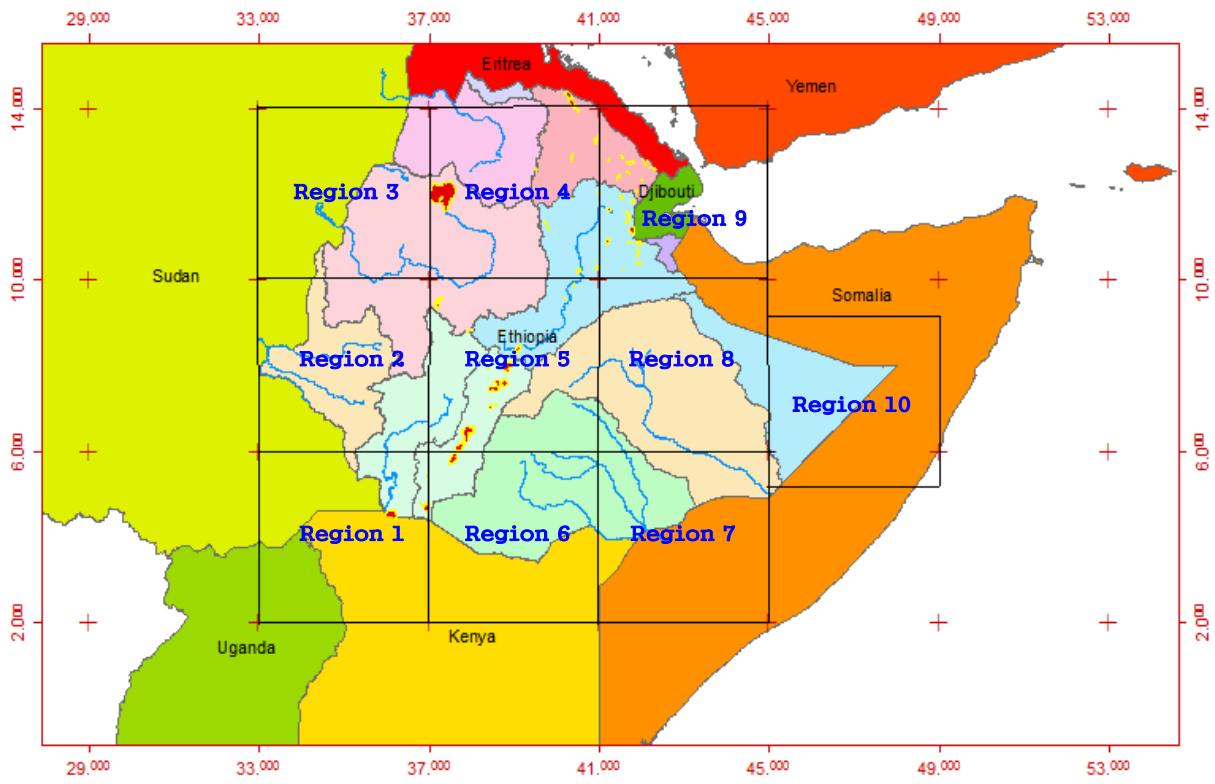

Figure 13: Ethiopia divided into ten study regions of 4^0 x 4^0 (440 Km x 440 Km) spatial resolution

3.3.1. GRACE derived TWS

Before converting the DDK3 filtered spherical harmonic coefficients, covering the period of January 2003 to December 2010, to TWS, first, the missing data of June in 2003 was filled using a linear interpolation. Then, the time-variable part of coefficients was computed by removing the long-term temporal mean of the coefficients over the period of study. The reason for removing the mean field is that it is dominated by the static component of the gravity field (Awange et al., 2007; Wahr, 2007). Finally, to convert the derivatives to TWS approach presented in Wahr et al. (1998) was adopted. For the entire 10 regions TWS data at 1^0 x 1^0 spatial resolutions, were generated at monthly temporal resolution over the study period.

3.3.2. GLDAS- Soil Moisture and TRMM-Rainfall

The monthly NOAA LSM WB data (soil moisture) was obtained at spatial resolution of 1^0 x 1^0, while the rainfall data over Ethiopia was acquired from TRMM satellite at spatial 0.25^0 x 0.25^0 and 3 hours temporal resolutions. As mentioned in section 3.2 these parameters were aggregated to 4^0 x 4^0 spatial and monthly temporal resolutions. Aggregating soil moisture or rainfall over a large areas (e.g., 4^0 x 4^0 regions considered in this study) that differ in climatic characteristics, vegetation types, and soil types could lead to possible over or under estimation. Also these parameters are used with GRACE satellite product, which cannot be down scaled to an area less than 4^0x4^0. Therefore, to be used in this study, while considering the problems mentioned as the downside, both data are aggregated spatially and temporally for the regions of interest over the study period.

3.3.3. Changes in Groundwater derived from GRACE and GLDAS

The most important variables to use when driving groundwater storage changes (ΔGWS) from derived GRACE ΔTWS data are; (i) changes in surface water storages (lakes or reservoirs) (ΔSWS), (ii) changes in soil moisture (ΔSM) and (iii) changes in snow water equivalent (ΔSWE). When compared to the land surface only about 0.7% of Ethiopia is covered by water bodies (MOWR, 2002). Winter et al., (1998) stated that surface water is often described as an intersection of the water table with the land surface. Adopting that view Rodell et al., (2007) suggests that it might be appropriate to neglect the surface water mass variability, given that the technique described supposes groundwater to be spatially continuous across the region of interest, and it would effectively eliminate surface water variations as a source of error. In addition to that, for instance, the largest surface water storage in the country (Lake Tana) which is located in region 4 (Fig. 1) has an area of 3,156 km^2, and accounts for about 1.6% of region 4.

Therefore, for studies of large spatial domains the surface water storage changes in Ethiopia can be neglected, while the snow water equivalent is negligible in Ethiopia. Soil moisture anomalies are computed by removing the long-term temporal mean of the monthly available soil moisture values. Then the monthly groundwater anomaly (ΔGWS) is obtained by subtracting the changes in soil moisture from TWS changes (Equation 26).

$$\Delta GWS = \Delta TWS - \Delta SM\,, \qquad 26$$

Where, ΔGWS is the Groundwater Storage anomaly, ΔTWS is TWS anomaly, and ΔSM is the Soil Moisture storage anomaly.

3.3.4. Total Water Storage Duration Curve (TDC)

In catchment hydrology, Flow Duration Curve (FDC) is known to be a very useful tool that has competence to reflect the characteristics of a given watershed. It is a frequency distribution formed from daily/monthly stream flow data and their exceedence probability (Sawicz et al., 2011; Yadav et al., 2007; Zhang et al., 2008). The TWS duration curve (TDC) developed in this study shares the same principle with FDC. All the available TWS data (96 months) are first listed in descending order and given a rank (the maximum will take the 1 and the minimum will take the last rank). Using the ranks (m), the probability of exceedence is computed using Weibul method (Equation 27), and then TDC is obtained by plotting the TWS on the y-axis against the probability of exceedence on the x-axis.

$$\%Exceedence = \frac{m}{N+1} * 100\,\%\,, \qquad 27$$

where m is rank and N is the sample size (number of data considered in the analysis)

Like the stream flow, the higher values of TWS may be attributed to extreme rainfalls and the lower values may be subject of severe drought throughout the period of analysis. For this reason, the slope of the TDC (S_{TDC}[-]) is calculated in a range where variation is not greatly subjected to both extremes (i.e. between the 33th and 66th TWS percentiles) using Equation 28 (modified to TWS case from Sawicz et al., 2011). In this case, the slope reflects the aquifer storage size and the aquifer through flow property. The purpose of computing S_{TDC}[-] is to concentrate the information of TWS variations into a single value, so that the information for judging the water storage characteristics will be simplified.

$$S_{TDC} = \frac{TWS(33\%) - TWS(66\%)}{(66 - 33)} \quad 28$$

3.3.5. Total Storage Deficit (TSD)

Total storage deficit over Ethiopia in each regions is computed from GRACE derived TWS anomalies using the approach stated by (Yirdaw et al., 2008),

$$TSD_i = \frac{TWSA_i - Mean\_TWSA_i}{Max\_TWSA_i - Min\_TWSA_i}, \quad 29$$

where, $TWSA_i$ is the TWS Anomaly in month i, $Mean\_TWSA_i$ is the long term monthly mean of TWSA in month i, Max_TWSA_i is the maximum TWSA recorded in month i over the study period, and Min_TWSA_i is the minimum TWSA recorded in month i over the study period.

The main rationale of computing the TSD in this study is to see the possibility of reduction/increment in crop production and yield related to moisture availability.

3.3.6. Correlation Analysis

To study the lag time of water storages variation (TWS and soil moisture) response to rainfall, a correlation analysis (e.g., Chatfield, 1989) was carried out between (a) TWS and rainfall, (b) soil moisture variation and rainfall, and (c) soil moisture variation and TWS.

3.3.7. Principal Component Analysis (PCA)

The PCA method, used in this paper, works based on eigen value decomposition of the data-derived auto-covariance matrix (Preisendorfer, 1988). In principle, PCA expands the derived TWS changes, within the 10 defined regions in terms of a new set of orthogonal vectors know as (EOFs) associated with their uncorrelated temporal evolutions known as principal components (PCs) (Forootan and Kusche, 2012). The components that are shown serve as the dominant TWS behaviour over Ethiopia, while those dropped ones are most often corresponding to the lower correlation with the overall TWS changes. North et al. (1982)'s rule of thumb was used to decide on the number of the dominant components.

CHAPTER FOUR

RESULTS

The variations of TWS over Ethiopia computed from GRACE, soil moisture from GLDAS and rainfall from TRMM are summarized in Fig. 14. The lower tail of the box plot indicates the smallest observation (sample minimum), the lower end of the box shows the lower quartile (25 %), the line across the box indicates the median, the upper end of the box specify the upper quartile (75 %), and the upper tail of the plot illustrates largest observation (sample maximum). The results show that the variation of TWS is strong in the western, north western and northern regions (respectively, regions 2, 3 and 4), while the far eastern corner of the country (region 10) shows relatively less variation. Highland dominated regions of the country (regions 2, 3, 4 and 5) shows a strong variation in rainfall and soil moisture, while the lowland dominated segments (see Fig. 12) have relatively less variability.

As an independent check on the results presented in Fig. 14, the PCA method was applied on TWS, soil-moisture and precipitation time series derived for the 10 pre-described regions. Applying the (North et al., 1982)'s rule of thumb shows that for the three data sets above, only the first two components are statistically significant, which are shown in Fig. 15. The first mode of PCA on TWS (EOF1 and PC1 of TWS) is equivalent to 65.83 % of total TWS variability, with PC1 showing a dominant annual variability and EOF1 showing that region 2,3,4 and 5 are the dominant regions thus confirming the results of Fig. 14. The same statement is also true for the first mode of soil-moisture (67.4 % of variance) and rainfall (70.1 % of variance). The second modes of all the three data sets extract mostly inter-annual variability in the data. There are also some annual and intra annual variations detectable on the second modes, which are due

to the incapability of the PCA method to perfectly separate such signals (see, e.g., Forootan and Kusche, 2012).

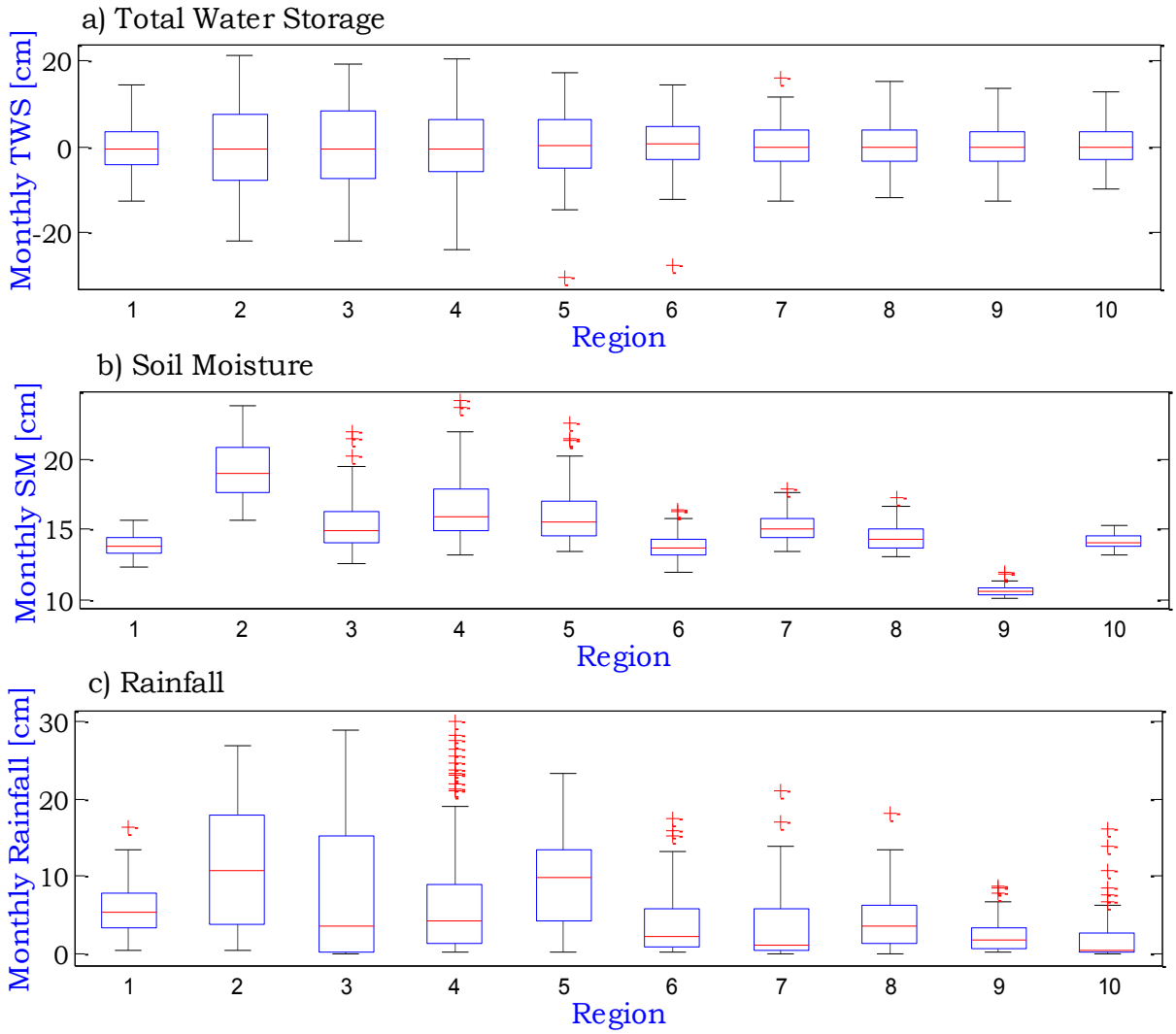

Figure 14: Summary of TWS, soil moisture and rainfall variations over Ethiopia

EOF2 and PC2 of TWS is equivalent with 14.9 % of total variance while EOF2 shows that the regions 2, 3, 6, 7, 8 and 9 are dominant. The dominant inter annual soil moisture variations are found for regions 1,2,6,7 and 8 (see EOF2 and PC2 of soil-moisture in Fig. 15, middle). Finally, the same regions of 1,2,6,7 and 8 are also found to exhibit the most inter-annual precipitation

(see EOF2 and PC2 of rainfall in Fig. 15, right). The PCA results confirm our finding shown in Fig. 14.

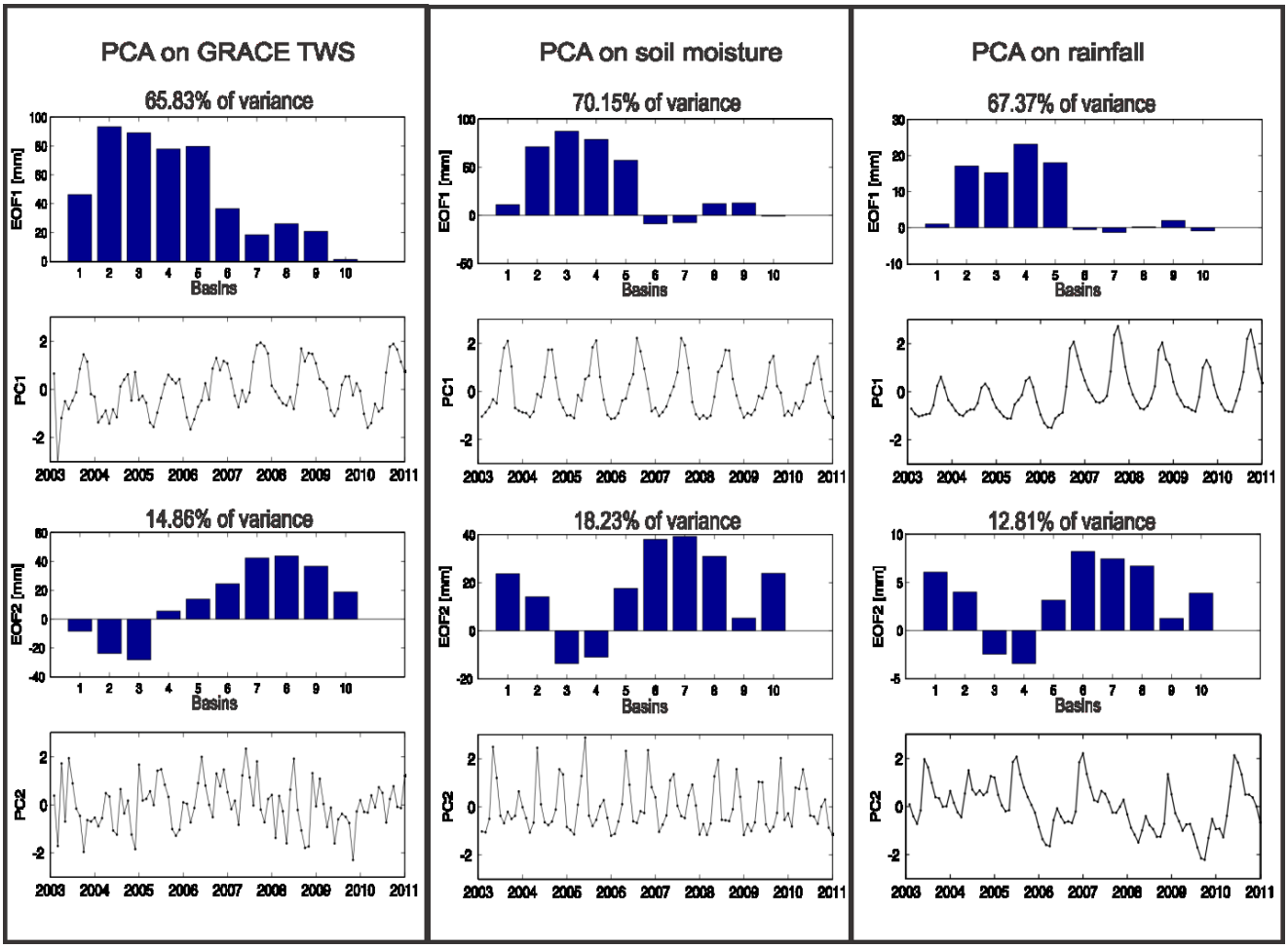

Figure 15: Results of PCA, applied on the time series of 10 predefined regions; (left) TWS data from GRACE, (middle) soil moisture data from GLDAS (right) and, (right) rainfall data from TRMM.

4.1. Annual and Seasonal Mean TWS

Figure 16 depicts the mean water mass lost /gained in cm/month aggregated at seasonal and annual time scales from monthly TWS derived from GRACE satellite using Equation 10. The annual mean indicates mass gain in the northern (region 4), central (region 5 and 8), southern (region 6 and 7) and eastern corner (region 10), while regions 1, 3, and 9 showed negative sign (Fig. 16, bottom). The results of the seasonal mean of TWS show regions 1, 2, 3, 4

and 5 having the same characteristics, where they lose water in winter and spring and gain in summer and autumn. Regions 7 and 8 reflect the same characteristics as the first group, but differ by their main losing season being winter and the gaining one being summer periods (see Fig. 16, top). The other three regions (region 6, 9 and 10) have differing characteristics from all regions. The only character that regions 6 and 10 have in common is that they obtain water mass 75 % of the time in a year, while it is 50 % for region 9. Our results, from both model and data, confirm the fact that summer is the main gaining season of Ethiopia.

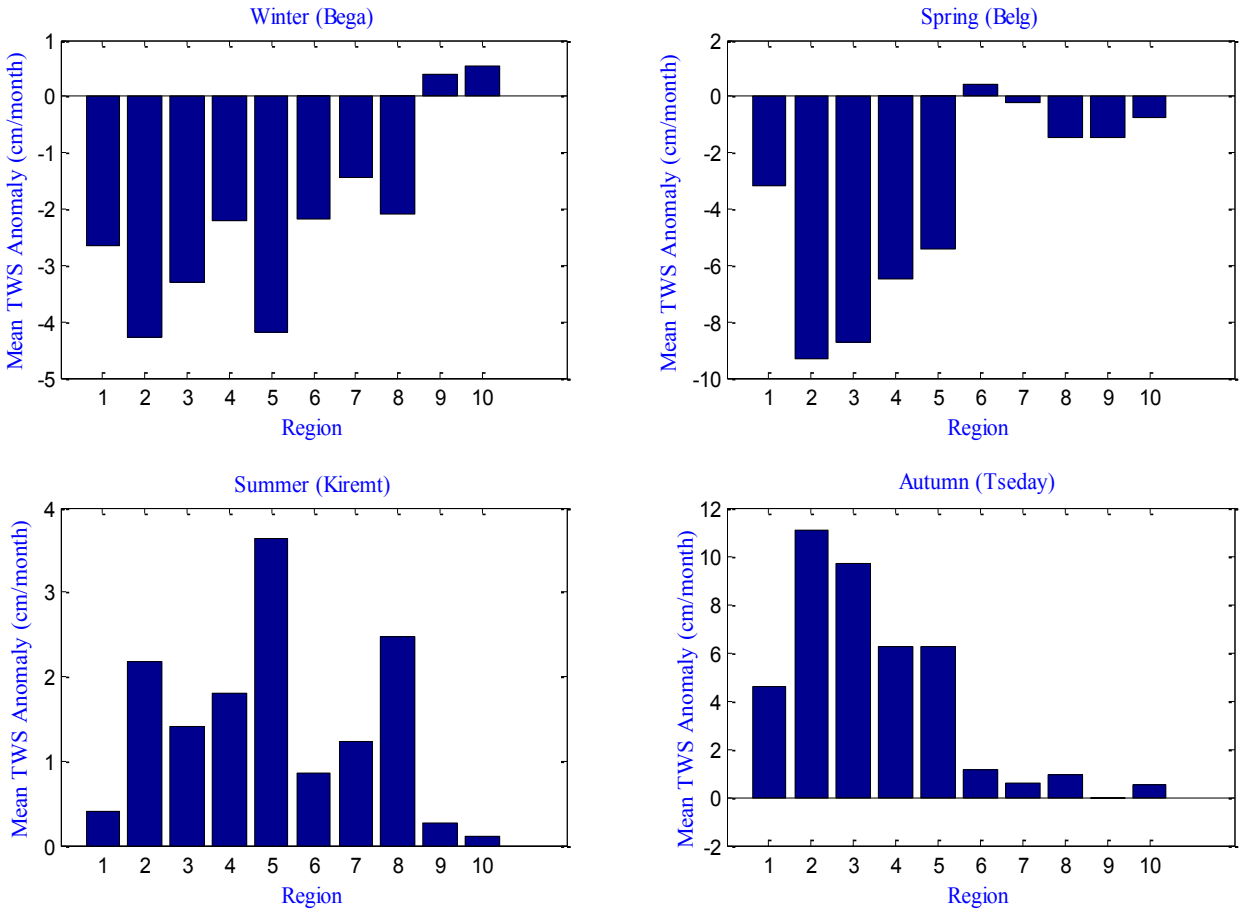

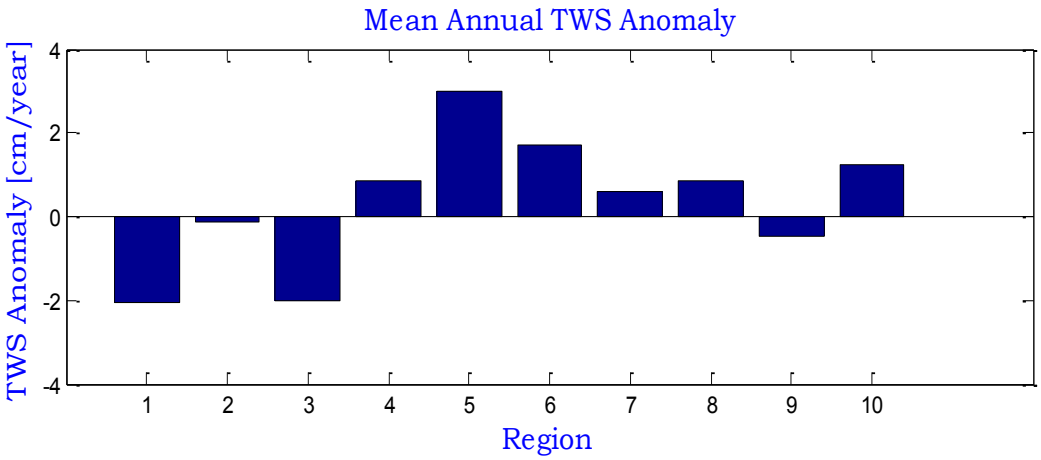

Figure 16: Seasonal (top) with Ethiopian naming for the seasons in bracket, and Annual (bottom) mean of TWS variation over Ethiopia derived from GRACE

The maximum mean annual water mass gain were recorded in region 5 in summer (Fig. 16), which may be attributed to three major facts; i) the larger part of the Rift Valley basin lakes lies in this region and there could be more of surface water influence. The Ethiopia rift valley lakes' basin (see Fig. 11) which lies in the Main Ethiopian Rift is a collection of cascade lakes which might have underground connections with other lakes. (ii) Regarding the amount of surface water, the rift lakes' valley basin is known to have closed watershed, there is water going into the lakes but have no surface water outlets (see also Chernet, 1993), and iii) the region is again the starting point for four basins that include the Awash, Omo-Ghibe, Ganale-Dawa and Wabishebele basins.

4.2. Inter-annual variation

To study the variability between years, we used the monthly TWS data derived from GRACE, soil moisture data from GLDAS and rainfall data from TRMM. The variation of TWS, soil moisture, rainfall and GWS anomaly over the study period in each month has been compiled in Fig. 17. The TWS year to year variation (Fig. 17, A) shows that except for a few months see, e.g., June (regions, 2, 4 and 9), July (regions, 7 and 8) and September (region 9) there is a

significant variation in TWS in all regions for every months. Figure 17, B also show that considerable variation in soil moisture in all months, where the variation is relatively strong in rainy seasons. The inter-annual plot of rainfall illustrated in Fig. 17, C describes that considerable variation exists in all months in regions 1 and 2, while all other regions show minor variabilities except in major rainy seasons of the country. The GWS plot (Fig. 17, D) also presents nearly same characteristics with soil moisture and TWS. As it is described above, the variation of TWS, SM and GWS anomaly is turned out to be less related to rainfall. This could be a sign that the anthropogenic effects such as land degradation, deforestation and overexploitation are contributing to the hydrologic changes in Ethiopia nearly more than the climatic factors.

For most regions (see, e.g., regions, 2, 3, 4, 5 and 6, in Fig. 17, A), the month of February seems to have the largest lower range bounding value of all months, with a minimum water loss of about 20 cm to 30 cm. This might be a sign of the propagation of drought in 2002 reported in e.g., Anderson and Choularton (2004) and Meze-Hausken (2004). Similar to the TWS, extreme depletion in groundwater storage over the study period is noticed in the western (region 2 and 3), central (region 5), northern (region 4) and southern (region 6) in February 2003, indicating that ground water storage have larger control than soil moisture over the TWS in Ethiopia.

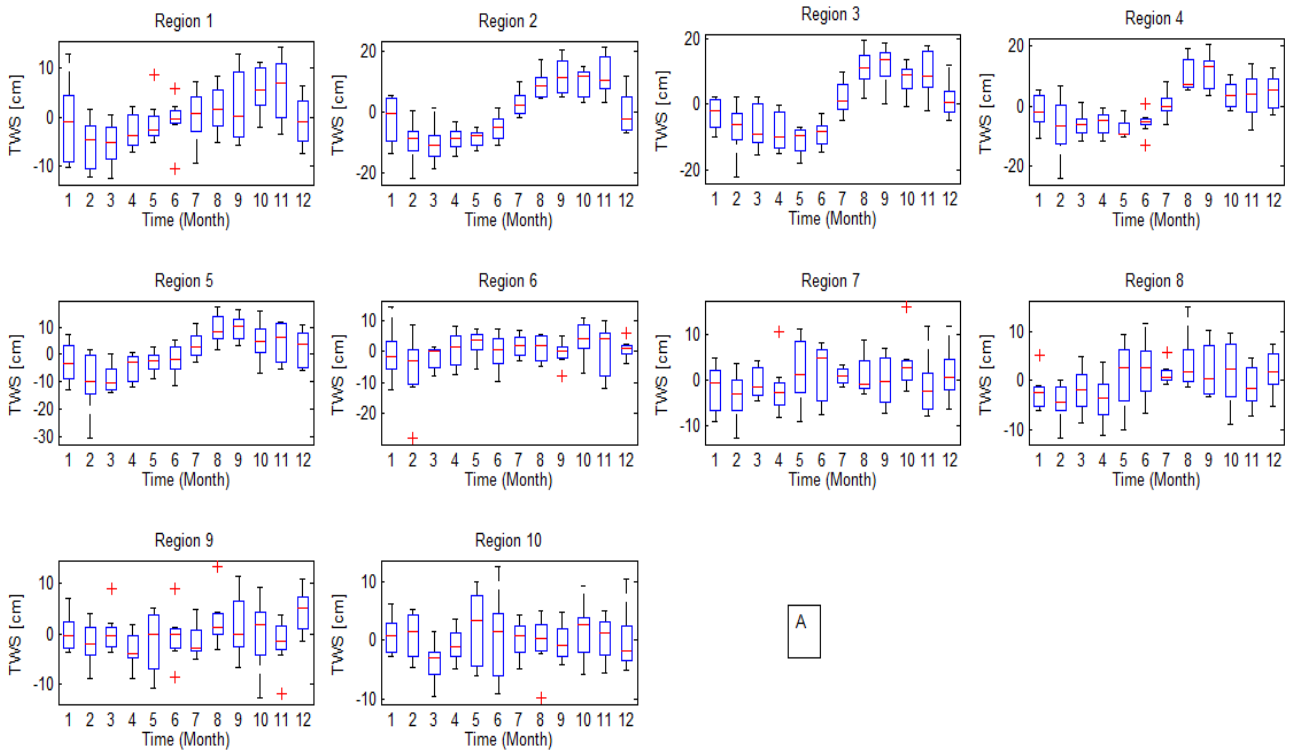
Region 1
Region 2
Region 3
Region 4
Region 5
Region 6
Region 7
Region 8
Region 9
Region 10
TWS [cm]
Time (Month)

A

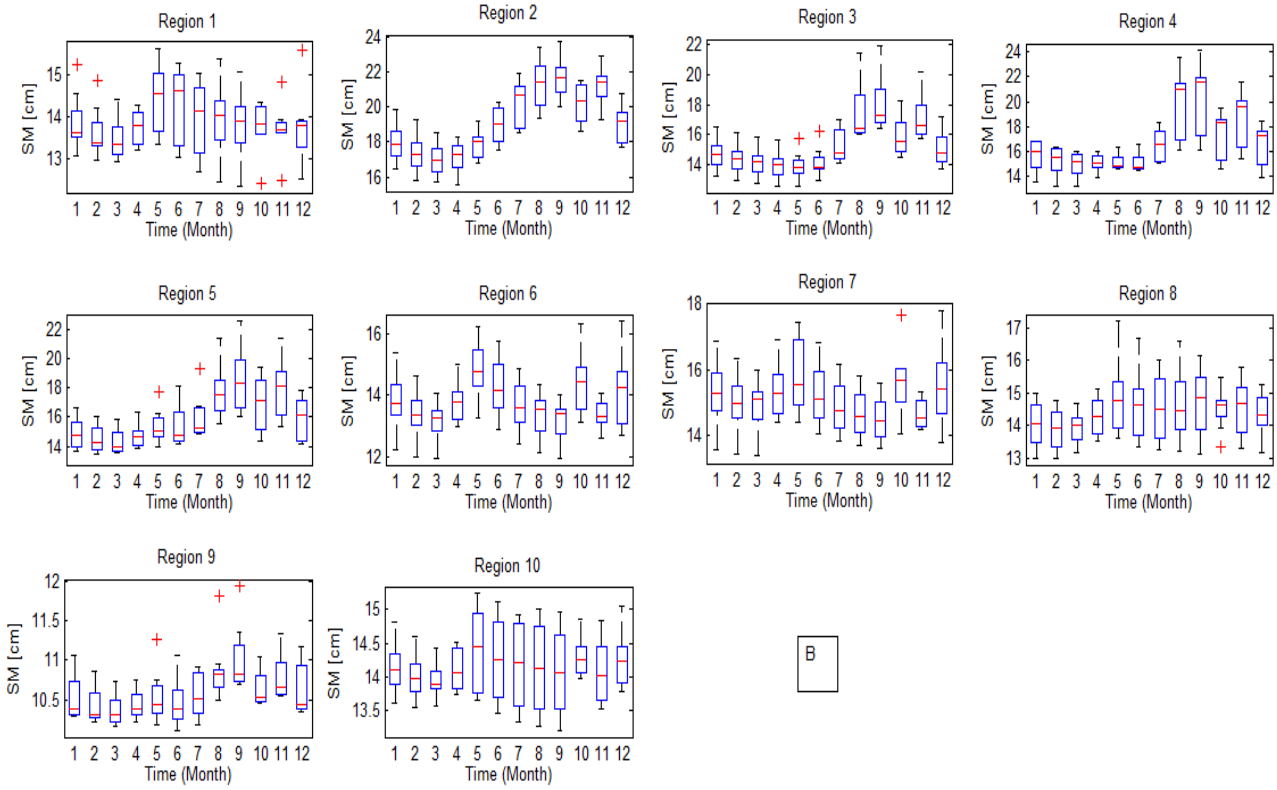
Region 1
Region 2
Region 3
Region 4
Region 5
Region 6
Region 7
Region 8
Region 9
Region 10
SM [cm]
Time (Month)

B

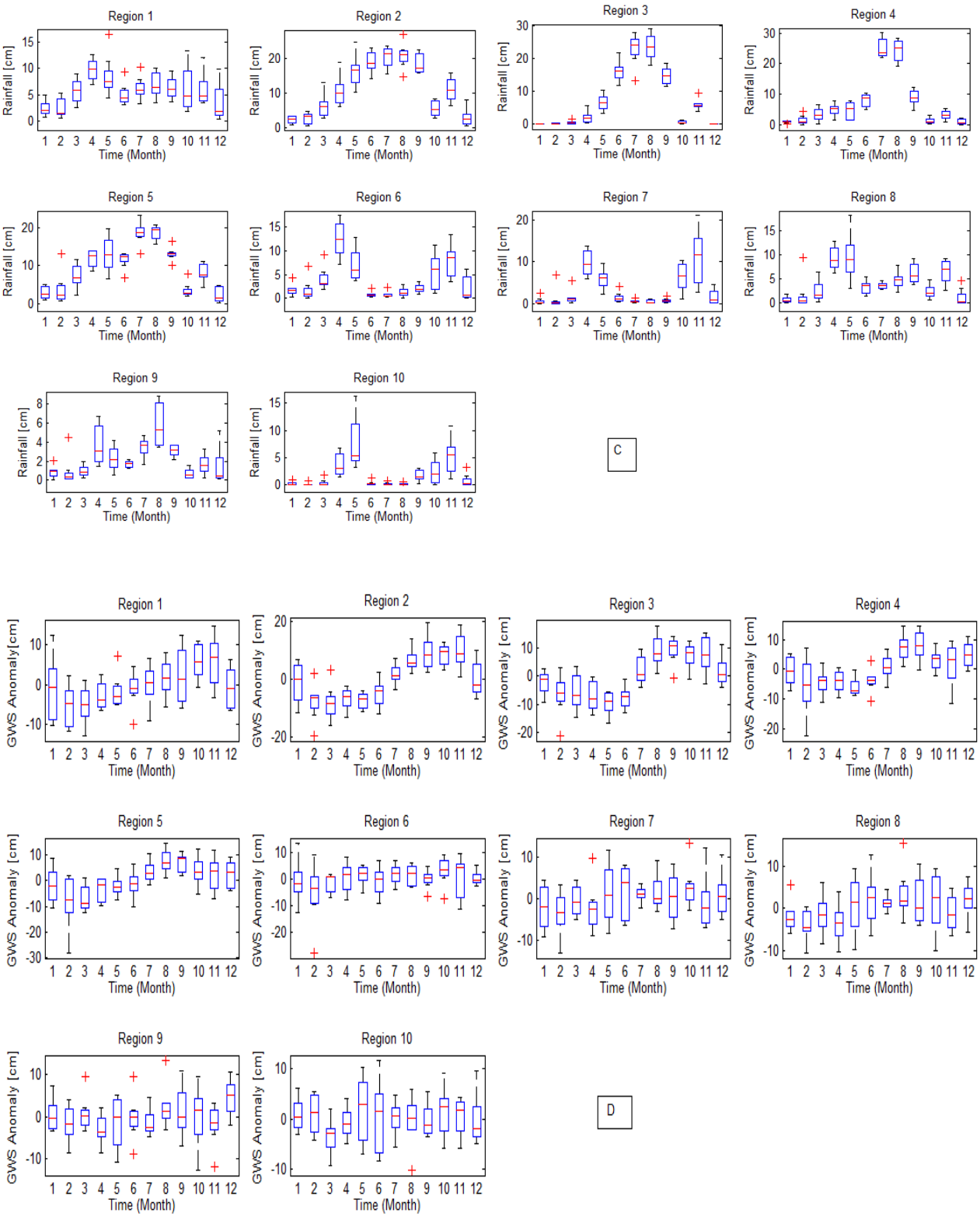

Figure 17: Inter-annual variability of TWS (A), Soil Moisture (B), Rainfall (C) and GWS anomaly (D) over Ethiopia.

4.3. Intra-annual variation

Figure 18 shows the intra-annual curve of four hydrological parameters (TWS, soil moisture anomaly, GWS anomaly and rainfall) developed from their mean monthly data. From the figure one can clearly see two distinct groups based on their TWS anomaly over the months. The first group includes regions 2, 3, 4 and 5, where the TWS and GWS anomalies shows three similar parts; i) the rising limb, which occurs from June to September, indicating the recovery period of TWS, ii) the peak, for most of them which occurs in October, except region 2 (i.e., November), iii) the recession or falling limb that covers a longer period than the previous ones, i.e., starting from a point at which the peak is attained (October/ November) and extending up to June. The results indicate that, like the rainfall patterns, TWS shows seasonality, having gaining seasons (JJA and some part of SON), while in the other two seasons the loss overcomes the gain in most regions of Ethiopia. This happens since the mentioned periods are the main rainy season in Ethiopia. The second group includes all the other regions with characteristics opposite to the first group. They have short duration recession curves with very long recovery or rising limb period, attaining their maximum peaks in the SON season. Despite the fact that SON is the long rainy period in this regions, the length of rising period might be attributed to the aquifer type and size, as well as recharge mechanism. Compared to the incoming rainfall and the response of GWS and TWS, one can see that there is no significant fluctuation in soil moisture.

From the intra-annual soil moisture plots in Fig. 19, one can visually extract extreme regions that include (i) the western part of Ethiopia (i.e. region 2), which has higher soil moisture content than any other parts, (ii) the north east (i.e. region 9), which has very low soil moisture than the others, and iii) the intermediate regions, that includes all the other regions. Apart from this, the country may be divided into two groups. The first group covers the western, north

western, northern and central regions. This group shows little variability over the first half of a year and significant raise in the second half, attaining their peaks in September. This is because the period is the main rainy season for most segments of the country. The other regions of the country portray almost same behavior to each other, having minimum values of about 14 cm/month and maximum of 16 cm/month.

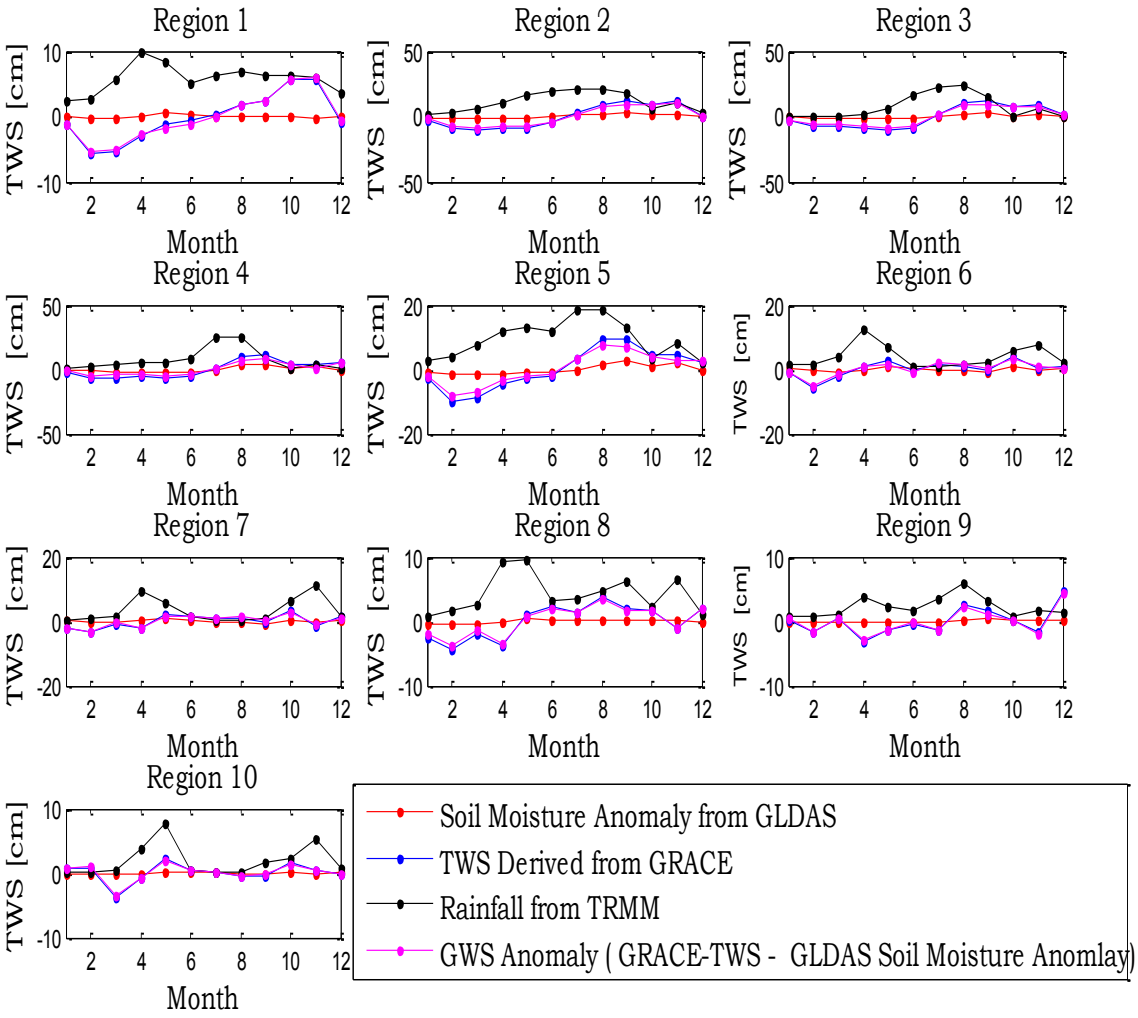

Figure 18: Intra-annual variability of TWS, SMA, GWS and rainfall over Ethiopia.

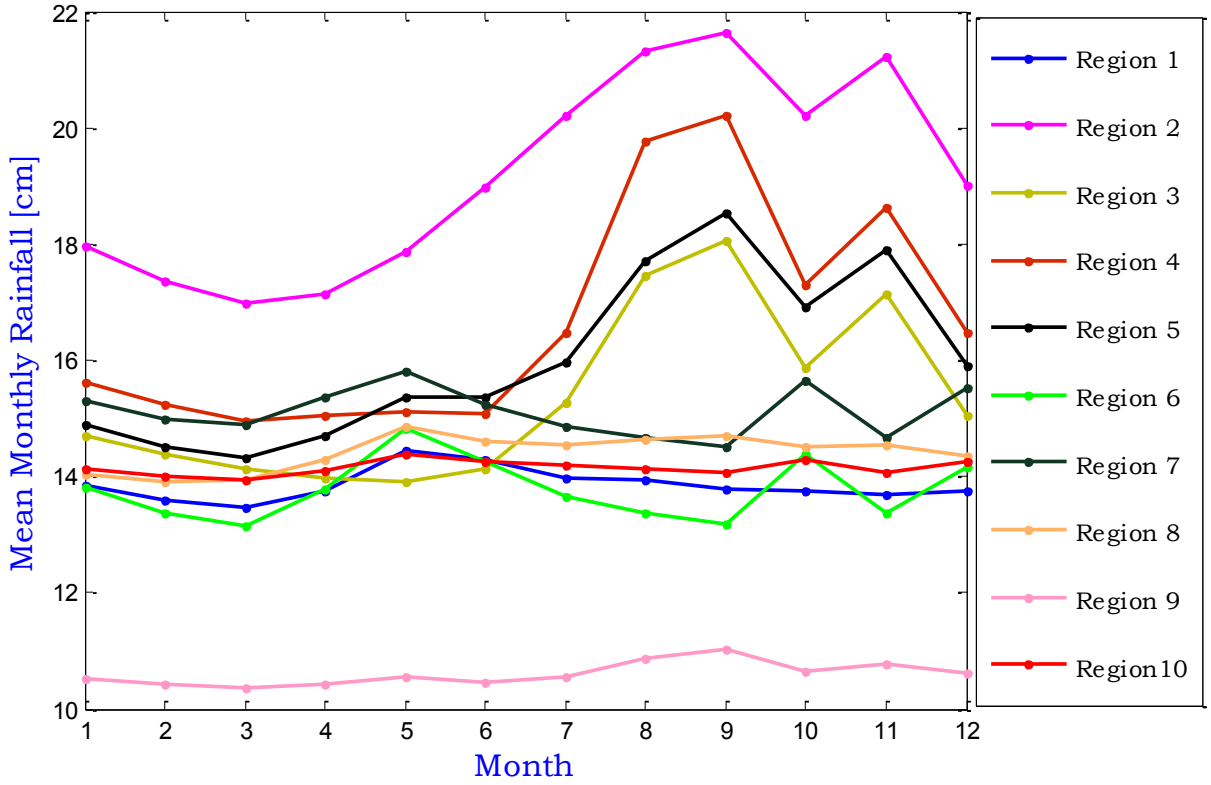

Figure 19: Intra-annual variability of soil moisture over Ethiopia

4.4. TWS Duration Curve (TDC)

The GRACE derived TWS duration curve (TDC) is developed and illustrated in Fig. 20. From the probability of exceedence at no loss/no gain point (i.e. point at which TWS equals zero) one can easily see that almost all regions received a water mass only 45 % of the time, while the other 55 % was losing period. TDC has also the capacity of reflecting the possibility of occurrence of TWS. The maximum water mass gain, which has a possibility of occurrence of less than 1 % over the study period ranges from 12 cm/month in region 10 to 23 cm/month in region 7. While the maximum water loss at a percentage exceedence of about 99 % ranges from -19 cm/month in region 2 to -9 cm/month in region 10.

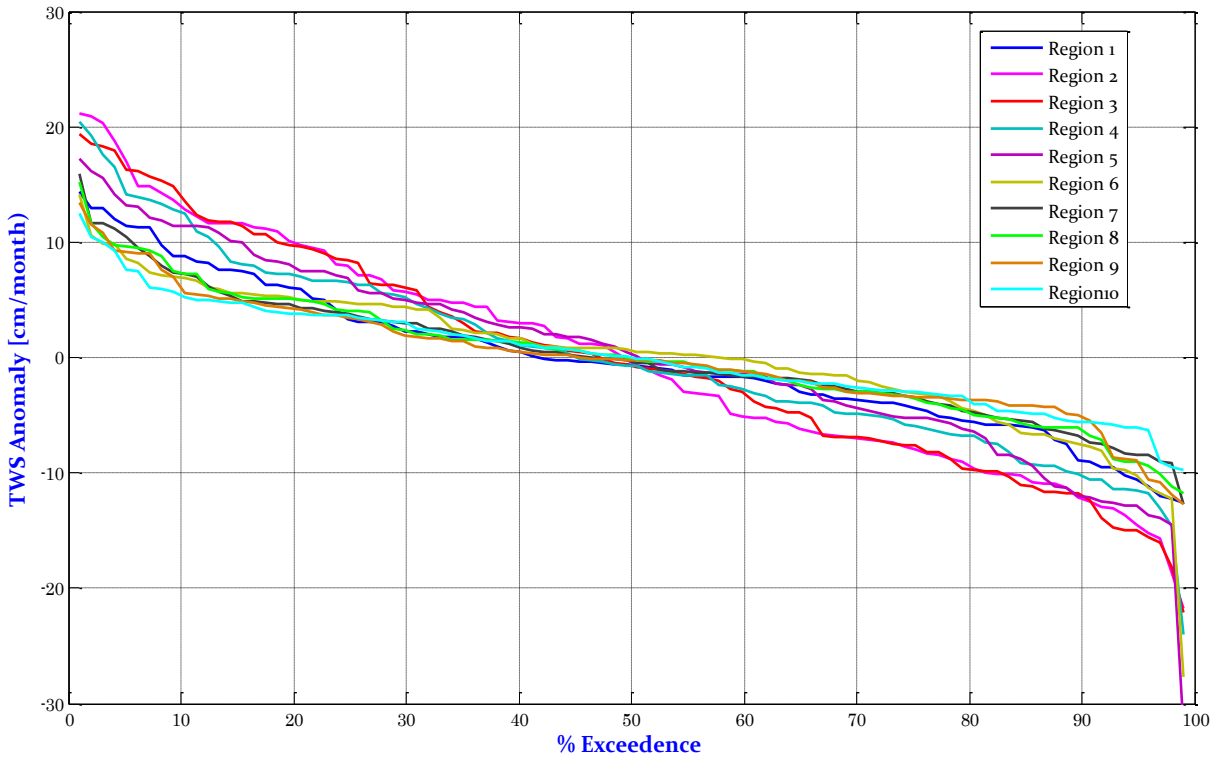

Figure 20: TDC of GRACE-based monthly TWS over the study period

To obtain the information of variability of TWS into a single value, a slope of the TDC is calculated using equation 29. The slopes registered in each region are tabulated in Table 4. A high slope value means rapid response and small storage potential while a low slope value means slow response to incoming water mass and large storage potential. For simplicity, we can group regions based on their TDC slopes as, i) $S_{TDC} > 30$ % (only region 2), ii) 20 % < S_{TDC} < 30 % (regions 3, 4 and 5) and iii) 10 % < S_{TDC} < 20 % (regions 1, 6,7,8,9 and 10). This indicates that over Ethiopia, the TWS variation is high in the western region and low in the north eastern region.

4.5. Cross-Correlation between Rainfall, Soil moisture and TWS

A correlation analysis is made using mean monthly data and illustrated in Figure 21, to study the time lag between rainfall and TWS, soil moisture anomaly and TWS, and soil moisture anomaly and rainfall. The analysis shows almost no lag between soil moisture and TWS in all regions, except regions 1 and 9 where lags of 5 and 1 month have been seen respectively. Strong correlation between rainfall and TWS have been seen in regions 2, 3 4 and 5. For TWS and rainfall, a lags of 1 month (regions 4 and 7), 2 months (region 3), 3 months (regions 2, 5 and 8), 4 months (region 9), 6 months (regions 1 and 6), and 0 in region 10 has been observed

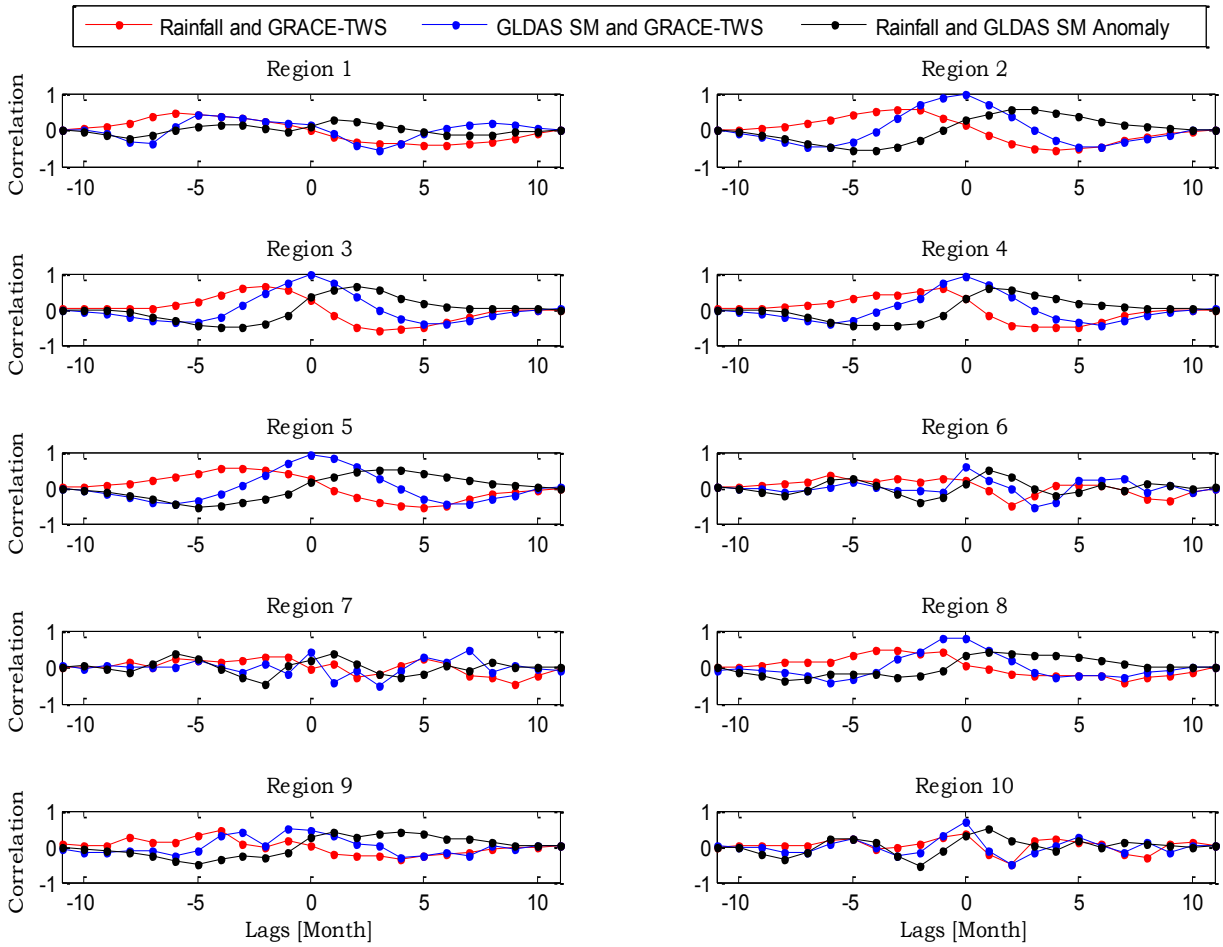

Figure 21: Cross-correlation between TWS, soil moisture and rainfall

The lags between TWS and rainfall obtained from Figure 21 are tabulated in Table 4

Table 4: Slope (m) of the TDC derived from GRACE-TWS, and Lag between GRACE-TWS and TRMM-rainfall for each region

Region	1	2	3	4	5	6	7	8	9	0
Lag (months)	6	3	2	1	3	6	1	3	4	0
m	-0.150	-0.344	-0.276	-0.236	-0.221	-0.146	-0.136	-0.138	-0.116	-0.138

Larger lag periods are indicative of water storages properties such as large size water storage, indirect dominant recharge mechanism or combination of both, while smaller values are more attributed to direct recharge mechanisms, smaller water storage size or effect of the combination.

4.6. Relationship between TRMM-Rainfall and GRACE-TWS

From Figures 17 and 18 one can see that there is no much significant delineation between plots of TWS and GWS. It is, therefore, thought that the very large influence of TWS over Ethiopia comes from the groundwater storage. The relationship between rainfall and TWS is presented in Fig. 22. This is developed by accounting for the lag duration of TWS from rainfall, as calculated in section 4.3. For example, in region 1, a lag of 6 months is used to see how much of rainfall observed in January has contributed to the TWS in July.

The correlation coefficients (R^2) of each region are as indicated in the Fig. 22. In all regions except regions 2, 4 and 5, correlation coefficients of less than 0.6 have been seen. For the regions where high values of R^2 are obtained (western, northern and central segments of the country), they could be attributed to two major facts, i.e. i) either the region is a source of water (e.g., regions 2 , 4 and 5) or, ii) there is no significant subsurface water mass contribution to the region. The results obtained here support our findings described in section 4.5.

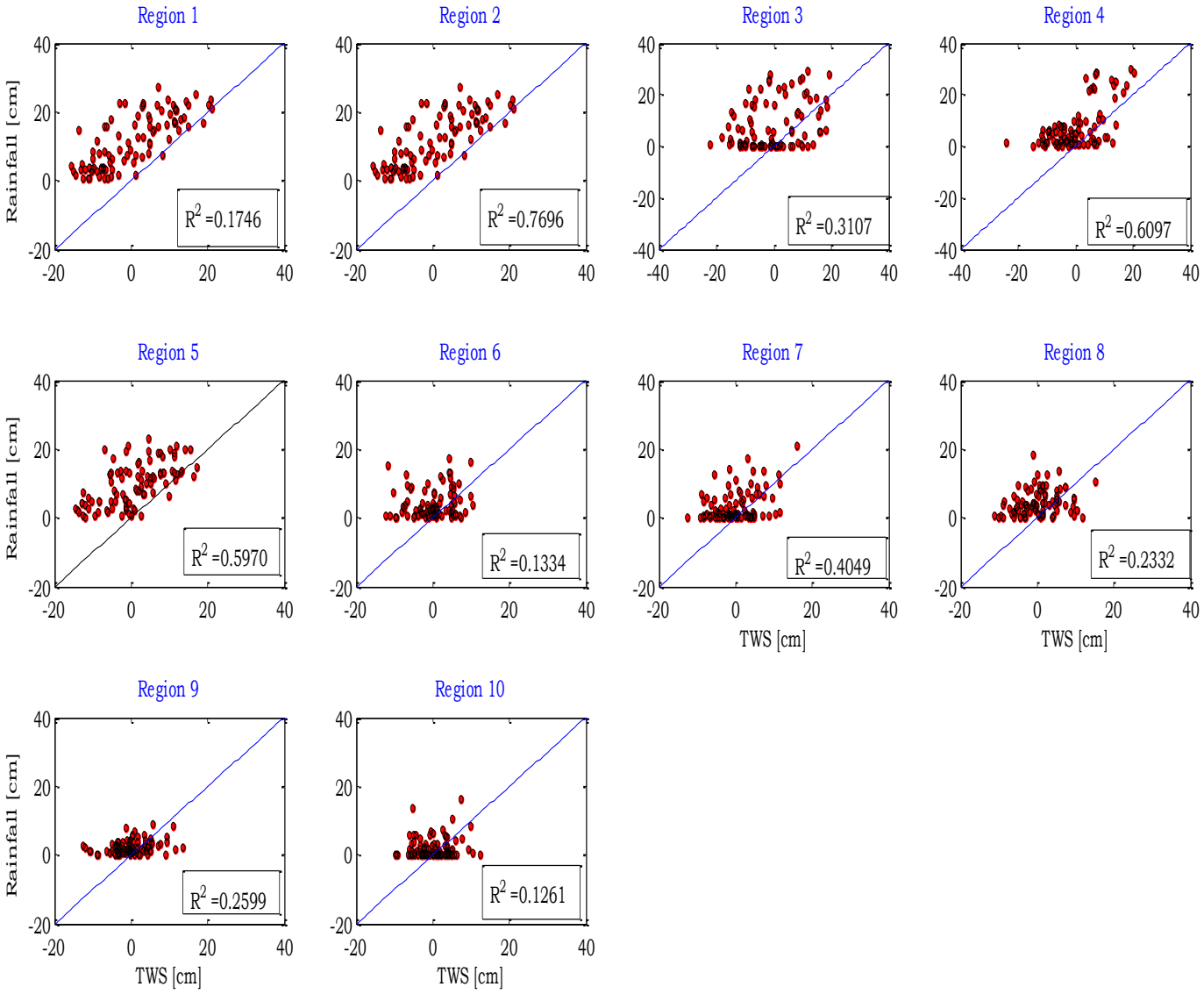

Figure 22: Relationship between TRMM rainfall and GRACE TWS in each region at their respective lags.

4.7. Total Storage Deficit (TSD)

TSD in percent are computed from GRACE-derived TWS anomaly and illustrated in Fig. 23. Depending on the pattern of their TSD, Ethiopia can be divided into three different groups. In the first group, we have regions 1 and 6; regions 7, 8, 9 and 10 are in the second

group, and regions 2, 3, 4 and 5 in the third group. For the three groups, TSD decreased from the beginning of 2003 and lasts up to mid-2006 for the groups of one and two and lasts up to January 2005 for the third group. Then for the first and third groups, it started rising in 2006, while the starting time for the second group is almost beginning 2007. The decrease in TSD starting from Jan-2003 indicates the dryness, which may be due to the propagation of the 2002 drought in Ethiopia (Anderson and Choularton, 2004; Meze-Hausken, 2004).

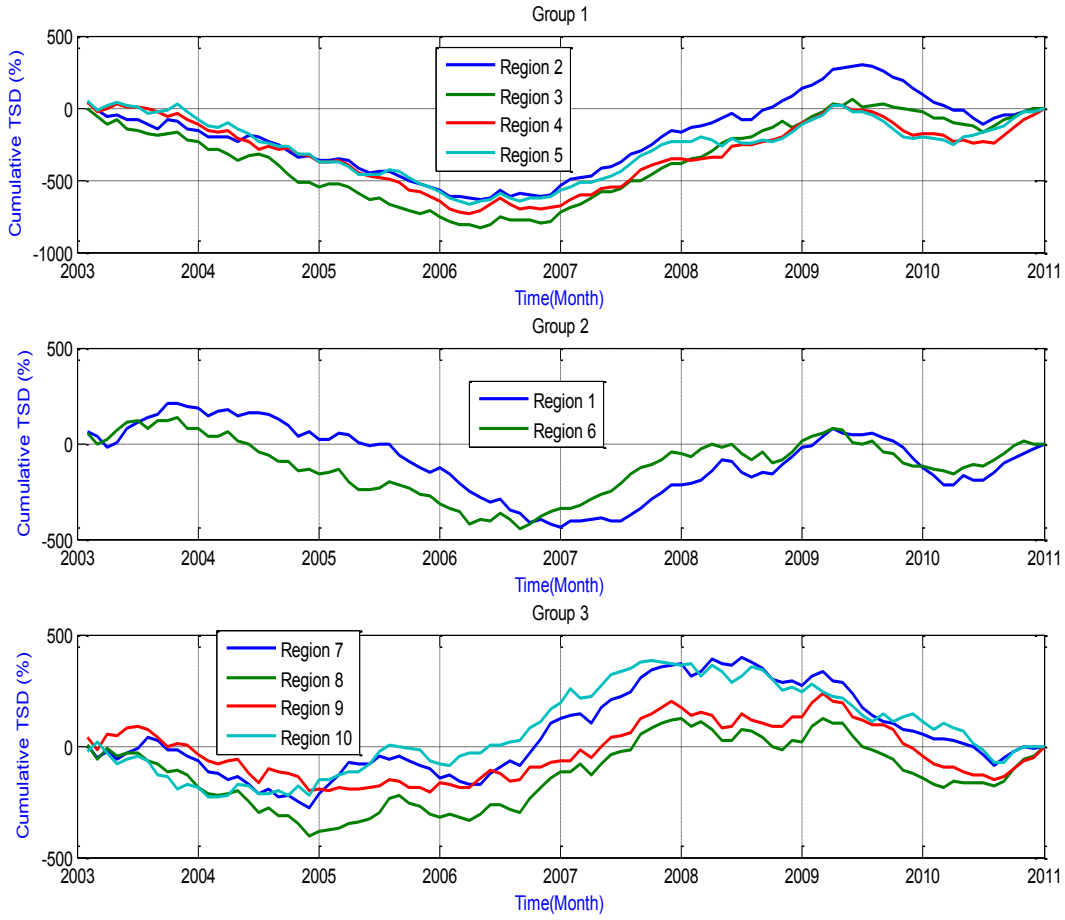

Figure 23: Total Storage Deficit over Ethiopia in percent

CHAPTER FIVE

DISCUSSION

Despite its coarser spatial domain, with other global datasets like TRMM and GLDAS, GRACE mission provides a possibility to characterize large scale water storage regimes in Ethiopia. From the inter-annual variation in Fig. 17, extreme depletion in TWS and GWS in certain regions for February 2003 was noticed. This is probably due to reported droughts in the year 2002. When considered together with the lag determined from TWS and rainfall correlation, one can conclude that the signs in February 2003 were due to rainfall shortage in the year 2002 as pointed out in Anderson and Choularton, (2004) and Meze-Hausken, (2004).

Rainfall over Ethiopia is known to be seasonal having dry and rainy seasons (Seleshi and Zanke, 2004). The effect of this seasonality seems to be reflected on the TWS anomalies over the country, having two distinct seasons on average, the loosing (winter (-2.13 cm/month) and spring (-3.66 cm/month)) and gaining (summer (1.437 cm/month) and autumn (4.101 cm/month). PCA results showed that the annual peaks of rainfall are also very important and highly correlated to the annual peaks of TWS, thus indicating that rainfall is the main driving parameter for rise and fall of TWS level in most parts of the Ethiopia.

The soil moisture variation over Ethiopia (Fig. 19) bears a resemblance to the agro-ecological zonation described in (Hurni, 1998). Depending on the dominant agro-ecological zone in each region, three different groups of regions may exist. These are; (i) Dega/Woyna Dega consisting of regions 2, 4 and 5, (ii) Bereha including regions 1, 6, 7, 8, 9 and 10, and (iii) the transitional zone Kolla/Dega comprising only of region 3. The Dega/Woyna Dega group has high soil moisture amounts with strong seasonality, while the Bereha group shows little

seasonality behavior as they receive little rainfall. Further Fig. 19 indicates two regions with extreme wetness and extreme dryness comparatively, regions 2 and 9 respectively. The possible reason for region 2 is the fact that i) the region receives rainfall almost throughout the year, comprising the area which obtains highest annual rainfall amount in the country and ii) the land cover in the region is highly dominated by rainforest. In region 9, the Danakil depression region, which shows lower soil moisture content, is known to be one of the dry regions in Ethiopia, where there is no significant river flow, short period bimodal rainfall, a dry land with no land cover and high temperature. Ertale, the area where volcanic magma can be seen at Earth surface also exists in this region.

From the developed TDC using 96 months of GRACE derived TWS data (Fig. 20), the lower end of the curve might be subjected to extreme water depletion cases, while the upper end is of high rainfall condition with long return period. So, to see the real variation of TWS, the slope of the TDC in the region where one can assume linearity is computed. In such a way, if we put it in percent, the slopes vary nearly from -14 % to -35 %. There are several factors that might affect the slope of TDC. These include soil moisture, the hydrogeologic setting, aquifer flow, storage type, storage potential, recharge rate and recharge mechanism.

The dominant hydrogeologic regime, recharge mechanism, recharge rates, aquifer flow and storage type for each region are presented, e.g., in Alemayehu, (2010), Chernet, (1993) and Wright and Burgess, (1992). Here we discuss the results obtained in relation to properties of the regions described in the Tables 6 and 7. The aquifers response lag to rainfall computed in this study is also described in Table 5. For same aquifer flow and storage type one can notice that there are different lag values, see, e.g., regions 2 and 3, this could be attributed to the recharge mechanism in the regions. Further, for regions that are dominated by inter-granular aquifer flow,

storage type has been seen to have a longer lag period (regions 1, and 6), while Krast dominated regions show a direct response to rainfall (region 10). In regions 1, 2, 3, 9 and 10, on the annual time scale, water mass loss has been found (see Fig. 16), when compared to recharge amount per year stated in Table 6, there is a huge loss of water. This might be attributed to manual extraction by human and large water mass outflow (subsurface, evapotranispiration) from the regions.

With the characteristics listed in the Tables 6 and 7, and their TDC slope, one can tell that i) region 2 , has smaller storage potential compared to others, ii) regions 2, 4 and 5 have relatively intermediate storage potential, and iii) all the other regions have relatively large storage potential. From Fig. 22, in regions other than 1 and 4, based on their correlation coefficients, there are clear views that certain percent of the TWS in the region are contributed from subsurface inter flow and dominant indirect recharges

Table 5: Hydrogeology, Aquifer flow and Storage type characteristics over Ethiopia (Source: Alemayehu, 2010; Chernet, 1993; Wright and Burgess, 1992)

Region	**Hydrogeologic Setting**	**Aquifer flow and Storage type**	**Lag (months)**
1	Unconsolidated sediment	Inter-granular	6
2	Volcanic rocks, Metamorphic rocks and Intrusive	Fracture	3
3	Volcanic and Metamorphic rocks and intrusive	Fracture	2
4	Metamorphic rocks and intrusive	Fracture	1
5	Metamorphic rocks and intrusive	Fracture	3
6	Metamorphic rocks and intrusive, Consolidated	Inter-granular	6
7	Consolidated sediment	Inter-granular and Fracture	1
8	Consolidated and Unconsolidated Sediment	Inter-granular and Fracture	3
9	Metamorphic rocks and intrusive	Fracture	4
10	Consolidated sediment Unconsolidated Sediment	Fracture(Krast)	0

Table 6: Recharge mechanisms and recharge rates over different regions of Ethiopia (Source: Alemayehu, 2010; Chernet, 1993; Wright and Burgess, 1992)

Reg.	Recharge Mechanism	Recharge Rate(mm/year)	GRACE-Mean Annual TWS (mm/year)
1	Recharge from wadi beds through local wadi floods	50-150	-20.64
2	Direct diffuse recharge through soil and root zone Recharge from wetland during high flood	150-250	-1.08
3	Wadi bed through local wadi floods, Selective recharge from heavy rainfall	50-150	-19.92
4	Selective recharges from heavy rain falls, direct diffuse + floods from highlands	50-150	8.64
5	Selective recharges from heavy rain falls , Mountain block and mountain font	50-250	30.12
6	Selective recharges from heavy rainfalls wadi beds through local wadi floods	50-150	17.04
7	Selective recharges from heavy rainfalls wadi beds through local wadi floods	<50	6.00
8	Selective recharges from heavy rainfalls wadi beds through local wadi floods	<50-150	8.64
9	Flood Water from the highlands	<50	-4.80
10	Recharge from wadi beds through local wadi floods	<50	12.48

In the northern (region 4) and south eastern (region 7), a lag of one month between TWS and rainfall have been obtained from cross correlation. This implies that the aquifer responds to the rainfall after about one month. The slope of TDC (S_{TDC}) indicates that region 4 has low storage potential than region 7. The rainfall in region 4 is a bit higher than in region 7. From the above information one can conclude that the chance that water can be transferred from rainy to non rainy season in such regions is very low. In this case, mostly the rise or fall in TWS in certain season is subjected to rainfall in that particular season.

In the north western segment a lag of 2 months is noticed (Table 3 and Figure 21). This shows that the life span of water contributed from rainfall in this region is not more than 2 months, making the transfer of water from season to season impossible. In addition to this, the S_{TDC} also indicates that the region has a lower storage potential compared to other regions next to the western part of the country (region 2). These imply that for most parts of Ethiopia the rainfall in previous season might have impact on the TWS of the current season at most, but cannot go further.

In the central parts of the country (regions 2, 5 and 8), the cross correlation between rainfall with TWS indicated a lag of 3 months (Table 5). Figure 22 also shows that there is a high correlation between rainfall and TWS in regions 2 and 5, indicating that the influences of rainfall on TWS in these regions are higher than subsurface inflow from adjacent regions. The S_{TDC} decreases from west to east and the water storing potential also follows the same route. Rainfall amount decreases from west to east. TWS in region 9 also recorded a lag of 4 months from the rainfall. This region has low rainfall and also poor correlation between rainfall and TWS anomaly (Fig. 22).

The mean annual rainfall regions 1 and 6 has slightly two peaks, with a lag of 6 months obtained from TWS/Rainfall cross correlation. The slope of the TDC (-0.15 for both) also supports the pervious statement, as this value indicates large storage potential condition. The autumn mass gain is mainly of rainfall received in winter. With characteristics described in Table 5 and 7, these regions have the property to transfer water mass gained from rainfall in certain year to the next one. According to Kebede (2012), three fourth of Ethiopia aquifers receives localized and indirect recharge. This implies that the possibility of having good correlation

between TWS and rainfall will be less than 25 %, the R^2 results obtained from correlation analysis in Fig. 22 supports this idea.

Ethiopia is a country where more than 85 % of its community is agrarian; there are different types of crops which are commonly grown in the region, the major crop producing zones have been described in Fig. 24. Normally the agricultural production in certain region is highly dependent on the TWS available. In Ethiopia, the principal grain crops are teff, wheat, barley (primarily cool-weather crops) and corn, sorghum, and millet (warm weather

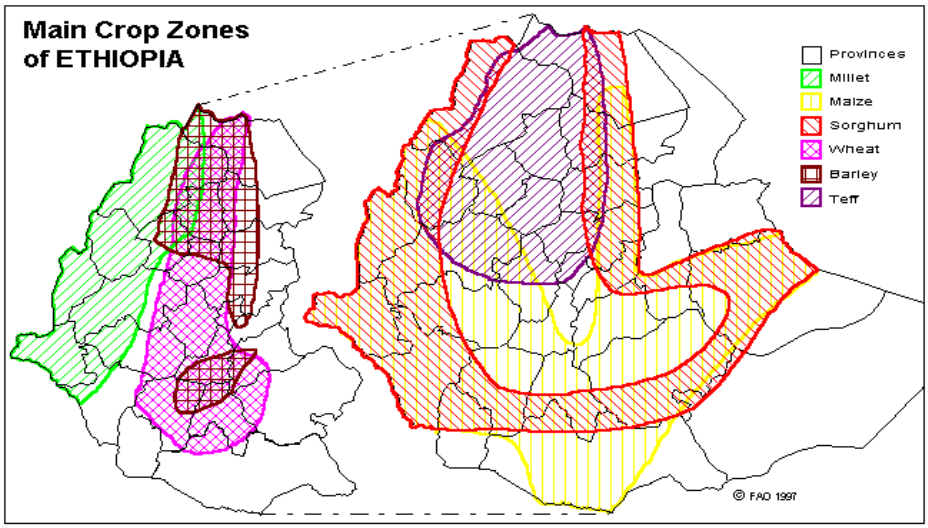

Figure 24 : Major crop producing zones of Ethiopia (Source: http://www.fas.usda.gov)

grain crops)[4]. In regions where significant TSD has been seen from 2003 to 2006 (e.g., Group 1 in Fig.13), the main crops are teff, sorghum, maize, wheat and millet. Despite the increase in TSD in the regions, there has been an increase in crop production area and yield in the region as stated by (Eberhardt, 2008) indicating that the crops can sustain the water deficit. On the other

[4] http://www.fas.usda.gov

hand, this indicates that the largest portion of this deficit in TWS is subjected to groundwater storage depletion.

CHAPTER SIX

CONCLUSIONS AND RECOMMENDATIONS

6.1. Conclusions

A time series of TWS, soil moisture and rainfall over Ethiopia were collected from GRACE, GLDAS and TRMM respectively. The inter-annual, intra-annual and seasonal variability of water storages, the relationship between water storage variations with rainfall and soil moisture, and the aquifers' characteristics and TWS anomalies has been made over a period of 8 years from 2003 to 2011. The study revealed the western segment and the north-eastern lowland of the country as a water losing regions. We were also able to see the impact of rainfall seasonality on TWS changes. The losing seasons are summer and autumn while the gaining seasons are spring and winter for vast part of the country. The TDC curve developed over the study period also indicated that almost in all segments of the country, water gain accounted only for 45 % of the time. Soil moisture and rainfall variations showed the dominant annual water variability in the western, north western, northern and central regions, and the dominant seasonal variability in the western and eastern regions. Change in soil moisture was seen to have less control over the total water storage in Ethiopia, while groundwater storage has a dominant control. From a correlation analysis between TWS and rainfall, we were able to observe a lag of 2 to 3 months in most of the regions, indicating the capacity of Ethiopian groundwater storages (aquifers) to transfer water mass gained in certain period to be less than 3 months. If validated at a finer spatial domain, this could be vital sign for water managers to know that if increase in TWS is needed to back up the water availability in dry seasons, one has to focus on increasing the soil moisture and surface water storages rather than groundwater storages. Significant TWS

deficit is subjected to the 2002 drought was also detected in the central highlands of the country over the period of three years between 2003 and 2006.

6.2. Recommendations

- Due to the spatial resolution of GRACE satellite this study was carried out at a coarse spatial domain of 440 km x 440 km grid. The results presented and interpretations made might not be suited to smaller size basins. In order to compel it applicable for small watersheds additional advancement in the science of GRACE remote sensors and generation of new approaches in computing the spherical harmonic coefficients is needed.
- The study made ignores the effect of surface water mass variability based on the fact that surface water covered regions in Ethiopia is very small. And under the concept stated by Rodell et al., (2007) that it might be appropriate to neglect the surface water mass variability, given that the technique described supposes groundwater to be spatially continuous across the region of interest, and it would effectively eliminate surface water variations as a source of error. But rather than neglecting this effect it is important to consider it while computing groundwater mass variabilities as it can be obtained through employing satellite altimetry products.
- As this study is the first attempt to apply GRACE satellite gravimetry product to calculate TWS over Ethiopia as a whole it needs to be validated through the use of hydrologic models or other products like the Mass Concentration (MASCON) anomaly data.

REFERENCES

Achamyeleh, K., 2003. The associated programme on flood management, integrated flood management case study, Ethiopia: Integrated flood Management, World Metrological Organization/Global Water Partnership.

Alemayehu, T., 2006. Groundwater occurrence in Ethiopia. Addis Ababa University, Addis Ababa, Ethiopia, 107 pp.

Alemayehu, T., 2010. An overview of the transboundary aquifers in East Africa. Journal of African Earth Sciences, 58: 684-691, doi:10.1016/j.jafrearsci.2009.10.003.

Anderson, S. and Choularton, R., 2004. Retrospective analysis: 2002/3 crisis in Ethiopia: early warning and response, The Regional Economic Development Services Office For East and Southern Africa (REDSO), 64pp.

Awange, J.L., Fleming, K.M., Kuhn, M., Featherstone, W.E., Heck, B. and Anjasmara, I., 2011. On the suitability of the 4^o X 4^o GRACE mascon solutions for remote sensing Australian hydrology. Remote Sensing of Environment, 115: 864875, doi:10.1016/j.rse.2010.11.014.

Awange, J.L., Sharifi, M.A., Ogonda, G., Wickert, J., Grafarend, E.W. and Omulo, M.A., 2007. The falling lake Victoria water levels: GRACE,TRIMM and CHAMP satellite analysis of the lake basin. Water Resour Manage, 22:775–796, doi: 10.1007/s11269-007-9191-y.

Awulachew, S.B., Yilma, A.D., Loulseged, M., Loiskandl, W., Ayana, M., Alamirew, T., 2007. Water resources and irrigation development in Ethiopia, Working Paper 123. International Water Management Institute, Colombo, Sri Lanka, 78 pp.

Ayenew, T., Demlie, M. and Wohnlich, S., 2008. Hydrogeological framework and occurrence of groundwater in the Ethiopian aquifers. Journal of African Earth Sciences, 52: 97-113, doi:10.1016/j.jafrearsci.2008.06.006.

Bedada, T., 2007. Combining space based GRACE gravity field measurement and climatologically averaged precipitation data to assess essential features of hydrological mass variation within the Nile Basin, MSc. Thesis Addis Ababa University, Addis Ababa, Ethiopia.

Berhane,G., Kristine, M., Nawal.,A. and Kristine W., 2013. Water leakage investigation of micro-dam reservoirs in Mesozoic sedimentary sequences in Northern Ethiopia. Journal of African Earth Sciences,79:98-110, http://dx.doi.org/10.1016/j.jafrearsci.2012.10.004

Beyene, E.G. and Meissner, B., 2010. Spatio-temporal analyses of correlation between NOAA satellite RFE and weather stations' rainfall record in Ethiopia .International Journal of Applied Earth Observation and Geoinformation 125, 569-575, doi:10.1016/j.jag.2009.09.006

Bonsor, H.C., Mansour, M.M., MacDonald, A.M., Hughes, A.G., Hipkin, R.G., and Bedada, T., 2010. Interpretation of GRACE data of the Nile Basin using a groundwater recharge model. Hydrology and Earth System Sciences, Discussions 7(45014533), doi: 10.5194/hessd-7-4501-2010.

Chatfield, C., 1989. The analysis of time series: an introduction. Chapman and Hall, 352pp, ISBN: 10:1584883170.

Chen, J.L., Wilson, C.R., Tapley, B.D., Longuevergne, L., Yang, Z.L., Scanlon, B.R., 2010. Recent La Plata basin drought conditions observed by satellite gravimetry. Journal of Geophysical Research, 115(D22108), doi: 10.1029/2010JD014689.

Chernet, T., 1993. Hydrogeology of Ethiopia and water resources development. Ethiopian Institute of Geological Surveys, Ministry of Mines and Energy, Addis Ababa, Ethiopia, 227 pp.

Conway, D., 1996. The impact of climate variablity and future climate change in Nile basin on water resources in Egypt. International Journal of Water Resoiurces Development, 12:3: 277-296, doi: 10.1080/07900629650178.

Conway, D., Lisa, E. and Schipper, F., 2011. Adaptation to climate change in Africa: Challenges and opportunities identified from Ethiopia. Global Environmental Change, 21: 227-237, doi:10.1016/j.gloenvcha.2010.07.013.

Crowley, J.W., Mitrovica, J.X., Bailey, R.C., Tamisiea, M.E. and Davis, J.L., 2006. Land water storage within the Congo Basin inferred from GRACE satellite gravity data. Geophysical Research Letter, 33(L19402), doi:10.1029/2006GL027070.

Crowley, J.W., Mitrovica, J.X., Bailey, R.C., Tamisiea, M.E. and Davis, J.L., 2008. Annual variations in water storage and precipitation in the Amazon Basin. Journal of Geodesy, 82(1): 9-13.

Demilie, M., Wohnlich, S., Gizaw, B. and Stichler, W., 2007. Groundwater recharge, flow and hydrogeochemical evolution in a complex volcanic aquifer system, central Ethiopia. Hydrogeology Journal, 15: 1169-1181, doi:10.1007/s10040-007-0163-3.

Demilie, M., Wohnlich, S. and Ayenew, T., 2008. Major ion hydrochemistry and environmental isotope signatures as a tool in assessing groundwater occurrence and its dynamics in a fractured volcanic aquifer system located within a heavily urbanized catchment, central Ethiopia. Journal of Hydrology, 353: 175-188, doi: 10.1016/j.jhydrol.2008.02.009.

Dinku, T., Ceccato, P., Grover-Kopec, E., Lemma, M.Connor, S.J., Ropelewski, C.F., 2007. Validation of satellite rainfall products over East Africa's complex topography. International Journal of Remote Sensing 28 (7), 1503-1526, doi: 10.1080/01431160600954688.

Dinku, T., Chidzambwa, S., Ceccato, P., Connor, S. J., and Ropelewski, C. F., 2008. Validation of high-resolution satellite rainfall products over complex terrain, Int. J. Remote Sens., 29(14), 4097–4110, doi:10.1080/01431160701772526.

Dinku, T., Ceccato, P., Cressman, K., Connor, S.J., 2010. Evaluating Detection Skills of Satellite Rainfall Estimates over Desert Locust Recession Regions. International Journal of Applied meteorology and Climatology 49, 1322-1332, doi: 10.1175/2010JAMC2281.1

Degefu, W., 1987. Some aspects of meteorological drought in Ethiopia. In: M.H. Glantz (Editor), Drought and Hunger in Africa: Denying Famine a Future. Cambaridge University Press, Cambaridge, UK, 23 – 36

Dubale, P., 2001. Soil and water resources and degradation factors affecting productivity in Ethiopian Highland agro-ecosystems. Northeast African Studies, 8:1: 27-52.

Eberhardt,M.,2008.Cereal production in Ethiopia :A brief historical overview of land under cultivation and yields,Centre for the Study of African Economies, University of Oxford, Oxford.

Engida, A.N. and Esteves, M., 2011. Characterization and disaggregation of daily rainfall in the Upper Blue Nile Basin in Ethiopia. Journal of Hydrology, 399: 226-234.

Fang, H., Beaudoing, H.K., Rodell, M., Teng, W.L. and Vollmer, B.E., 2009. Global Land Data Assimilation (GLDAS) Products, Service and Application from NASA Hydrology Data and Information Service Center (HDISC), ASPRS Annual Conference, Baltimore, Maryland.

FAO, 2005. 2005-AQUASTAT-Survey, Irrigation in Africa in Figures.

Ferguson, A.J.D. and Harbott, B.J., 1982. Geophysical, Physical and Chemical aspects of Lake Turkana. In: E. Hopson (Editor), Lake Turkana: A report of the findings of the Lake Turkana project 1972-1975. Overseas Development Administration, London, UK.

Flechtner, F., 2007. GFZ Level-2 Processing Standards Document for Product Release 04, GeoForschungszentrum, Postdam, Germany.

Forootan, E., Awange, J.L., Kusche, J., Heck, B. and Eicker, A., 2012. Independent patterns of water mass anomalies over Australia from satellite data and models Remote Sensing of Environment, 124: 427-443, doi:0.1016/j.rse.2012.05.023.

Forootan, E., Kusche, J., 2012. Separation of global time-variable gravity signals into maximally independent components. Journal of Geodesy Vol.86 (7): 477-497, doi:10.1007/s00190-011-0532-5.

Frappart, F., Papa, F., Güntner, A., Werth, S., Silva, J.Sd., Tomasella, J., Seyler, F., Prigent, C., Rossow, W.B., Calmant, S., Bonnet. M.P., 2011. Satellite-based estimates of groundwater storage variations in large drainage basins with extensive flood plains. Remote Sensing of Environment, 115: 1588-1594, doi:10.1016/j.rse.2011.02.003.

Funk, C., Williams, A.P. and Robertson, J., 2011. More Frequent Drought Likely in Eastern Africa, USGS, News Release.

Furi, W., Razack, M., Haile, T., Abiye, T.A. and Legesse, D., 2011. The hydrogeology of Adama–Wonji basin and assessment of groundwater level changes in Wonji wetland, Main Ethiopian Rift: results from 2D tomography and electrical sounding method. Journal of Environmental Earth Science, 62(6): 1323-1335, doi: 10.1007/s12665-010-0619-y.

Furi, W., Razack, M., Abiye, T.A., Kebede, S. and Legesse, D., 2012. Hydrochemical characterization of complex volcanic aquifers in a continental rifted zone: the Middle Awash basin, Ethiopia. Hydrogeology Journal, 20: 385-400, doi: 10.1007/s10040-011-0807-1.

Gamachu, D., 1977. Aspects of climate and water budget in Ethiopia. Addis Ababa University Press, Addis Ababa, Ethiopia, 71 pp.

Gebeto, P.J., 2010. No more thirst: The citizens of the Nile. Rehobot Printers, Addis Ababa, Ethiopia, 282 pp, ISBN: 9966-05-291-7.

Gray, C. and Mueller, V., 2012. Drought and population mobility in rural Ethiopia. World Development, 40(1): 134-145.

Haile, T., 1988. Causes and characteristics of drought in Ethiopia. Ethiopian Journal of Agricultural Science, 10: 85-97.

Hirpa, F. A., Gebremichael, M., and Hopson, T., 2010. Evaluation of High Resolution Satellite Precipitation Products over Very Complex Terrain in Ethiopia, J. Appl. Meteorol. Clim. IPWG Special Collection, 49(5), 1044–1051, doi:10.1175/2009JAMC2298.1

Huffman, G. and Bolvin, D., 2012. TRMM and other data precipitation data set documentation. Mesoscale Atmospheric Processes Laboratory, NASA Goddard Space Flight Center and Science Systems and Applications, Inc.

Huffman, G.J., Adler, R.F., Bolvin, D.T., Gu, G.-J., Nelkin, E.J., Bowman, K.P., Hong, Y., Stocker, E.F., Wolff, D.B., 2007. The TRMM multisatellite Precipitation Analysis (TMPA): Quasi-Global, multiyear, combined-sensor precipitation estimates at fine scales. Jornal of Hydrometeorology, 8: 38-55.

Hurni, H., 1998. Agroecological Belts of Ethiopia: Explanatory notes on three maps at a scale of 1:1,000,000, Soil Conservation Research Programme,Ministry of Agriculture / Centre for Development and Environment, University of Berne, Bern, Switzerland.

Johanson, D.C. and Edey, M.A., 1981. The beginnings of Humankind. Penguin, London, UK.

Kebede, S., 2012. Ground Water in Ethiopia: Features, Numbers and Opportunities. Springer Hydrogeology, Verlag Berlin, 292 pp, ISBN:978-3-642-30390-6.

Kebede, S., Travi, Y., Alemayehu, T. and Ayenew, T., 2005. Groundwater recharge, circulation and geochemical evolution in the source region of the Blue Nile River, Ethiopia. Applied Geochemistry, 20: 1658-1676, doi:10.1016/j.apgeochem.2005.04.016.

Kebede, S., Travi, Y., Asrat, A., Alemayehu, T., Ayenew, T. and Tessema, Z., 2008. Groundwater origin and flow along selected transects in Ethiopian Rift volcanic aquifers Hydrogeology Journal, 16: 55-73, doi: 10.1007/s10040-007-0210-0.

Kummerow, C., Barnes, W., Kuzo, T., Shiue, J. and Simpson, J., 1998. The Tropical Rainfall Measuring Mission (TRMM) sensor package. Journal of Atmospheric and Oceanic Technology, 15: 809-817.

Kummerow, C., Simpson, J., Thiele, O., Barnes, W., Chang, A.T.C., Stocker, E., Iguchi, T., Kuroiwa, H., Im, E., Haddad, Z., Huffman, G., Ferrier, B., Olson, W.S., Zipser, E., Smith, E.A., Wilheit, T.T., North, G., Krishnamurti, T., Nakamura, K., 2000. The status of the Tropical Rainfall Measuring Mission (TRMM) after two years in orbit. Journal of Applied Meteorology, 39: 1965-1982.

Kusche, J., 2007. Approximate decorrelation and non-isotropic smoothing of time-variable GRACE-type gravity field models. Journal of Geodesy, 81: 733-749, doi: 10.1007/s00190-007-0143-3.

Kusche, J., Schmidt, R., Petrovic, S. and Rietbroek, R., 2009. Decorrelated GRACE time-variable gravity solutions by GFZ, and their validation using a hydrological model Journal of Geodesy, 83 903-913, oi:10.1007/s00190- 852009-0308-3. 853.

MacDonald, A.M., Calow, R.C., Nicol, A.L., Hope, B. and Robins, N.S., 2001. Ethiopia: water security and drought. British Geological Survey, Natural Environment Research Council, Nottingham, UK.

Melesse, A., Abtew, W., Dessalegne, T. and Wang, X., 2010. Low and high flow analyses and wavelet application for characterization of the Blue Nile River system. Hydrological Processes, 24: 241-252, doi: 10.1002/hyp.7312.

Melesse, A.M. (Editor), 2011. Nile River Basin: hydrology, climate and water use. Springer, New York, 448 pp, ISBN: 978-94-007-0688-0.

Meze-Hausken, E., 2004. Contrasting climate variability and meteorological drought with perceived drought and climate change in northern Ethiopia. Climate Research, 27: 19-31.

MoWR, 1999. Water Resource Management Policy (WRMP), Ministry of Water Resources, Addis Ababa: Ethiopia.

MoWR, 2002. Water Sector Development Program (WSDP), Ministry of Water Resources, Addis Ababa, Ethiopia.

MoWR, 2012. Ministry of Water Resources Web page, Accessed on September 05, 2012, Addis Ababa, Ethiopia, http://www.mowr.gov.et/index.php?pagenum=2.1&pagehgt=5495px.

North, G.R., Bell, T.L. and Cahalan, R.F., 1982. Sampling errors in the estimation of empirical orthogonal functions. Monthly Weather Review Vol. 110: 699-706.

Nyssen, J., Clymans, W., Descheemaeker, K., Poesen,J., Vandecasteele, I., Vanmaercke, M., Amanuel Zenebe, Van Camp, M., Mitiku Haile, Nigussie Haregeweyn, Moeyersons, J., Martens, K., Tesfamichael Gebreyohannes, Deckers, J., Walraevens, K., 2010. Impact of soil and water conservation on catchment hydrological response -a case in north Ethiopia. Hydrological Processes, 24(13): 1880-1895

Preisendorfer, R., 1988. Principal component analysis in meteorology and oceanography. Elsevier, Amsterdam.

Ramillien, G., Frappart, F., Cazenave, A. and Guntner, A., 2005. Time variations of land water storage from an inversion of 2 years of GRACE geoids. Earth and Planetary Science Letters, 235: 283-301, doi:10.1016/j.epsl.2005.04.005.

Reager, J.T. and Famiglietti, J.S., 2009. Global terrestrial water storage capacity and flood potential using GRACE. Geophysical Research Letter, 36(L23402), doi: 10.1029/2009GL040826.

Rodell, M., Chen, J., Kato, H., Famiglietti, J.S., Nigro, J., Wilson, C.R., 2007. Estimating groundwater storage changes in the Mississippi River basin (USA) using GRACE. Hydrogeology Journal, 15: 159-166, doi: 10.1007/s10040-006-0103-7.

Rodell, M. and Famiglietti, J.S., 2001. An analysis of terrestrial water storage variations in Illinois with implications for the Gravity Recovery and Climate Experiment (GRACE). Water Resources Research, 37: 1327–1339, doi: 10.1029/2000WR900306.

Rodell M, Houser, P.R., Jambor, U., Gottschalck, J., Mitchell, K., Meng, K., Arsenault, C.-J., Cosgrove, B., Radakovich, J., Bosilovich, M., Entin, J.K., Walker, J.P., Lohmann, D., and Toll, D. (2004). The Global Land Data Assimilation System. Bulletin of the American Meteorological Society, 85 (3), 381-394.

Romilly, T.G. and Gebremichael, M., 2011. Evaluation of satellite rainfall estimates over Ethiopian river basins. Hydrology and Earth System Sciences, 15: 1505-1514, doi: 10.5194/hess-15-1505-2011.

Rui, H., 2011. README Document for Global Land Data Assimilation System Version 1 (GLDAS-1) Products. Goddard Earth Sciences Data and Information Services Center (GES DISC), National Aeronautics and Space Administration (NASA).

Sawicz, K., Wagene, T., Sivapalan, M., Troch, P.A. and Carrillo, G., 2011. Catchment classification: empirical analysis of hydrologic similarity based on catchment function in the eastern USA. Hydrology and Earth System Sciences, 15: 2895-2911, doi:10.5194/hess-15-2895-2011.

Schmidt, R., Schwintzer, P., Flechtner, F., Reigber, C., Guntner, A., Doll, P., Ramillien, G., Cazenave, A., Petrovic, S., Jochmann, H., Wunsch, J.,2006. GRACE observations of changes in continental water storage. Global and Planetary Change, 50: 112-126, doi:10.1016/j.gloplacha.2004.11.018.

Schmidt, R., Flechtner, F., Meyer, U., Neumayer, K.-H., Dahle, C., Konig, R., Kusche, J., 2008. Hydrological Signals Observed by the GRACE Satellites. Surv Geophys, 29: 319-334, doi: 10.1007/s10712-008-9033-3.

Seleshi, Y. and Camberlin, P., 2006. Recent changes in dry spell and extreme rainfall events in Ethiopia. Theor. Appl. Climatol., 24: 181-191.

Seleshi, Y. and Zanke, U., 2004. Recent changes in rainfall and rainy days in Ethiopia. International Journal of Climatology, 24: 973-983, doi: 10.1002/joc.1052.

Shang, H., Yan, J., Gebremichael, M. and Ayalew, S.M., 2011. Trend analysis of extreme precipitation in the Northwestern Highlands of Ethiopia with a case study of Debre Markos. Hydrology and Earth System Sciences, 15: 1937-1944, doi:10.5194/hess-15-1937-2011.

Simpson, J., Adler, R.F. and North, G.R., 1988. A Proposed Tropical Rainfall Measuring Mission (TRMM) Satellite. Bulletin American Meteorological Society, 69(3): 278-294.

Strassberg, G., Scanlon, B.R. and Chambers, D., 2009. Evaluation of groundwater storage monitoring with the GRACE satellite: Case study of the High Plains aquifer, central United States. Water Resour Research, 45(W05410), doi:10.1029/2008WR006892.

Sutcliffe, J.V. and Parks, Y.P., 1999. The hydrology of Nile. International Association of Hydrological Sciences, Special Publication No.5, Oxfordshire, UK, 192 pp.

Swenson, S., Famiglietti, J., Basara, J. and Wahr, J., 2008. Estimating profile soil moisture and groundwater variations using GRACE and Oklahoma Mesonet soil moisture data. Water Resour Research, 44(W01413), doi:10.1029/2007WR006057.

Syed, T.H., Famiglietti, J.S., Rodell, M., Chen, J. and Wilson, C.R., 2008. Analysis of terrestrial water storage changes from GRACE and GLDAS. Water Resources Research, 44(W02433), doi:10.1029/2006WR005779.

Tapley, B.D., Bettadpur, S., Ries, J.C., Thompson, P.F., and Watkins, M., 2004). GRACE measurements of mass variability in the Earth system Science 305, 503-505, doi:10.1126/science.1099192.

Taye, M.T. and Willems, P., 2012. Temporal variability of hydroclimatic extremes in the Blue Nile basin. Water Resources Research, 48(W03513), doi:10.1029/2011WR011466.

UNEP/DEWA, 2012. Support to sustainable development in the Lake Turkana Basin for human well-being, regional assessment 47. Global International Waters Assessment and United Nations Environment Programme, University of Kalmar, Kalmar, Sweden.

United Nation, 2008. Handbook on the least developed country category: inclusion, graduation and special support measures. Committee for Development Policy and United Nations, Department of Economic and Social Affairs, New York, 101 pp.

Uitto, J. and A. Duda. 2002. Management of transboundary water resources: lessons from international cooperation for conflict prevention. The Geographical Journal Vol. 168, (4):363-378

Wahr, J., Molenaar, M. and Bryan, F., 1998. Time-variability of the Earth's gravity field: Hydrological and oceanic effects and their possible detection using GRACE. . Journal of Geophysical Research, 103 (B12) 3220530229, doi: 10.1029/98JB02844.

Wahr, J.M., 2007. Time-Variable Gravity From Satellites. In: T. Hearing (Editor), Treatise on Geophysics. Elsevier, Boston.

Werth, S., A.Guntner, R.Schmidt and Kusche, J., 2009. Evaluation of GRACE filter tools from a hydrological perspective. Geophys J Int 179: 14991515, doi:10.1111/j.1365-246X.2009.04355.x.

Wolde-Georgis, T., 1997. El Niño and Drought Early Warning in Ethiopia. Internet Journal of African Studies, http://www.esig.ncar.edu/ijas/ijasno2/wolde-georgis.htm..

World Bank, 2006. World Bank Country Water Resources Assistance Strategy, Ethiopia: Managing Water Resources to Maximize Sustainable Growth, REPORT NO. 36000-ET. The World Bank Agriculture and Rural Development Department, Washington, DC, 119 pp.

World Bank., 2009. Disaster Risk Management Programs for Priority Countries Global Facility for Disaster Reduction and Recovery, Washington, DC, USA.

Wright, P.E. and Burgess, W.G. (Editors), 1992. The hydrogeology of crystalline basement aquifers in Africa, 66. British Geological Society, London, UK, 264 pp.

Yadav, M., Wagener, T. and Gupta, H., 2007. Regionalization of con-straints on expected watershed response. Adv. Water Resour., 30: 1756-1774, doi:10.1016/j.advwatres.2007.01.005.

Yeh, P.J.-F., Swenson, S.C., Famiglietti, J.S. and Rodell, M., 2006. Remote sensing of GW storage changes in Illinois using the Gravity Recovery and Climate Experiment (GRACE). Water Resour Research, 42(W12203), doi:10.1029/2006WR005374.

Yirdaw, S.Z., Snelgrove, K.R. and Agboma, C.O., 2008. GRACE satellite observations of terrestrial moisture changes for drought characterization in the Canadian Prairie. Journal of Hydrology, 356: 84-92, doi:10.1016/j.jhydrol.2008.04.004.

Yitbarek, A., Razack, M., Ayenew, T., Zemedagegnehu, E. and Azagegn, T., 2012. Hydrogeological and hydrochemical framework of Upper Awash River basin, Ethiopia: with special emphasis on inter-basins groundwater transfer between Blue Nile and Awash Rivers. Journal of African Earth Sciences 65: 46-60, doi:10.1016/j.jafrearsci.2012.01.002.

Zhang, Z., Wagener, T., Reed, P. and Bhushan, R., 2008. Reducing uncertainty in predictions in ungauged basins by combining hydrologic indices regionalization and multi objective optimization. Water Resources Research, 44(W00B04), doi: 10.1029/2008WR006833

PART-II

Hydrological Characterization and Classifications of Baro-Akobo Watersheds in Western Ethiopia using Remote Sensing Datasets and Models

ABSTRACT

The use of remotely sensed data and models are increasingly used as a way of approaching hydrologic behaviors in ungauged and remote watersheds, particularly in developing countries where the availability of observed data is limited. The aim of this study was to apply remotely sensed data and model to Baro-Akobo watersheds in west Ethiopia in order to i) hydrologically characterize the watersheds, and ii) classify the watersheds based on their hydrologic similarity. The procedure consists of (1) generating annual synthetic runoff data using dynamic water balance model with satellite rainfall and evapotranispiration inputs, (2) driving the watersheds climate, functional response and form indicators from remote sensing and synthetic runoff data, and (3) characterizing and classifying catchments based on their hydrologic similarity. The sources data used in this study includes; TRMM (rainfall), MODIS (potential and actual evaporation) and ASTER (digital elevation model). The results shows that, about 70% of the watersheds in the basin have evaporative index value of greater than 0.7, and more than 80% of the watersheds have runoff coefficient of less than 0.40, indicating that much of the water coming to the basin leaves as green water. Stream flow elasticity analysis also implies that basin watersheds are highly sensitive to change in precipitation. The morphometric analysis (hypsometric curve) of the watersheds describes that more than 60% of the watersheds have reached their equilibrium stage while only less than 10% are at their in-equilibrium stage. The analysis made on spatial distribution of wetness index showed that nearly 40% of the watersheds TWI distribution function follows Generalized Pareto type while it is Wakeby lower bound distribution type for 30% of the catchments. The catchment classification made using the agglomerative hierarchical cluster analysis shows that most of the highland dominated catchments in eastern regions fall under similar category.

Keywords: catchment climate, catchment functions, catchment forms, water balance, ungauged catchments

CHAPTER ONE

INTRODUCTION

Catchments hold uniqueness and complexity in their behaviors (Beven, 2000). Despite the advancements in watershed hydrology over the past decades, full understanding of the interactions between climate inputs and landscape characteristics has been a challenge for hydrologists. The supreme challenge comes from changes in the forces acting on the landscape and the way change is transmitted through the various associated systems and subsystems(Black, 1997;Schaefli et al., 2011). The tremendous heterogeneities in climatic inputs and landscape properties also hold the responsibilities (Sivakumar and Singh, 2012). One way to press forward our understanding of watershed hydrology is to classify watersheds based on their influential parameters(McDonnell et al., 2007). This will enable us to sort and group the tremendous variability in space, time, and process(McDonnell and Woods, 2004), but a classification system should characterize the mechanisms of movement and storage of water. Even though studies in watershed hydrology continued to characterize and catalogue the enormous heterogeneity and complexity of rainfall runoff processes based on their degree of similarity, the ability to generalize these findings to ungauged regions remains out of reach(McDonnell et al., 2007).

Classification based on hydrologic similarity is a crucial step in improving predictions in ungauged basins (Sivapalan et al., 2003), and also to synthesize our understanding of the interaction between climate variability and catchment characteristics(Carrillo et al., 2011;McDonnell and Woods, 2004;Wagener et al., 2007). Like many other watersheds of Ethiopia most of the Baro-Akobo basin sub catchments are ungauged. The available stream and metrological gauging stations in the basin are mostly located along the main river system and

also placed along the road ways throughout the region. This has been leading to limited knowledge about the watersheds, error in water availability estimations and improper water resources exploitation. In order to classify ungauged catchments under their most likely group we need to understand why a given catchment belongs to certain groups of hydrologic behavior (Carrillo et al., 2011).One of the major obstacles to this issue is lack of reliable quantitative information about the ungauged catchments which block the opportunity to observe their resemblance to certain class.

Numerous studies have been conducted in different parts of the world focused on the grouping of catchments based on their hydrologic similarities while considering different perspectives. For instance, Burn, 1997 used cluster analysis to group catchment based on their similarity for regional flood frequency analysis. Sawicz et al. 2011 classified 280 catchments in the US based on their empirically retrieved hydrologic signatures using a Bayesian clustering scheme and reported that nine group of catchments exist. Similarly, Carrillo et al. 2011 investigated catchment classification using process-based modeling to interrogate how climate and catchment characteristics interact to produce observed hydrologic response. They presented that only limited number of model parameters can be related to observable landscape features. Ley et al., 2011 also introduces similarity approach based on self organizing maps, to group gauged catchments in Germany considering runoff behaviors.

Wagener et al., 2007, described that catchment classification in hydrology can be based on structural catchment characteristics in form of dimensionless numbers, curves or distributions, and conceptual and mathematical models. When it is done based on hydroclimatic characteristics, where the main variables are precipitation, potential evaporation, and runoff, a valuable way of combining these variables is through a dimensionless numbers like climatic

dryness index (Wagener et al., 2007). They also argued that behavioral signatures which should include stream flow should be used to classify catchments based on their functional response.

1.1. Relevance of the research

Characterization and classification of catchments requires intensively collected data at fine spatial and temporal resolutions. In regions where data from conventional measurement approaches are scares remote sensing data provides an alternative source of information. The data used in this study includes rainfall from the Tropical Rainfall Measuring Mission (TRMM) satellite, actual evapotranispiration (AET) and potential evapotranispiration (PET) from the MOderate Resolution Imaging Spectroradiometer (MODIS) remote sensor, and the 30m-Digital Elevation Model (DEM) data from Advanced Spaceborn Thermal Emission and Reflection Radiometer (ASTER). The approach employed in this paper uses TRMM-3B42 version 7 rainfall, and MOD16 AET and PET to derive catchment climate indices. The dynamic water balance model framework was also used to extract catchment function signatures as well as the ASTER-DEM to obtain the catchment structure descriptors. Then following Ward, 1963, the agglomerative hierarchical cluster analysis (AHCA) method is used to group catchments based on their similarity. In this study, AHCA is first applied on individual parameter. Then on catchment climate, catchment function and catchment form to make them categorized. Finally, all parameters are combined to form a first stage preliminary classification.

1.2. Research Objectives

General Objective

The main objective of this study is to employ remotely sensed data and models to hydrologically characterize and catalogue watersheds based on their hydrologic similarity in data limited regions.

Specific Objectives

The specific objectives of current study includes,

(i) To characterize Baro-Akobo watersheds based on indexes, distribution function and/or curves,

(ii) To classify catchments based on their climate (evaporative and dryness index), function signatures (runoff coefficient and stream flow elasticity) and structure (topographic wetness index and hypsometric curve), and

(iii) To provide preliminary stage catchment classification, this is important to give a clue of ungauged catchments resemblance.

1.3. Research Questions

- Can we characterize the Baro-Akobo basin using remotely sensed climatic and watershed variables?

- How can we cluster the Baro-Akobo basin into hydrologically homogenous regimes using catchment signatures derived from remotely sensed data's?

1.4. Structure of the thesis

The remainder of the study is organized as follows; the study region and satellites and models employed are presented in sections 2 and 3, followed by, data and methods of analysis in section 4, results in section 5, discussion in section 6 and conclusions and recommendations in section 6.

CHAPTER TWO

STUDY REGION

Geographically the Baro-Akobo basin extends between 5 ^{0} 31'N to 10 ^{0} 54'N latitudes and 33 ^{0} 00'E to 36 ^{0} 17' E longitudes. The basin emanates from Central Highlands of Ethiopia and oriented towards West of Ethiopia, making a part of the Nile drainage system (Fig. 1). The drainage area of the basin is about 6.9 % of Ethiopia (75, 912 Km^2). Despite its size, the basin has the second largest annual flow next to Abbay, the second highest irrigation potential which is located next to Genale-Dawa and is also counted as the third hydro electric potential after Abbay and Omo-Ghibe(Awulachew et al., 2007). The estimated annual runoff and groundwater potential is about 23.6 and 1 billion cubic meters respectively (MoWR, 2012), which accounts about 26 % of the total annual flow of the Nile river. The altitude of Baro-Akobo basin ranges from 395 m at Ethio-Sudanese border to 3,266 m above mean sea level in Central Highlands. The annual rainfall varies from about 1,800 mm to over 2,200 mm; the mean annual evapotranispiration is about 1800 mm and the mean annual temperatures in the basin range from about 17.5°C on the highlands to about 27.5°C on the flood plains(MoWR, 2012). The topographical setting and hydrological characteristics of the lower Baro-Akobo regions have led to the creation of extensive waterlogged areas, basically categorized into two; i) the watersheds are characterized by the land surface covered with water throughout the year forming a marshland and ii) the other type is when waterlogged land is under water for part of the year(Woube, 1999).

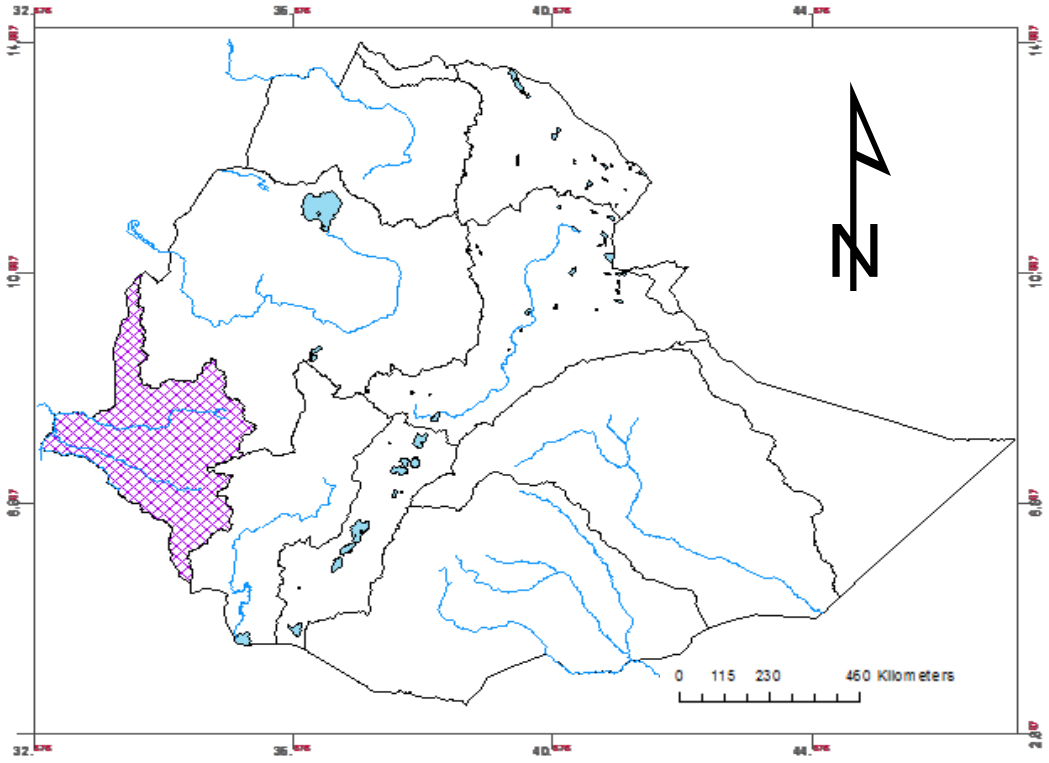

Figure 25: Location of Baro-Akobo basin (shaded)

CHAPTER THREE

REMOTE SENSORS AND MODELS USED

3.1. Satellites

3.1.1. Moderate Resolution Imaging Spectroradiometer (MODIS)

MODIS is the National Aeronautics and Space Administration (NASA) payload scientific instrument which was launched in December 1999 on board Terra satellite, and in 2002 on board Aqua satellite. Terra MODIS and Aqua MODIS orbit around the earth at an altitude of 705 Km, and viewing the entire Earth's surface every 1 to 2 days. MODIS mission is to provide measurements in large-scale global dynamics including changes in Earth's cloud cover, radiation budget and processes occurring in the oceans, on land and in the lower atmosphere. The instruments capture data in 36 spectral bands ranging in wavelength from 0.4 μm to 14.4 μm and at varying spatial resolutions (2 bands at 250 m, 5 bands at 500 m and 29 bands at 1 km).

A) Terra B) Aqua

Figure 26: MODIS Terra and Aqua Satellites

MODIS Evapotranispiration Algorithm

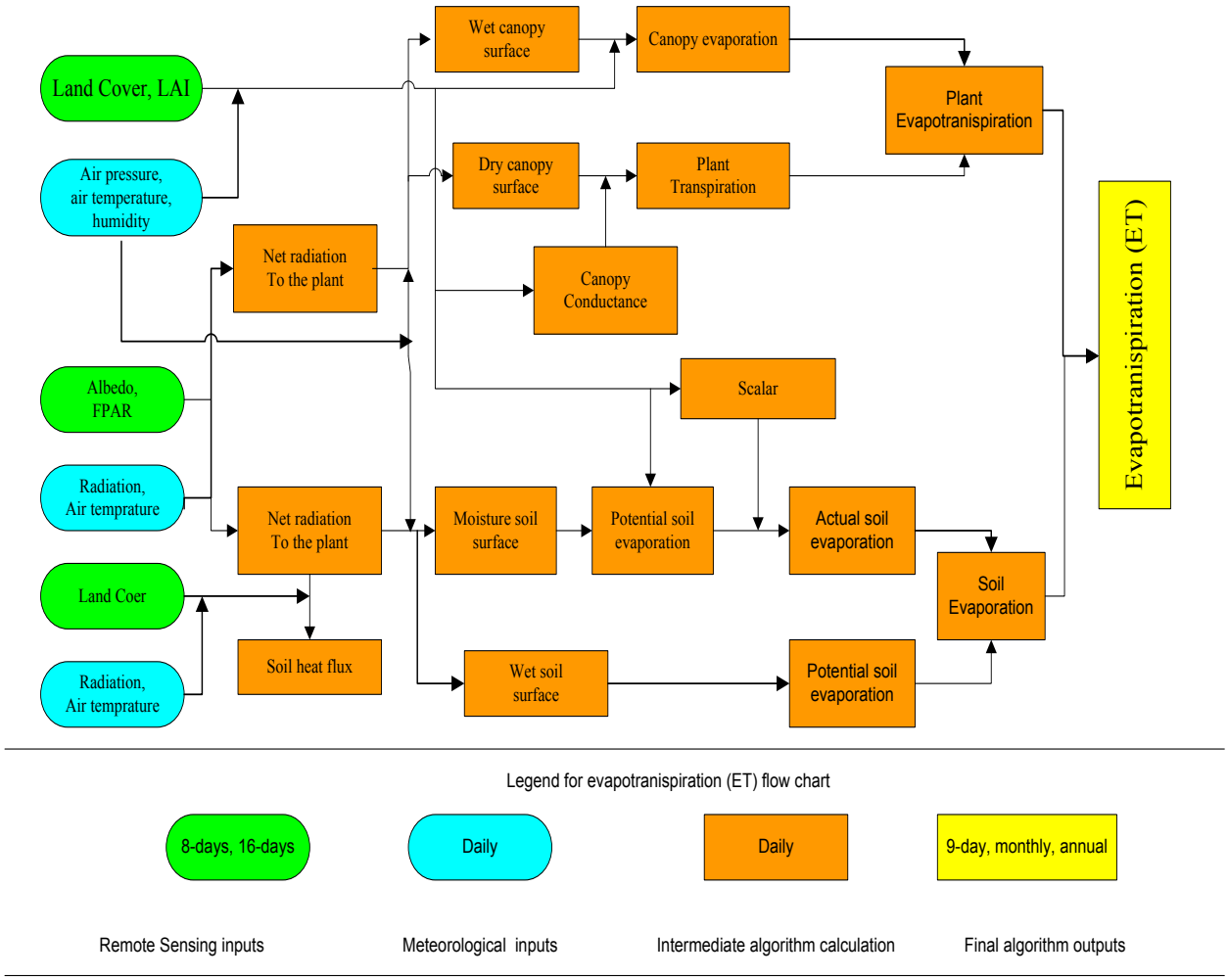

Figure 27: MODIS Evapotranispiration Algorithm (Source: Mu, et al., 2011)

3.1.2. Tropical Rainfall Measuring Mission (TRMM)

TRMM has been discussed in detail in section 2.5 of part one of this thesis

3.1.3. Advanced Spaceborn Thermal Emission and Reflection Radiometer (ASTER)

ASTER is a joint remote sensing mission between NASA, Japan's Ministry of Economy, Trade and Industry (METI), and Japan Space Systems. It was launched in December 1999 onboard Terra (Fig. 26 A). The ASTER instrument consists of three subsystems which include

the Visible and Near Infrared (VNIR), the Shortwave Infrared (SWIR), and the Thermal Infrared (TIR). The ASTER Global Digital Elevation Model (ASTER GDEM) has two products which are released for distribution at no charge to all users on 29 June 2009 (Version 1), and on October 17, 2011 (Version 2). They are one of the most complete mapping of the earth ever made, covering 99% of the Earth's landmass (±180 longitudes and ±83 latitudes), both have a spatial resolution of 30m.

3.2. Models

3.2.1. The Dynamic Water Balance Model

The dynamic water balance model derivation approach expressed in this subsection is adopted from Zhang et al., (2008). The dynamic water balance of any watershed can be written as

$$\frac{d}{dt}w(t) = P(t) - E(w,t) - Q(w,t) \quad (1)$$

Where w (t) is the soil water store in the catchment, and P (t), E (w, t), and Q (w, t) are precipitation, evapotranspiration and runoff. When equation (1) is integrated over a time interval T, one obtains,

$$\frac{w(T)-w(0)}{T} = P - E - Q \quad (2)$$

Where P, E and Q are time-averaged water fluxes

$$P = \frac{1}{T}\int_0^T P(t)dt, E = \frac{1}{T}\int_0^T E(t)dt, Q = \frac{1}{T}\int_0^T Q(w,t)dt \quad (3)$$

The left hand side of equation (2) accounts for the effect of water storage changes in the time-averaged water balance and decreases relative to the right hand side as T increases. If T is long

enough, i.e., decades, the storage term can be neglected relative to the fluxes and equation (2) becomes,

$$\mathbf{0} = \boldsymbol{P} - \boldsymbol{E} - \boldsymbol{Q} \quad (4)$$

This is thought as the "equilibrium" or "steady-state" water balance. It is a holistic approach that assumes the equilibrium water balance is controlled by water availability and atmospheric demand. The water availability can be approximated by precipitation; the atmospheric demand represents the maximum possible evapotranspiration and is often considered as potential evapotranspiration. Based on phenomenological considerations, Fu (1981) developed the following relationships for estimating mean annual evapotranspiration:

$$\frac{\boldsymbol{E}}{\boldsymbol{P}} = \mathbf{1} + \frac{\boldsymbol{E_o}}{\boldsymbol{P}} - \left[\mathbf{1} + \left(\frac{\boldsymbol{E_o}}{\boldsymbol{P}}\right)^{\boldsymbol{\alpha}}\right]^{\mathbf{1}/\boldsymbol{\alpha}} \quad (5)$$

Where E_0 is potential evaporation and α is a model parameter.

The method of Fu (1981) is similar to Budyko (1958) and assumes that the equilibrium water balance is controlled by water availability and atmospheric demand. On mean annual time scale, the water availability can be approximated by precipitation, while the atmospheric demand is represented by potential evapotranspiration. By combining equations (4) and (5), one obtains the following expression for mean annual runoff:

$$\mathbf{Q} = \left(\boldsymbol{P}^{\boldsymbol{\alpha}} + \boldsymbol{E}_{\boldsymbol{o}}^{\boldsymbol{\alpha}}\right)^{\mathbf{1}/\boldsymbol{\alpha}} - \boldsymbol{E_o} \quad (6)$$

Dynamic water balance model

In moving from mean annual to shorter time scale, i.e., decreasing T, one generally has to account for the effect of catchment water storage change on the water balance. Unlike the

equilibrium water balance modelling, little effort has been made to address the issue of inter annual variability in water balance. Koster and Suarez (1999) assumed that inter annual changes in catchment water storage are much smaller than the annual precipitation, evaporation, and runoff. As result, they suggested the following expression for evaporation ratio in a given year i:

$$\left(\frac{E}{P}\right)_i = F\left(\left(\frac{E_o}{P}\right)_i, \alpha\right) \quad 7$$

Where F is equation (5). Based on the above relationship and by assuming negligible inter annual variations in potential evapotranspiration, Koster and Suarez (1999) further showed that the ratio of the standard deviation of annual evaporation to that of annual precipitation can be expressed as a function of index of dryness:

$$\frac{\sigma_E}{\sigma_P} = F(\varphi) - \varphi F'(\varphi) \quad 8$$

Where Φ, is the dryness index. Equation (8) is called the evaporation deviation ratio. Large values of this ratio indicate that most of precipitation variability becomes evapotranspiration variability, whereas small values mean that evapotranspiration variability is largely insensitive to variability in rainfall. From this relationship, Koster and Suarez (1999) showed that the ratio of the standard deviation of annual runoff to the standard deviation of annual precipitation can also be expressed as:

$$\frac{\sigma_Q}{\sigma_P} = 1 - \frac{\sigma_E}{\sigma_P} \quad 9$$

Equation (9) can be used to describe inter-annual variability of stream flow (Sankarasubramanian and Vogel, 2002). One can also estimate annual runoff from equation (10) in analogy to equation (6) by ignoring inter annual water storage change:

$$Q_i = (P_i^{\alpha} + E_{oi}^{\alpha})^{1/\alpha} - E_{oi} \quad (10)$$

Where subscript i represents year.

3.2.2. Watershed Hypsometric Curve Properties

A hypsometric curve is a graphical representation of the distribution of area with elevation (Langbein, 1947) or the relative proportion of the watershed area that lies at or above a given height relative to total watershed relief (Strahler, 1952). Hypsometric curve can distinguish watersheds dominated by surface runoff (fluvial landforms – concave hypsometry) from watersheds dominated by subsurface runoff (terrestrial sapping landform – convex hypsometry). The most used parameter representing the shape of a hypsometric curve is the hypsometric integral (Luo 2000; Vivoni et al 2008) with a value of 0.5 representing a threshold between concave (<0.5) and convex (≥0.5) hypsometric forms.

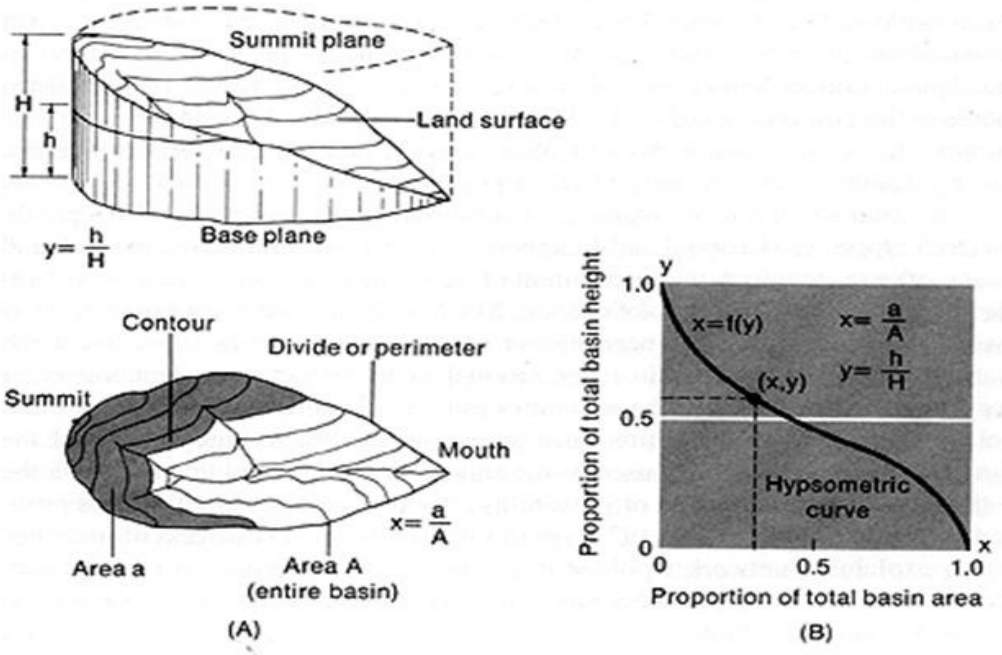

Figure 28: Watershed hypsometric curve descriptions

However, Strahler (1952) used values of <0.35 as a monadnock stage, 0.35 to 0.6 as the equilibrium stage, and ≥0.6 as the young (inequilibrium) stage. But as certain hypsometric integral value might be resulted from two very different hypsometric curves, the use of hypsometric integral only in catchment classification is not reliable. Therefore, we need to add some basic parameters which describe a given hypsometric curves distinctly, this includes hypsometric skewness, hypsometric kurtosis, density skewness and density kurtosis. The following equations, which are used to calculate the descriptors of the curves, are adopted from Harlin, (1998).

Hypsometric Integral (HI):

$$\boldsymbol{HI} = \iint_{\boldsymbol{R}} \boldsymbol{dxdy} \tag{11}$$

Where R = the region under the hypsometric curve, x= relative area, and y= relative height.

Hypsometric Skewness (SK):

$$\boldsymbol{SK} = \frac{\boldsymbol{\mu_{30}}}{\left(\boldsymbol{\mu_{20}^{1/2}}\right)^{3}} \tag{12}$$

Where, $\mu_{30} = the\ third\ moment\ about\ x.$

$$\boldsymbol{\mu_{30}} = \frac{\boldsymbol{1}}{\boldsymbol{HI}} \iint (\boldsymbol{x} - \boldsymbol{\mu_{20}})^{\boldsymbol{3}} \boldsymbol{dxdy} \tag{13}$$

$\mu_{20} = the\ second\ order\ moment\ about\ x\ or\ variance$

$$\boldsymbol{\mu_{10}} = \frac{\boldsymbol{1}}{\boldsymbol{HI}} \iint (\boldsymbol{x} - \boldsymbol{\mu_{10}})^{\boldsymbol{2}} \boldsymbol{dydx} \tag{14}$$

$$\boldsymbol{\mu_{10} = the\ first\ order\ moment\ about\ x\ or\ X - mean}$$

$$\boldsymbol{\mu_{10} = \frac{1}{HI}\iint_R xdydx} \quad 15$$

Hypsometric Kurtosis (KURT):

$$\boldsymbol{KUR = \frac{\mu_{40}}{\left(\mu_{20}^{1/2}\right)^4}} \quad 16$$

Where $\mu_{40} = the\ fourth\ order\ moment\ about\ x$

$$\boldsymbol{\mu_{40} = \frac{1}{HI}\iint (x - \mu_{10})^4 dydx} \quad 17$$

Density skewness (DSK) and density kurtosis (DKUR) are defined similarly except that y is the first derivative of the hypsometric curve (i.e., the density function of the hypsometric curve replacing y with y').

3.2.3. L-Moment

L-moments are expectations of certain linear combinations of order statistics. L-moment statistics are used for computing sample statistics for data at individual sites; for testing homogeneity/heterogeneity of proposed groupings of sites (regions); for conducting goodness-of-fit tests for identifying a suitable probability distribution(s); and for solving for distribution parameters for the selected probability distribution. The L-moment measure of location and L-moment ratio measures of skewness and kurtosis are:

L-Skewness (τ_3):

$$\boldsymbol{\tau_3 = L_3 / L_2} \quad 18$$

L-Kurtosis (τ_4):

$$\tau_4 = L_4/L_2 \quad (19)$$

Where:

$$L_1 = \beta_o \quad (20)$$

$$L_2 = 2\beta_1 - \beta_o \quad (21)$$

$$L_3 = 6\beta_2 - 6\beta_1 + \beta_o \quad (22)$$

$$L_4 = 20\beta_3 - 30\beta_2 + 12\beta_1 - \beta_o \quad (23)$$

Where the data ($x_{1:n}$) are first ranked in ascending order from 1 to n and:

$$\beta_o = n^{-1} \sum_{j=1}^{n} x_j \quad (24)$$

$$\beta_1 = n^{-1} \sum_{j=1}^{n} x_j[(j-1)/(n-1)] \quad (25)$$

$$\beta_2 = n^{-1} \sum_{j=1}^{n} x_j[(j-1)(j-2)/(n-1)(n-2)] \quad (26)$$

$$\beta_3 = n^{-1} \sum_{j=1}^{n} x_j[(j-1)(j-2)(j-3)/(n-1)(n-2)(n-3)] \quad (27)$$

A distribution type or category under which our sample data falls, we need to use L-Moment ratio diagram. A diagram based on L-Moment ratios (measure of skewness versus measure of kurtosis). To identify the distribution type L-moment ratio diagram for some common distribution should be plotted with sample L-moment ratios on the same graph (Fig 6.).

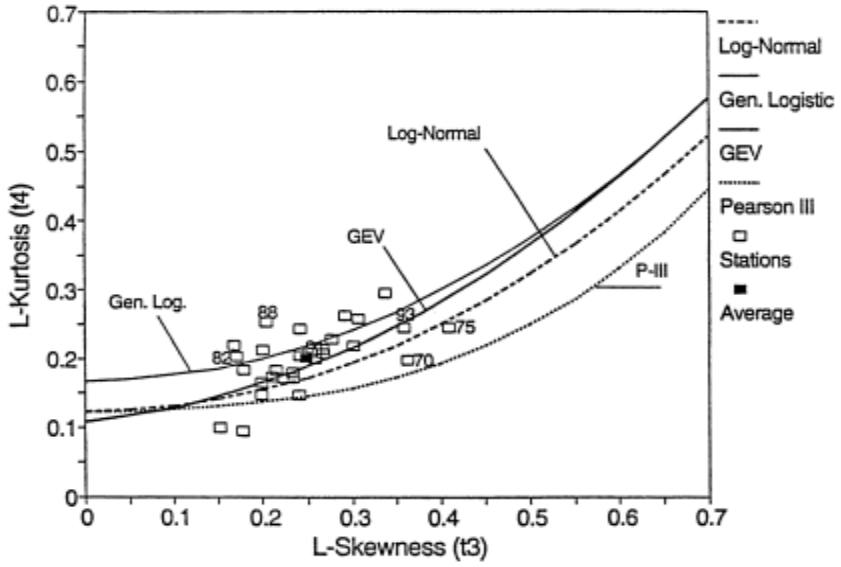

Figure 29: L-Moment ratio diagram

3.2.4. Cluster Analysis

Cluster Analysis groups data objects based only on information found in the data that describes the objects and their relationships. The goal is that the objects with in a group be similar to one another and different from the objects in other groups. The greater the similarity within a group and the greater the difference between groups the better or more distinct the clustering. There are various types of clustering. From different perspectives they can be categorized as hierarchical (nested) and partitional (unnested), exclusive, overlapping and fuzzy, and complete and partial clustering. The most commonly discussed distinction among those types of clustering is whether the set of clusters is nested or unnested. A partitional clustering is simply a division of the set of data objects into non-overlapping subsets such that each data object is in exactly one subset. The hierarchical clustering allows clusters to have sub-clusters; it is a set of nested clusters organized as a tree. Each cluster in the tree (except for leaf nodes) is union of its children (sub-clusters), and the root of the tree is the cluster containing all the objects. Based on where the clustering

starts the hierarchical clustering can be classified into two different approaches, the agglomerative (bottom up) and divisive (top-down) clustering. In this study we employed the agglomerative hierarchical clustering method, so only this approach has been discussed in detail in the following subsection.

Agglomerative Hierarchical Clustering Method

It begins with as many clusters as objects. Clusters are successively merged until only one cluster remains. This approach requires defining the notion of clustering proximity. It is often displayed graphically using a tree-like diagram called a dendrogram. A dendrogram is a visualization tool used to display data points and the value they represent (Fig. 30). In this application, the catchments are considered points of data and the values they represent are values of each signature/distribution.

There are different ways of the clustering proximity or distance (y axis of Fig. 30). The most commonly used and the one employed in this study is the Ward's clustering method of calculating distances, which is expressed in equation 28. It is the most useful type of combining values in order to preserve the amount of information within each point of data (Ward, 1963).

$$\mathbf{ESS} = \sum_{\mathbf{i=1}}^{\mathbf{n}} \mathbf{z_i^2} - \frac{\mathbf{1}}{\mathbf{n}} \left(\sum_{\mathbf{i=1}}^{\mathbf{n}} \mathbf{z_i}\right)^{\mathbf{2}} \qquad \mathbf{28}$$

Where ESS is the error sum of squares, z_i, is the z-score of the i^{th} catchment which is given by

$$\mathbf{z_i} = \frac{\boldsymbol{\alpha_i} - \bar{\boldsymbol{\alpha}}}{\boldsymbol{\sigma}}$$

Where $\alpha_i$data is value at data point location i, $\bar{\alpha}$ is the mean of the data series and σ is the standard deviation of the data series. The purpose of using z-score is to none dimensionalize and normalize all of the different data series.

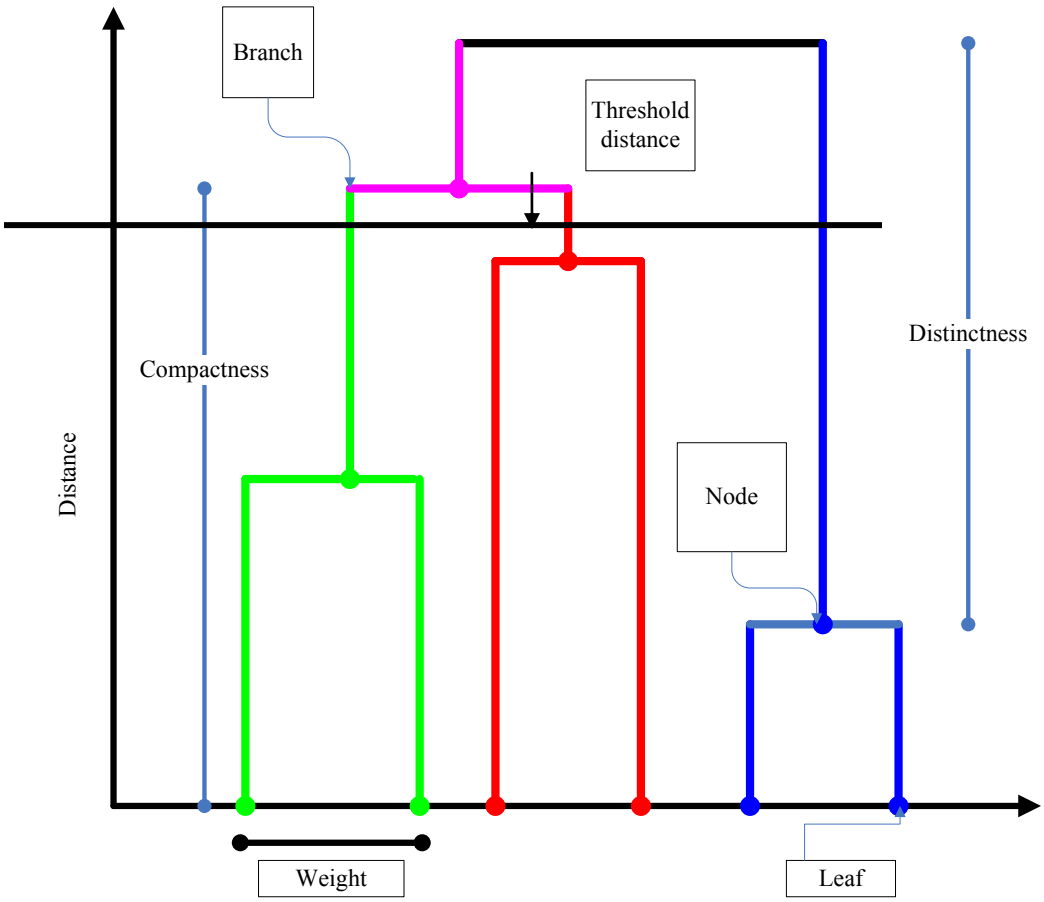

Figure 30: Schematic dendrogram introducing the descriptive terminology. The vertical axis represents a distance metric used in determining how close or far one catchment is to another catchment in signature space. The horizontal axis represents an order of catchments based on the cluster analysis. The distance threshold is shown as a black horizontal line, whereas the groups are shown in red and blue.

CHAPTER FOUR

DATA AND METHODS

4.1. Data

4.1.1. MODIS

MODIS data are placed under two broad categories, the daily scenes and derived products. These products are further separated into Land, Atmosphere, Cryosphere, and Ocean groups. The data used in this study is MOD16 derived land product data which covers the time period of twelve years (2000 – 2011). It provides global evapotranspiration (ET), latent heat flux (LE), potential ET (PET) and potential LE (PLE) datasets at 1 Km spatial domain and monthly time scale. The ET algorithm is based on the Penman-Monteith equation(Mu et al., 2007;Mu et al., 2011).

4.1.2. TRMM

Of its many products, TRMM-3B42 is one of the widely used products. The version used herein is its last TRMM version 7 data (Huffman and Bolvin, 2012). The TRMM data are 3-hourly rainfall rates, which has a fair spatial resolution of 0.25^0 x 0.25^0, obtained from NASA GES DISC. The 3-hourly rainfall rates have been converted to rainfall amount and aggregated to monthly then to annual basis.

4.1.3. ASTER

The ASTER Global Digital Elevation Model (ASTER GDEM) has two products which are released for distribution at no charge to all users on 29 June 2009 (Version 1), and on October 17, 2011 (Version 2). They are one of the most complete mapping of the earth ever made, covering 99% of the Earth's landmass (±180 longitudes and ±83 latitudes), both have a

spatial resolution of 30m. The improved product (GDEM V2) adds 260,000 additional stereo-pairs, improving coverage and reducing the occurrence of artifacts. The refined production algorithm provides improved spatial resolution, increased horizontal and vertical accuracy, and superior water body coverage and detection. The product used in this study was the ASTER GDEM version 2 obtained from the METI.

4.2. Methods of Analysis

The important classes of catchment behaviors which are believed to govern catchment hydrologic similarity are the catchment climate, catchment functions and catchment structures(Wagener et al., 2007). In this paper, (a) dryness index (DI) and evaporative index (EI) are selected from catchment climate, while (b) runoff coefficients (RC) and stream flow elasticity (SE) are from catchment function, and finally (c) hypsometric curves (HC) and topographic wetness indexes (TWI) are used as descriptors of catchment structures. The selection of the indexes/distributions was done due to their popularity and possibility of estimating them from remotely sensed data. The derivation of this indexes and distributions through remote sensing data and models are individually described in the following subsections. The Baro-Akobo watersheds which are to be classified are extracted using 30m ASTER GDEM. Out of the 41 extracted only 4 catchments has gauged stream flow data at their outlets (Fig. 29B (yellow)). The drainage areas of the watersheds range from 133 (Fig. 29B (blue)) to 5911 Km^2 (Fig. 29B (red)).

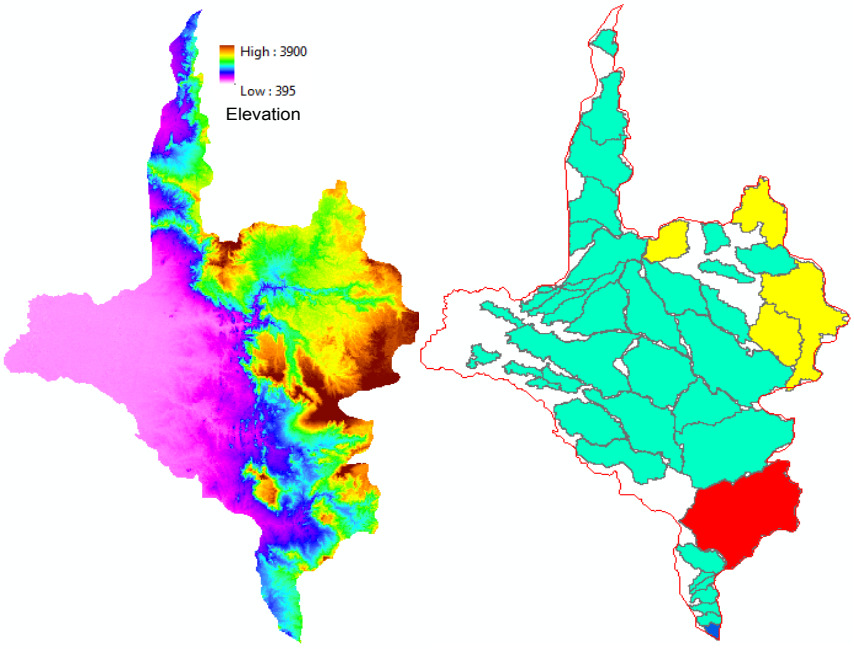

Figure 29: Baro-Akobo Basin Digital Elevation Model and derived sub-catchments

4.2.1. Catchment Signatures

a) **Catchment Climate Indexes**

Here, following (Budyko, 1958), the dryness index (DI) is defined as the ratio of Potential Evapotranispiration (PET) to Precipitation (P), while the evaporative index (EI) is the ratio of the actual potential evapotranispiration (AET) to precipitation. The precipitation data used was aggregated to monthly basis from TRMM-3B42 3-hourly product, while the AET and PET are obtained from MODIS.

b) Catchment Function Signatures

The catchment function signatures like runoff ratio, base flow index, slope of the flow duration curve, stream flow elasticity and recession coefficient are dependent on the gauged stream flow data. But out of the catchments to be classified, only five of them have runoff data at

their outlets (Fig. 29B). To overcome this, the total annual runoff is estimated for each watershed using the Budyko framework of dynamic annual water balance model approach presented in (Zhang et al., 2008)

Runoff coefficient

Runoff Coefficient (RC [-]) is a good signature of how much of the rainfall over the catchment have been converted to runoff. RC is defined as the ratio of long-term average stream flow to long-term average precipitation.

Stream flow Elasticity

Stream flow elasticity (SE [-]) is a descriptor of sensitiveness of the catchment's stream flow to the change in precipitation. SE can be computed as the ratio of change in stream flow to change in precipitation normalized by runoff coefficient. The median value is recommended as the robust measure since it filters out the outliers(Sawicz et al., 2011). For instance, a value of 1% indicates that 1% variation in precipitation will lead to 1% variation in stream flow. A value of greater than 1 indicates the catchment is elastic (i.e., sensitive to change in precipitation) and if it is less than 1 the catchment is insensitive to change in precipitation.

c) Catchment Structure

Topographic Wetness Index

Topographic wetness index (TWI) describes the propensity of a location in the catchment to become saturated. Distribution functions of this index for catchments form the basis of Top model(Beven and Kirkby, 1979). It is the ratio of the upslope contributing area (α) and the local surface topographic slope ($\tan \beta$). For characterization and classification of Baro-Akobo basin TWI is estimated from ASTER-30m GDEM. The analysis for all sub-catchments has been done

in System for Automated Geoscientific Analysis (SAGA). The distribution functions for gridded TWI data, generated from DEM, were obtained using L-moment method(Rao and Hamed, 2000). In this study, first the L-moment ratio diagrams of twelve commonly used distribution types namely, Uniform, Exponential, Gumble (Extreme Value I), Logistic, Normal, Generalized Pareto, Generalized Logistic, Generalized Extreme Value, Gamma and Pearson III, Lognormal, Wakeby lower bound and Overall lower bound have been developed. Second, the sample L-moments have been derived for each catchment and plotted over the common L-moment ratio diagram. Finally, the distribution types for each catchment are identified as the one to which their sample moments are very close. For catchment classifications, the first four sample moments of the each watersheds TWI are used.

Hypsometric Curve

The area beneath the hypsometric curve which is called hypsometric integral is an important pointer of watershed conditions (Ritter et al., 2002), but do not exactly differ catchments, as two different shapes have possibility of giving same answers. In addition to hypsometric integral the widely used ways of differing hypsometric curve of one catchment from the others is through the use of statistical moments of the curve. Following (Harlin, 1978), the statistical moments used in this study are skewness of hypsometric curve (SK), kurtosis of hypsometric curve (KU), skewness of hypsometric density function (DSK) and kurtosis of the hypsometric density function (DKU).

4.2.2. Catchments Clustering

In this study the Agglomerative Hierarchical Cluster Analysis (AHCA) method (Ward, 1963) was used to group catchments based on their hydrologic similarity. The data was centered and scaled using z-scores. The Euclidean distance of clustering which is calculated using Ward

method (Ward, 1963) is used to quantify distance between objects or group of objects. First the classification was made using all indexes, including curves (HC) and distributions (TWI) separately. Second, the indexes are combined as catchment climate, catchment function and catchment forms to be used for classifying the watersheds based on their climatic, response and structural similarity. Finally, the general classification of the watersheds in the basin has been made using all parameters.

CHAPTER FIVE

RESULTS

5.1. Catchment Characterizations

i) Based on Catchment Climate

Figure 30 shows the two prominent climate indexes, the dryness index (DI) and the evaporative index (EI). The numbers labeled on the maps describe dryness indices (Fig. 30A) and evaporative indices (Fig. 30B). The DI value ranges from 0.98 in the (western region) of the basin to 3.89 (eastern region). The lower values are obtained in the highland regions while they are higher in lowland regions of the basin (Fig. 29A). The lower values (< 1.54) indicate humid regions and the higher values are indicators of arid and semi arid region (> 2.0).

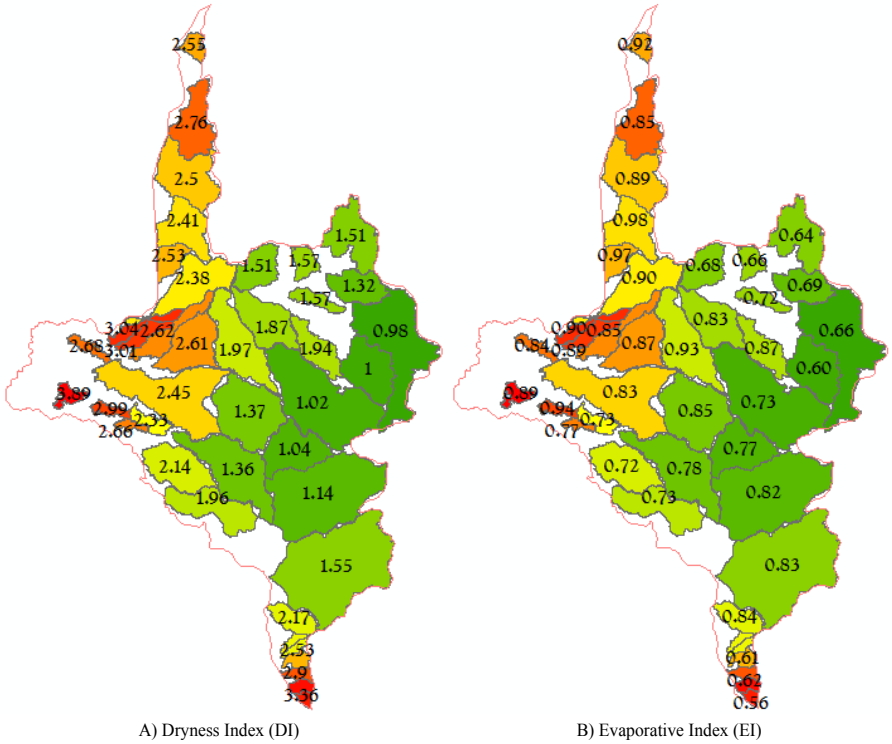

A) Dryness Index (DI) B) Evaporative Index (EI)

Figure 30: Climatic Indices (DI and EI) of the Baro-Akobo watersheds

The transition values between lower and higher values ($1.54 < DI \leq 2.0$) represent the dry sub humid regions. The evaporative index value in the basin ranges between 0.55 and 0.98. A higher evaporative index value indicates that larger portion of water coming to the catchment leaves as green water. The results indicate that most of the watersheds exist in medium region and only few of them are close to the energy limited and water limited lines.

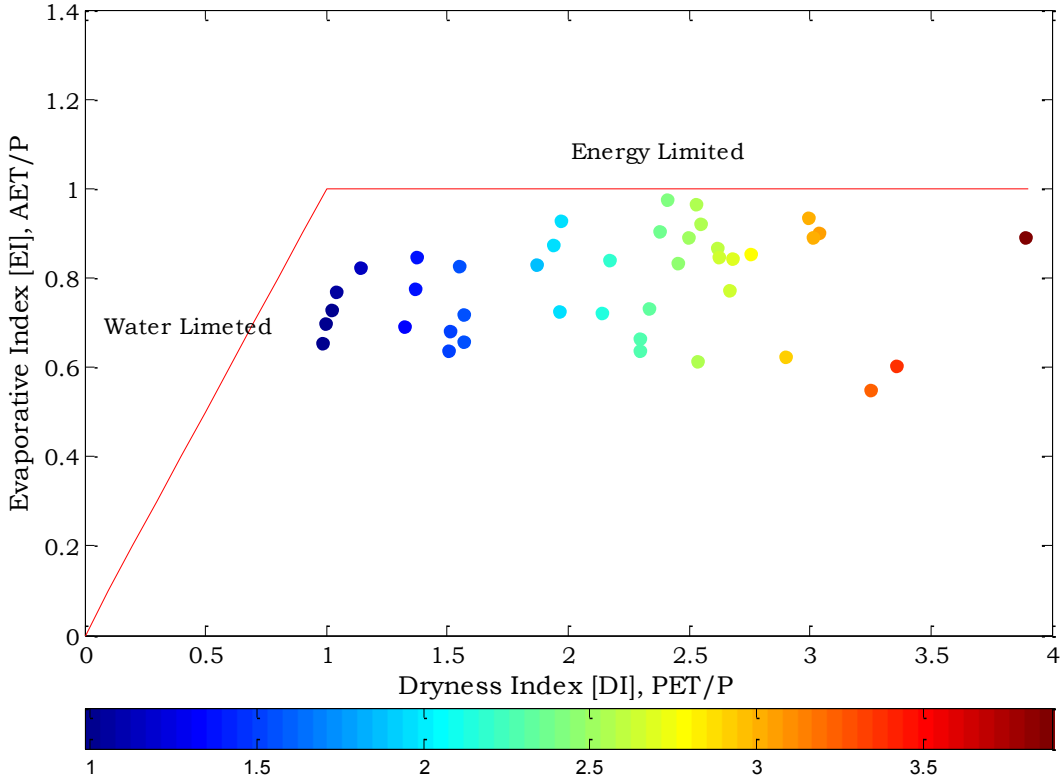

Figure 31: Budyko type curve for Baro-Akobo basin

ii) Based Catchment Functions

The scatter plots in Fig. 31 are fitted using Fu's equation (Fu, 1981), were the model parameter w is calibrated manually (Tekleab et al., 2011). Figure 32 shows a group of Fu curves with different model parameters and the catchments have been grouped based on their best fit

curve. Then using dynamic annual water balance model approach presented in (Zhang et al., 2008), synthetic annual runoff data for twelve years (2000 to 2011) have been generated for 41 sub catchments of Baro-Akobo basin. Using this data together with annual rainfall data obtained from TRMM, two basic catchment functions (runoff coefficient and stream flow elasticity) have been derived.

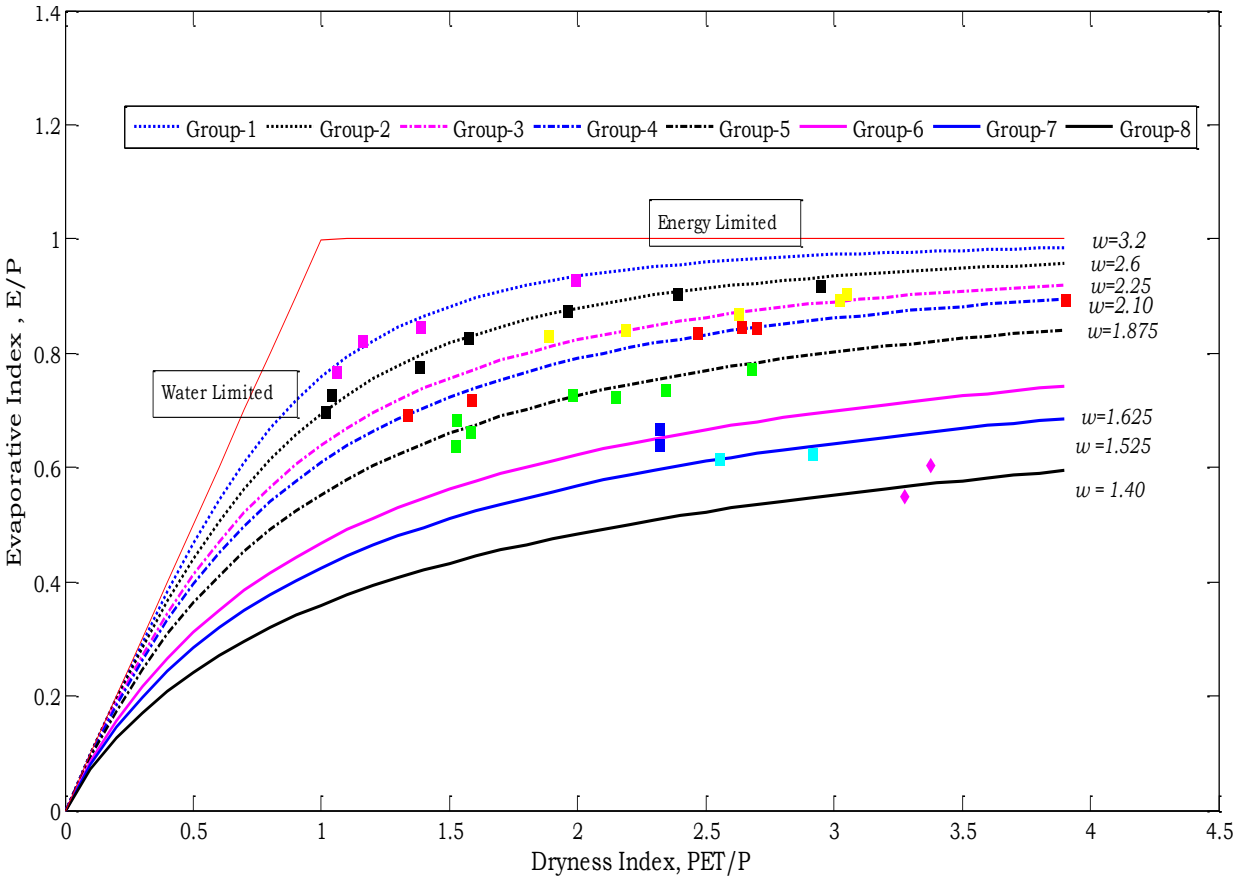

Figure 32: The ratio of mean annual evapotranspiration to rainfall (AET/P) as a function of the index of dryness (PET/P) for different values of parameter w fitted to Baro-Akobo basin watersheds.

The derived runoff coefficients and stream flow elasticity are described in Fig. 33. The runoff coefficients in the basin ranges from 0.09 to 0.76, with the higher coefficients indicating

large amount of water exiting the catchment as blue water and low value implies that larger portion of water available in the region leaves the catchment through evapotranispiration (i.e., green water). The minimum stream flow elasticity have been seen as 0.12 and the maximum is 2.29 with high values indicating a catchment that is relatively sensitive to changes in precipitation input between years and low values implying the catchment is insensitive to the inter annual variation of precipitation.

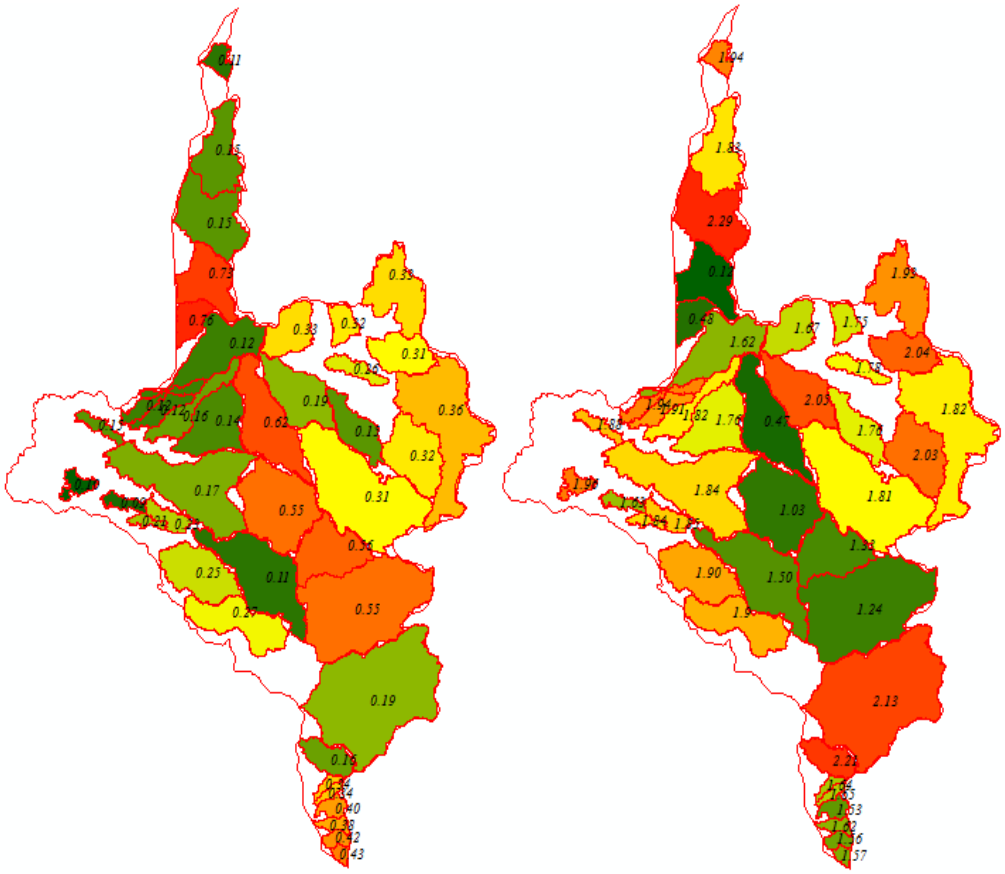

A) Runoff Coefficients B) Stream flow Elasticity

Figure 33: Runoff Coefficients and Stream flow elasticity of Baro-Akobo basin watersheds.

iii) Based On Catchment Structure

The two catchment form indicators (TWI and HC) have been derived from ASTER-30m DEM. To identify the characteristics of the TWI of 41 catchments in Baro-Akobo basin, the

spatial distributions of the TWI have been fitted to the twelve different distribution functions mentioned in section 3.1(c). The distribution function selection was done using L-moment ratio diagram method. The results obtained (Fig. 34A) shows that the Baro-Akobo basin watersheds fall under five distribution types (Lognormal, Gamma and Pearson III, Generalized Pareto, Generalized Extreme value and Wakeby lower bound). The catchments and their distribution types are shown in Fig. 34B.

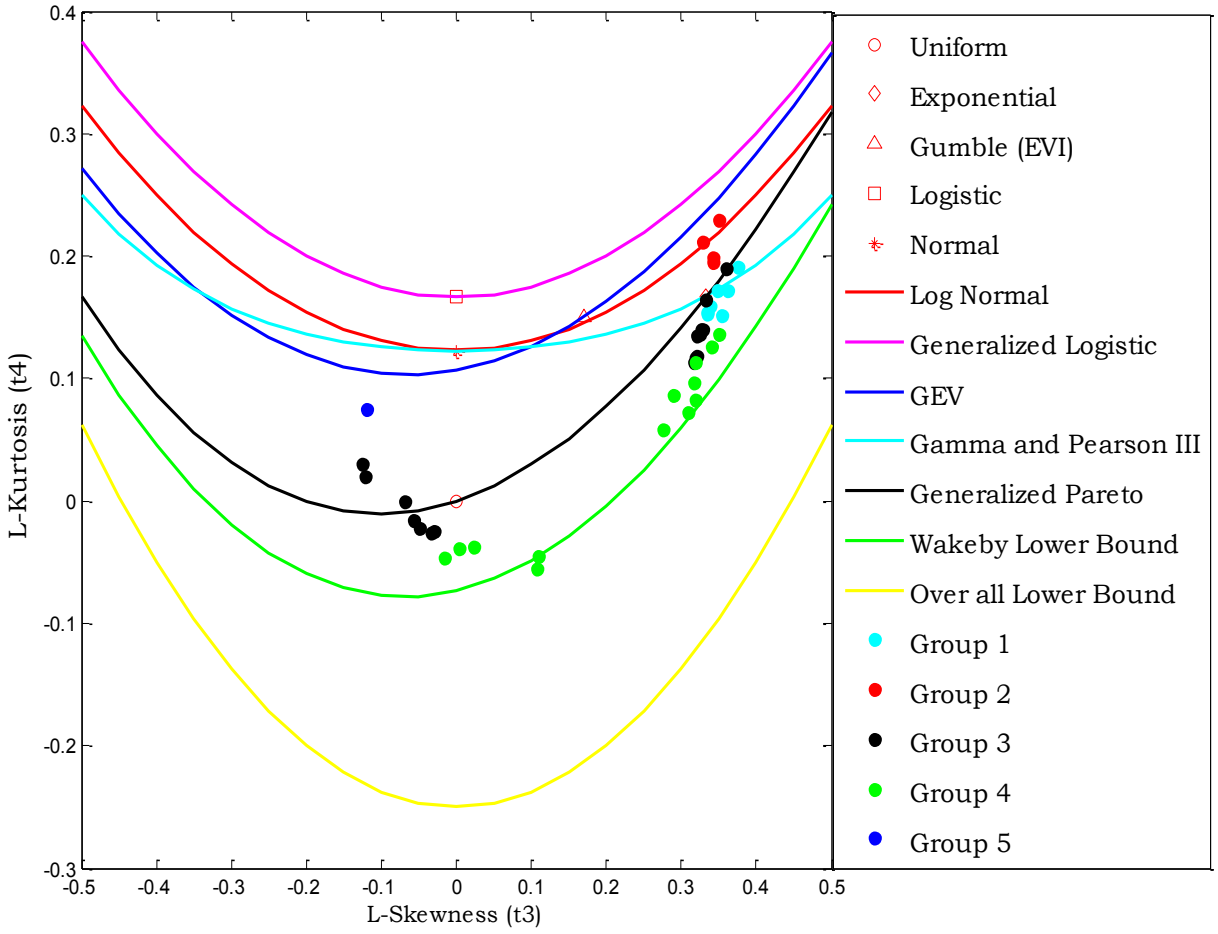

Figure 34A: L-Moment ratio diagram for 12 distribution types and sample moments of 41 sub-catchments of Baro-Akobo basin grouped based on the distribution type towards which they bear a resemblance.

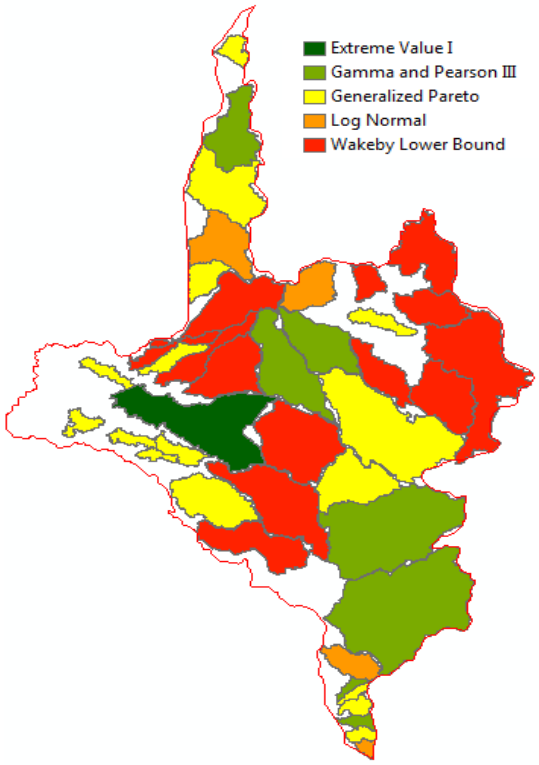

Figure 35B: Distribution functions of Baro-Akobo basin watersheds topographic wetness index.

Figure 35A and 35B describes the characteristics of Baro-Akobo watersheds based on their hypsometric curves. The hypsometric integral is one of the most used parameter, for representing the shape of a hypsometric curve (Luo, 2000;Vivoni et al., 2008), which is defined as the area under the hypsometric curve, with a value of 0.5 representing a threshold between concave (<0.5) and convex (≥0.5) hypsometric forms. According to (Strahler, 1952), catchment with hypsometric integral values of <0.35 are at their monadnock stage, 0.35 to 0.6 are at their equilibrium stage, and ≥0.6 at their young (inequilibrium) stage.

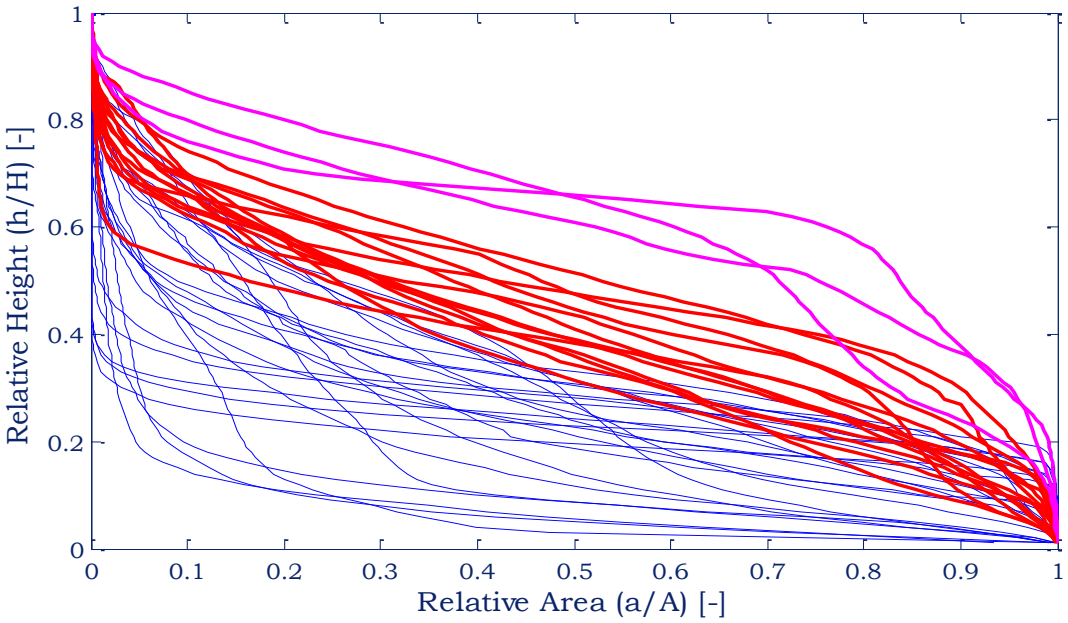

Figure 36A: Hypsometric curves of 41 Baro-Akobo basin watersheds describing the catchments at monadnock stage (blue), equilibrium stage (red) and inequlibrium stage (magenta)

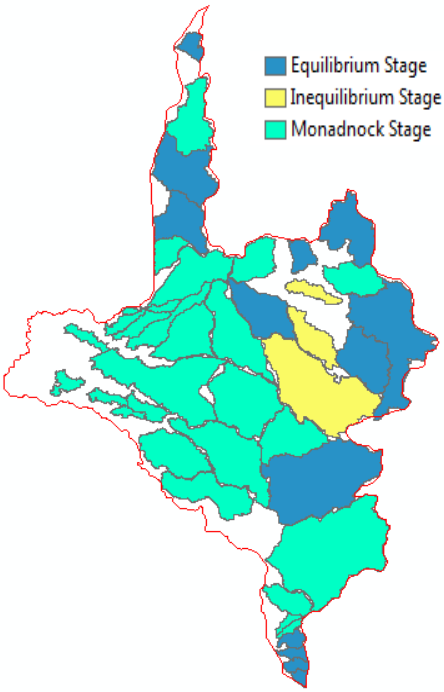

Figure 37B: The morphometric characteristics of Baro-Akobo basin watersheds using hypsometric curves.

5.2. Catchment Classification

i) Based on catchment indices and curves

The grouping in AHC is highly based on the Euclidean distance which has been fixed differently for all classifications through manual inspection as 0.8, 0.6, 0.6, 0.7, 3 and 1.4 for DI, EI, RC, SE, HC and TWI respectively. It is also fixed for catchment climate, function and structure as 2.5, 1.5 and 5.5 respectively, while it is 6 for over all classification.

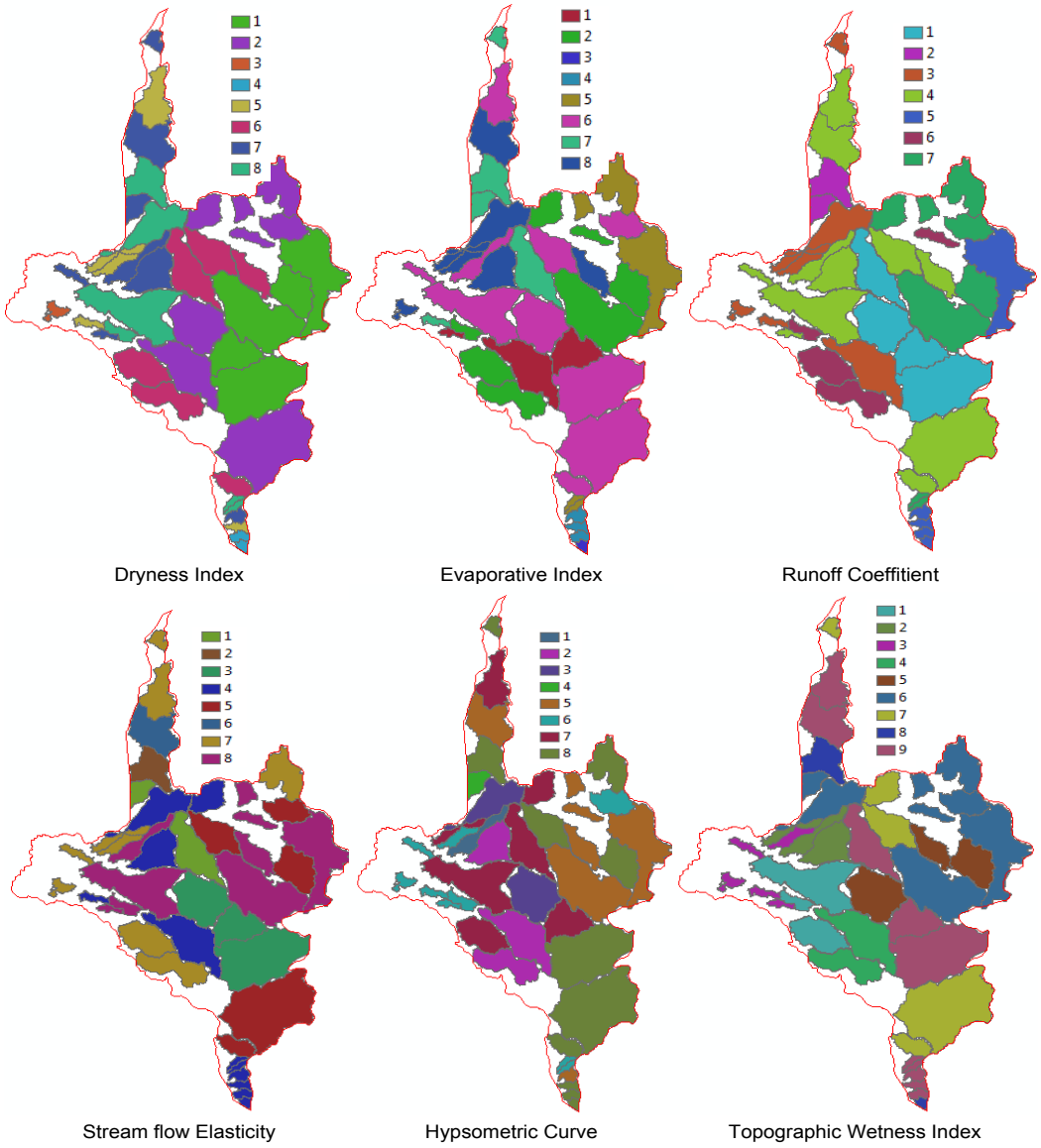

Figure 38: Classification of Baro-Akobo basin watersheds based on six catchment indices

ii) Based on Catchment Climate, Functions and Forms

To see the hydrological similarities of the Baro-Akobo basin watersheds based on three major divisions of a given catchment hydrology (catchment climate, catchment function and catchment structure) the indexes derived under each class have been combined to give a single classification for each section (Fig. 37). Climate wise catchments near to each other (e.g., the upper Baro-Akobo, central regions of the basin) happen to exhibit similar characteristics.

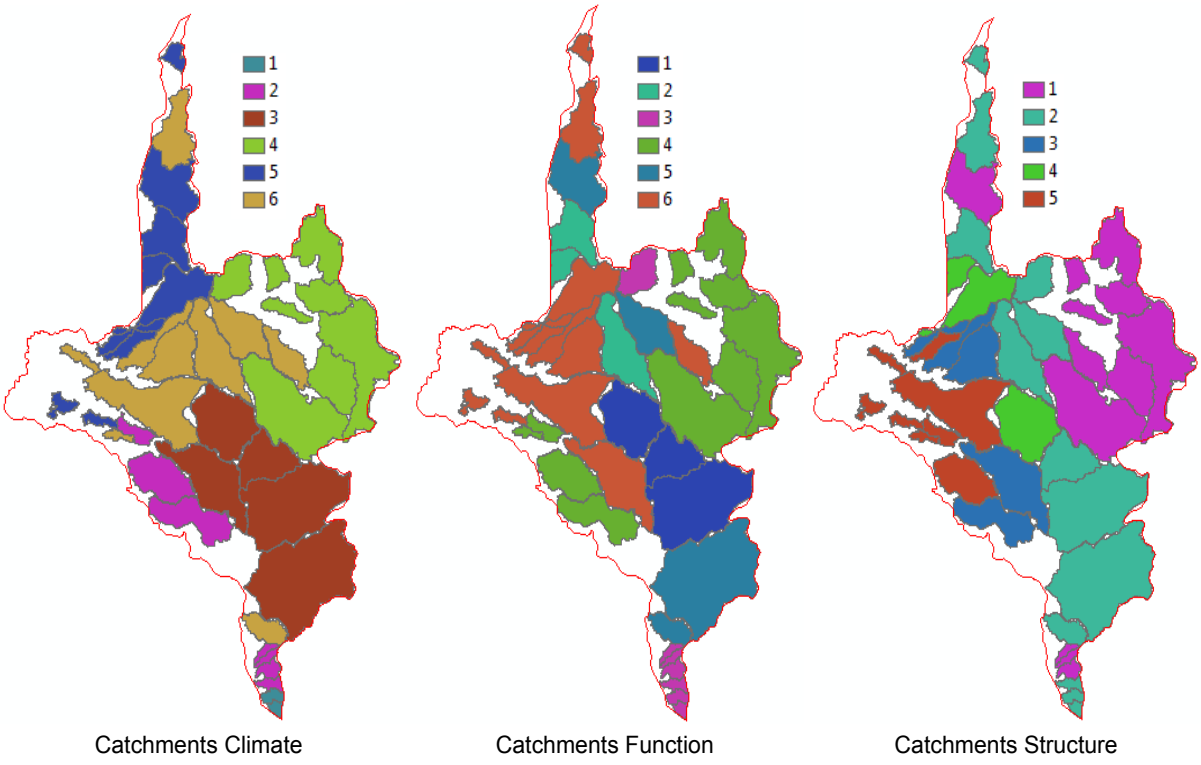

Figure 39: Classification of Baro-Akobo watersheds using selected catchment climate, function and structure indices.

iii) Baro-Akobo Basin Watersheds General First Stage Classification

Finally all the parameters derived for catchment climate (2), catchment function (2) and catchment form (2) are combined together to give hydrologically similar classes. Figure 38

illustrates the hydrologically similar groups of Baro-Akobo basin watersheds. The highland catchments happen to have similar characteristics, which is also true for catchments situated in lowlands

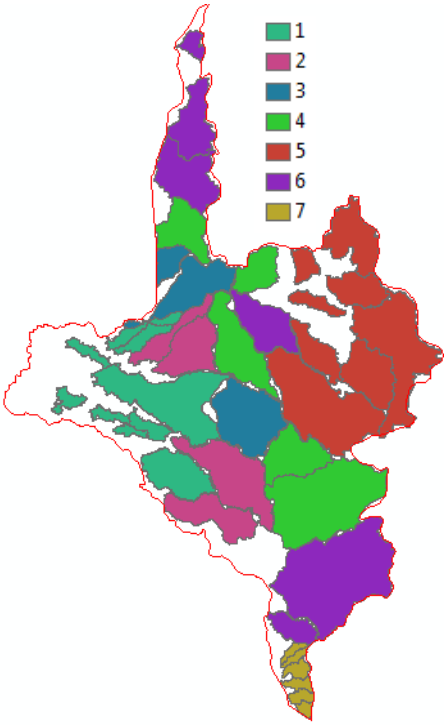

Figure 40: Baro-Akobo basin watersheds classified into seven hydrologically similar classes

CHAPTER SIX

DISCUSSION

6.1. Catchment Characterization

The Baro-Akobo basin watershed characterizations have been done based on their climate, functions and structures. With climatic perspective (Fig. 30), since dryness index is the inverse of humidity index, it indicates that catchments in the lower Baro-Akobo basin (western), southern and northern part falls under the arid and semi arid climate, while most of the highland and intermediate elevation watersheds show humid and dry sub-humid climate type respectively. With regard to the evaporative index, about 70% of the watersheds in the basin have evaporative index value of greater than 0.7, indicating that, much of the water coming to the basin leaves as a green water. When the dryness indexes are seen with the land cover classes of the basin, one can see that most of the humid regions catchments land are covered by natural forest and the left are cultivation land. While the arid and semi arid regions are dominated by wetlands and wood lands, most of the dry sub-humid catchments are partially wood land and partially natural forest.

Regarding the catchment functions, more than 80% of the watersheds have runoff coefficient of less than 0.40, this also indicates that the portion of the incoming water leaving the catchments as blue water is minimal. If we took a close look at topography of the Baro-Akobo basin, it can be grouped into three distinct regions, rugged (western region), flat (eastern) and the transition between them is a steep slope escarpment. Catchments located in the transition region have higher runoff coefficients of up to 0.73, while the rugged highland region has values between 0.26 and 0.36. The low land region were we can notice only a few meters elevation difference at hundreds of kilometers horizontal distance, the runoff coefficients are as minimum

as 0.09. On the side of stream flow elasticity, large numbers of catchments (more than 90%) in the basin have value greater than 1, indicating that the basin watersheds are highly sensitive to change in precipitation.

The characterization based on catchment structures; topographic wetness index and hypsometric curve has also been made to see morphometric characteristics of watersheds in the basin. Accordingly, from the hypsometric curve analysis (based on their hypsometric integral), about 60% of the watersheds are found to be at their monadnock stage, 32% have reached their equilibrium stage while only 7% are at their in-equilibrium stage. From the analysis of TWI it is been found that the basins watersheds wetness index spatial distribution falls under five categories of distribution, of which about 39% falls under Generalized Pareto distribution type, more than 30% under Wakeby lower bound distribution type. Most of the highland region watersheds are dominated by Wakeby lower bound, while Generalized Pareto took the lead in lowland watersheds.

6.2. Catchment Classification

The result of individual indexes/distributions clustering shows that most the catchment adjacent to each other demonstrated similar behavior. Classification with dryness index shows that the watersheds in the eastern corner of the basin are dominated by two classes, similarly few of the lowland catchment adjacent to each other falls under same category. The evaporative index based cataloging shows some similarity for watersheds in the northern and lowland region of the basin. Runoff coefficient wise some regional behaviors have been seen in the lowland, highland and transition regions, while the stream flow elasticity oriented classes show some similarity between adjacent watersheds in the northern tip and highlands. The categorization based on their

hypsometric curve and TWI has shown a very good similarity with most of the adjacent catchments being under same classes.

Many of the highland dominated catchments in eastern regions of the basin have been seen to fall under same classes, climatically, functionally and structurally (Fig. 37). The classes of catchments in other parts of the basin differ from each other. In the general first stage classification which is done combining climate, catchment function and forms characteristics, most of the northern, southern, highland (western), as well as low land (eastern) catchments of the basin falls under like groups (Fig. 38). In the central part of the basin catchments of different characteristics exists.

CHAPTER SEVEN

CONCLUSIONS AND RECOMENDATIONS

7.1. Conclusions

Catchment classification based on their hydrologic similarity is an open theme at the forefront of today's hydrological sciences. In regions were the incoming and outgoing water mass observations are collected intensively using reliable scientific instruments classification can be done at once using different approaches. When it comes to regions were those data's are not available either because of economy, skilled man power or inaccessibility, hydrological characterization and classification of catchments based on hydrologic similarity is the most difficult problem. In such areas, we cannot jump into general classifications of the catchments at once, so a preliminary or first stage classification will be needed. And also we need to look for data sources which might help with this preliminary approach that is when the necessity of global datasets and models get visible. In this study, 41 Baro-Akobo basin watersheds are derived from ASTER 30m-GDEM were only five of them has stream flow data at their outlets. The data employed for the analysis are TRMM (precipitation) and MODIS (AET and PET) over twelve years (2000-2011), were as dynamic annual water balance model is used to generate synthetic runoff data. Hydrological characterizations of the watersheds have been done from three different angles: climate, hydrologic response and forms. The classification has also been done at three stages; based on individual dimensionless indexes (dryness index, evaporative index, runoff coefficient, and stream flow elasticity), distributions (hypsometric curve and topographic wetness index), based on combined climatic indexes (evaporative index, dryness index), catchment functions (runoff coefficients and stream flow elasticity) and catchment forms (hypsometric curves and topographic wetness indexes). Finally the general first stage

classifications have been done combining climate indexes, catchment functions and catchment forms. The hydrological characterization has shown some expected behaviors of the watersheds and also seems to reflect the big difference which exists in the basin due to topography. In the same way the classified watersheds also showed that adjacent catchments in the highland and lowland regions falling under same category most of the times. The next move of this concept will be to interrogate selected watersheds in each group with experimental data through the use process based models to identify the behavior pedals of the regions hydrology.

7.2. Recommendations

- The numbers of signatures/distributions used in the study are limited to two per categories. For better understanding of watershed characteristics and to do better classifications.
- The model employed in this study is a dynamic water balance model which has only precipitation and evapotranispiration as an input in addition to manually calibrated single model parameter. Therefore, more process based modelling which accounts other influential parameters like soil moisture should be applied for better results.
- The classification method, agglomerative hierarchical cluster analysis, only depends on the single parameters computed over a periods and nothing else. To check the weight of classification approach employed in this paper, the watersheds should be revisited by more sophisticated approaches which consider spatial and temporal variabilities of the watersheds signatures.

REFERENCES

Awulachew, S. B., Yilma, A. D., Loulseged, M., Loiskandl, W., Ayana, M., and Alamirew, T., 2007. Water Resources and Irrigation Development in Ethiopia, International Water Management Institute, Colombo, Sri Lanka, Working Paper 123, 78p.

Beven, K. J., and Kirkby, M. J., 1979. A physically based,variable contributing area model of basin hydrology, Hydrological Sciences-Bulletin, 24, 43-69.

Beven, K. J., 2000. Uniqueness of place and process representations in hydrological modelling, Hydrology and Earth System Sciences, 4 (2), 203-213.

Black, P. E., 1997. Watershed Functions, Journal of the American Water Resources Association, 33 (1).

Budyko, M. I., 1958. The Heat Balance of the Earth's Surface, U.S. Department of Commerce, Washington, D.C.

Burn, D. H., 1997. Catchment similarity for regional flood frequency analysis using seasonality measures, Journal of Hydrology, 202, 212-230, doi:10.1016/S0022-1694(97)00068-1.

Carrillo, G., Troch, P. A., Sivapalan, M., Wagener, T., Harman, C., and Sawicz, K., 2011. Catchment classification: hydrological analysis of catchment behavior through process-based modeling along a climate gradient, Hydrology and Earth System Sciences, 15, 3411-3430, doi:10.5194/hess-15-3411-2011.

Fu, B. P., 1981. On the calculations of the evaporation from land surface, Sci. Atmos. Sin., 5 (1), 23-31.

Harlin, J. M., 1978. Statistical moments of the hypsometric curve and its density function, Math. Geol., 10, 59-72, doi:10.1007/BF01033300.

Huffman, G., and Bolvin, D., 2012. TRMM and other data precipitation data set documentation, Mesoscale Atmospheric Processes Laboratory, NASA Goddard Space Flight Center and Science Systems and Applications, Inc.

Koster, R.D. and M.J. Suarez., 1999. A simple framework for examining the inter-annual variability of land surface moisture fluxes. Journal of Climate, 12, 1911-1917.

Kummerow, C., Barnes, W., Kuzo, T., Shiue, J., and Simpson, J., 1998 The Tropical Rainfall Measuring Mission (TRMM) sensor package, Journal of Atmospheric and Oceanic Technology, 15, 809-817.

Langbein, W. B., 1947. Topographic Characteristics of Drainage Basins,Water-Supply Paper 968-C, Washington.

Ley, R., Casper, M. C., Hellebrand, H., and Merz, R., 2011. Catchment classification by runoff behaviour with self-organizing maps (SOM), Hydrology and Earth System Sciences, 15, 2947-2962, doi:10.5194/hess-15-2947-2011.

Luo, W., 2000. Quantifying groundwater-sapping landforms with hypsometric technique, Journal of Geophysical Research, 105, 1685-1694.

McDonnell, J. J., and Woods, R., 2004. Editorial: On the need for catchment classification, Journal of Hydrology, 299 (1-2), 2-3.

McDonnell, J. J., M.Sivapalan, Vache, K., Dunn, S., Grant, G., Haggerty, R., Hinz, C., Hooper, R., Kirchner, J., Roderick, M. L., Selker, J., and Weiler, M., 2007. Moving beyond heterogeneity and process complexity: A new vision for watershed hydrology, Water Resources Research, 43, W07301, doi:10.1029/2006WR005467.

MoWR, 2012. Ethiopian River Basins, accessed: December, 2012.

Mu, Q., Heinsch, F. A., Zhao, M., and Running, S. W., 2007 Development of a global evapotranspiration algorithm based on MODIS and global meteorology data, Remote Sensing of Environment, 111, 519-536, doi:10.1016/j.rse.2007.04.015.

Mu, Q., M.Zhao, and Running, S. W., 2011. Improvements to a MODIS Global Terrestrial Evapotranspiration Algorithm, Remote Sensing of Environment, 115, 1781-1800, doi:10.1016/j.rse.2011.02.019.

O'Sullivan, D., and Unwin, D., 2003. Geographic Information Analysis, John Wiley and Sons, Hoboken, New Jersey, US, 436 pp.

Rao, A. R., and Hamed, K. H., 2000. Flood Frequency Analysis, CRC Press, Florida, US, 355 pp.

Ritter, D. F., Kochel, R. C., and Miller, J. R., 2002. Process Geomorphology, McGraw-Hill, 560 pp.

Sawicz, K., T.Wagener, Sivapalan, M., A.Troch, P., and Carrillo, G., 2011. Catchment classification: empirical analysis of hydrologic similarity based on catchment function in the eastern USA, Hydrology and Earth System Sciences, 15, 2895-2911, doi:10.5194/hess-15-2895-2011.

Schaefli, B., Harman, C. J., Sivapalan, M., and Schymanski, S. J., 2011. HESS Opinions: Hydrologic predictions in a changing environment: behavioral modeling, Hydrology and Earth System Sciences, 15, 635-646, doi:10.5194/hess-15-635-2011.

Sivakumar, B., and Singh, V. P., 2012. Hydrologic system complexity and nonlinear dynamic concepts for a catchment classification framework, Hydrology and Earth System Sciences, 16.

Sivapalan, M., Bloschl, G., Zhang, L., and Vertessy, R., 2003. Downward approach to hydrological prediction, Hydrological Processes, 17, 2101-2111, doi: 10.1002/hyp.1425.

Strahler, A. N., 1952 Hypsometric (Area-Altitude) Analysis of Erosional Topography, Geological Society of America Bulletin, 63, no. 11, 1117-1142, doi: 10.1130/0016-7606(1952)63[1117:HAAOET]2.0.CO.

Tekleab, S., Uhlenbrook, S., Mohamed, Y., Savenije, H. H. G., Temesgen, M., and Wenninger, J., 2011. Water balance modeling of Upper Blue Nile catchments using a top-down approach, Hydrology and Earth System Sciences, 15, 2179-2193, doi:10.5194/hess-15-2179-2011.

Vivoni, E. R., Benedetto, F. D., Grimaldi, S., and Eltahir, E. A. B., 2008. Hypsometric control on surface and subsurface runoff, Water Resources Research, 44, W12502, doi:10.1029/2008WR006931.

Wagener, T., Sivapalan, M., Troch, P., and Woods, R., 2007. Catchment Classification and Hydrologic Similarity, Geography Compass, 1/4, 901-931, doi:10.1111/j.1749-8198.2007.00039.x.

Ward, J. H., 1963. Hierarchical Grouping to Optimize an Objective Function, Journal of the American Statistical Association, 58 (301).

Woube, M., 1999. Flooding and sustainable land–water management in the lower Baro–Akobo river basin, Ethiopia, Applied Geography, 19 (3), 235-251, doi:10.1016/S0143-6228(99)00004-1.

Zhang, L., Potter, N., Hickel, K., Zhang, Y., and Shao, Q., 2008. Water balance modeling over variable time scales based on the Budyko framework – Model development and testing, Journal of Hydrology, 360, 117-131, doi:10.1016/j.jhydrol.2008.07.021.